
# BRNO UNIVERSITY OF TECHNOLOGY

VYSOKÉ UČENÍ TECHNICKÉ V BRNĚ

## FACULTY OF MECHANICAL ENGINEERING

FAKULTA STROJNÍHO INŽENÝRSTVÍ

## INSTITUTE OF MACHINE AND INDUSTRIAL DESIGN

ÚSTAV KONSTRUOVÁNÍ


# OPERATIONAL SAFETY AND RELIABILITY ENHANCEMENT OF LARGE-SCALE HYDROSTATIC BEARINGS

NAVYŠOVÁNÍ PROVOZNÍ BEZPEČNOSTI A SPOLEHLIVOSTI VELKOROZMĚRNÝCH HYDROSTATICKÝCH LOŽISEK

**DOCTORAL THESIS**

DIZERTAČNÍ PRÁCE


**AUTHOR** — Ing. Jan Foltýn

AUTOR PRÁCE

**SUPERVISOR** — doc. Ing. Petr Svoboda, Ph.D.

ŠKOLITEL



**BRNO 2026**

# STATEMENT

I hereby declare that I have written the PhD thesis *Operational Safety and Reliability Enhancement of Large-Scale Hydrostatic Bearings* on my own according to the advice of my supervisor doc. Ing. Petr Svoboda, Ph.D., and using the sources listed in the references.

.....

Jan Foltýn

# BIBLIOGRAPHICAL REFERENCE

FOLTÝN, Jan. *Operational Safety and Reliability Enhancement of Large-Scale Hydrostatic Bearings.* Brno, 2026. 87 p. PhD thesis. Brno University of Technology, Faculty of Mechanical Engineering, Institute of Machine and Industrial Design. Supervisor doc. Ing. Petr Svoboda, Ph.D.

# ACKNOWLEDGEMENT

I would like to express my deepest gratitude to my supervisor, doc. Ing. Petr Svoboda, Ph.D., who provided consistent guidance and support throughout my studies. I also wish to extend my sincere thanks to Ing. Michal Michalec, Ph.D., and to the head of the department, prof. Ing. Martin Hartl, Ph.D., for their support and valuable advice during my academic work.

Furthermore, I am grateful to my colleagues from the Department of Mechanical and Industrial Engineering for creating a supportive, collegial, and motivating working environment. I particularly appreciate my office mates, with whom I shared many professional experiences and memorable moments.

My greatest thanks belong to my family and friends, whose support and encouragement accompanied me throughout my entire academic journey.

# ABSTRACT

This dissertation investigates the operational safety of large-scale hydrostatic bearings, in which load capacity is provided by an externally pressurized lubricating film separating sliding surfaces. Although hydrostatic lubrication enables negligible wear and very low friction even at zero speed, bearings of large diameter exhibit reduced safety margins. Segmentation of pads and tracks, assembly inaccuracies, structural compliance, thermal effects, and hydraulic disturbances can locally reduce film thickness and move the system toward contact-prone conditions. The dissertation therefore adopts a safety-oriented perspective in which the minimum lubricating film thickness and its distribution are treated as the key parameters governing reliability in rigid, segmented hydrostatic bearings. The main aim of this dissertation is to investigate, through analysis and experimental validation, how geometric deviations, hydraulic instabilities, and operating conditions affect the minimum lubricating film thickness in large-scale hydrostatic bearings, and to assess lubricating film thickness and its distribution as safety-relevant indicators of proximity to surface contact in rigid segmented bearing arrangements. The work is structured as three peer-reviewed journal papers. The first paper develops a contactless optical point tracking method for measuring lubricating film thickness without permanently installed sensors and validates it experimentally. The second paper examines pad alignment as a direct safety factor by comparing mechanical leveling, pressure-based alignment, and optical coordinate measurement method, demonstrating that optical alignment provides the most uniform film thickness distribution. The third paper applies the methodology to the hydrostatic bearing system of the Very Large Telescope, where contactless measurements reveal film-thickness variations caused by segmentation and simulated restrictor faults. Overall, this dissertation provides experimentally validated diagnostic tools and supports a preventive, film-thickness-based safety strategy for large hydrostatic bearings.

# KEYWORDS

Tribology, Hydrostatic lubrication, Lubricating film thickness, Bearing safety, Lubricating film distribution

# ABSTRAKT

Tato disertační práce se zabývá provozní bezpečností hydrostatických ložisek velkých rozměrů, u nichž je nosnost zajištěna tlakovým mazivem, tvořícím film oddělující kluzné povrchy. Přestože při hydrostatickém mazání prakticky nedochází k opotřebení a tření i při nulové rychlosti, ložiska velkých průměrů vykazují omezené bezpečnostní rezervy. Segmentace kapes a pojezdových drah, montážní nepřesnosti, poddajnost konstrukce, tepelné vlivy a hydraulické poruchy mohou lokálně snižovat tloušťku mazacího filmu a přibližovat systém ke stavům náchylným ke kontaktu, a tedy kolizi. Práce proto uplatňuje bezpečnostně orientovaný přístup, v němž jsou minimální tloušťka mazacího filmu a její rozložení považovány za klíčové parametry určující spolehlivost pevných segmentovaných hydrostatických ložisek. Hlavním cílem této disertační práce je analyticky i experimentálně prozkoumat, jak geometrické odchylky, hydraulické nestability a provozní podmínky ovlivňují minimální tloušťku mazacího filmu u velkorozměrových hydrostatických ložisek, a posoudit tloušťku mazacího filmu a její rozložení jako bezpečnostně relevantní indikátory vzniku kontaktu mezi kluznými povrchy v tuhých segmentovaných ložiskových uspořádáních. Práce je strukturována do tří recenzovaných článků. První článek vyvíjí bezkontaktní optickou metodu sledování bodů pro měření tloušťky mazacího filmu bez trvale instalovaných snímačů a experimentálně ji ověřuje. Druhý článek se zabývá ustavením kapes jako přímým bezpečnostním faktorem porovnáním konvenčních měřidel, ustavení na základě tlaků a optického měření a ukazuje, že optické ustavení poskytuje nejrovnoměrnější rozložení tloušťky mazacího filmu. Třetí článek vychází z předešlých poznatků a zabývá se hydrostatickým ložiskem teleskopu Very Large Telescope, kde bezkontaktní měření odhalují změny tloušťky mazacího filmu způsobené segmentací a simulovanými poruchami škrticích prvků. Celkově tato disertační práce přináší experimentálně ověřené diagnostické nástroje a podporuje preventivní, na tloušťce mazacího filmu založenou strategii bezpečnosti pro hydrostatická ložiska velkých rozměrů.

# KLÍČOVÁ SLOVA

Tribologie, Hydrostatické mazání, Tloušťka mazacího filmu, Bezpečnost ložiska, Rozložení mazací vrstvy

# CONTENT

# 1 INTRODUCTION

Hydrostatic bearings belong to the class of fluid film bearings in which a pressurized lubricant is supplied between sliding surfaces to generate load-carrying capacity. The externally pressurized lubricating film ensures complete separation of the contacting surfaces, thereby eliminating direct contact, significantly reducing wear, and enabling smooth motion with very low friction. A key advantage of hydrostatic bearings is their ability to maintain a stable lubricating film even at low or zero relative speed, which distinguishes them from hydrodynamic and rolling element bearings. These properties make hydrostatic systems particularly suitable for applications requiring high positioning accuracy, long service life, and effective vibration damping, such as precision machine tools, large rotary tables, antennas, and astronomical telescopes.

Unlike rolling bearings, whose performance is governed by discrete contact points, or hydrodynamic bearings, which rely on relative motion to generate pressure, hydrostatic bearings operate independently of speed. However, this benefit is accompanied by strict requirements on the control of the lubricating film. The thickness and pressure distribution of the oil film must remain within a narrow operational window to ensure safe and reliable performance. In large-diameter hydrostatic bearings, maintaining a consistent film thickness becomes increasingly challenging, as even small deviations in geometry, alignment, or loading conditions can lead to local instabilities in the lubricating layer. Such instabilities may manifest as excessive pressure gradients, local film thinning, or, in extreme cases, collapse of the lubricating film and direct contact between sliding surfaces.

As the size of the supported structure increases, so do the technological, manufacturing, and logistical challenges associate with the bearing system. Bearings with diameters of several meters, and in some cases tens of meters, cannot be manufactured as monolithic components. Instead, both the bearing pads and the mating track surfaces are typically divided into multiple segments to enable feasible production, transport, and installation. While segmentation is unavoidable in large-scale systems, it introduces assembly-related inaccuracies such as height offsets, angular misalignments, and local deviations from flatness and parallelism. These imperfections directly influence the distribution of the lubricating film and the load-sharing behavior of individual bearing pads.

## 1.1 Motivation

The motivation for this research arises from the need to better understand how these deviations affect the safety and reliability of the hydrostatic lubrication regime. In segmented bearing systems, minor misalignments or local geometric errors can cause uneven pressure distribution among bearing recesses, leading to localized reduction of film thickness. Such conditions significantly increase the risk of lubricating film collapse and unintended contact between sliding surfaces, which can result in severe damage, costly repairs, and extended downtime.

Since perfect flatness, parallelism, and alignment across very large diameters are practically unattainable, a certain level of geometric imperfection must be expected and systematically managed. This necessitates reliable methods for bearing alignment, precise measurement of lubricating film thickness, and diagnostic techniques capable of identifying critical states before irreversible damage occurs. The motivation of this work is therefore to contribute to a deeper understanding of how assembly precision, hydraulic behavior, and diagnostic methods interact in large-scale hydrostatic bearings, and how this knowledge can be used to improve operational safety and robustness in applications where absolute geometric perfection cannot be guaranteed.

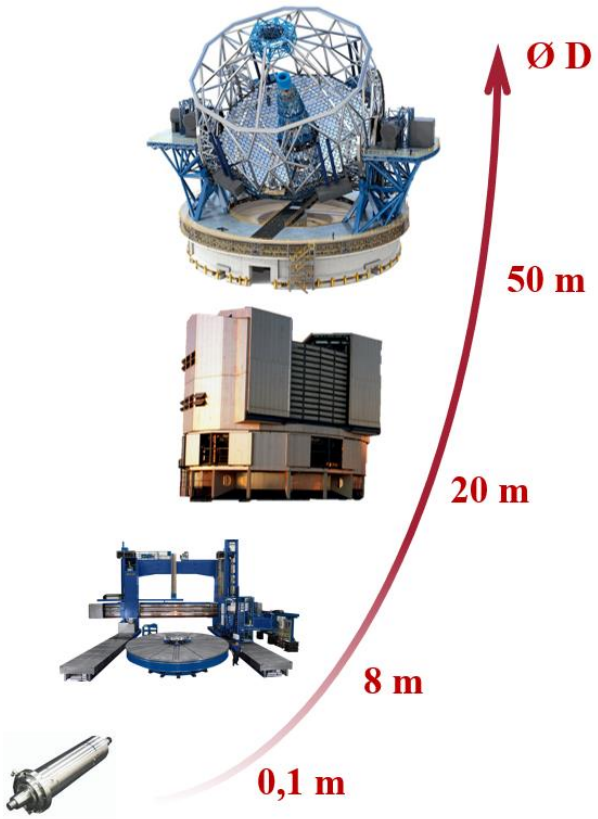


Figure 1 Scheme of hydrostatic bearings applications size comparison.

# 2 STATE OF THE ART

Hydrostatic bearings were first introduced by L.D. Girard in 1851 [1] as a water-lubricated bearing for railway applications. The concept was publicly presented at the Paris International Exposition in 1878. Since then, hydrostatic bearings have found widespread use in machinery, with components ranging in size from a few millimeters to several tens of meters. In 1989 Rowe [2] published paper about advances in this field. The main progress shifted from basic concepts to optimization and application: numerical methods and design charts were developed for hybrid bearings operating over wide power-ratio ranges, new geometries such as slot- and hole-entry, partial-arc and combined journal–thrust configurations were introduced, and cavitation, thermal and dynamic stability phenomena were incorporated into design practice. Next, in 1992 Bassani and Piccigallo [3] wrote book about main aspects of hydrostatic bearings. In 2014, Li et al. [4] analyzed research progress of large hydrostatic bearings. He stated that future focus in hydrostatic bearings will be in optimization of thermal influence. Liu et al. [5] evaluated development of hydrostatic bearings in basic theory and applications. In his opinion, future research will focus on reliability of these bearings. Later, Michalec et al. [6] summarized design and optimization of large hydrostatic bearings. He stated that the challenges will lie in estimation of tolerable error specification and failure prevention.

## 2.1 Hydrostatic bearings

The fundamental principle of hydrostatic bearing is the supply of pressurized fluid into the gap between two sliding surfaces. This creates a thin pressurized film that supports the load and prevents direct surface contact [7]. Unlike hydrodynamic bearings, hydrostatic bearings do not require relative motion between surfaces to generate a load-bearing film, which is a key advantage during machine startup and shutdown. From a design perspective, hydrostatic bearings are classified by the type of fluid (oil, water [8,9], or cryogens [10]), and by configuration (radial, thrust, or combined). Recently, hybrid bearings combining hydrostatic and hydrodynamic principles have emerged [11–14], enabling efficient operation at high speeds where part of the load is carried hydrodynamically. The bearing receess (Figure 2) formed within the pad is supplied with pressurised lubricant from a hydraulic power unit through an inlet hole. The bearing pad is loaded with a force $F$. Once the pressure source is activated (Figure 3), the pressure in the recess increases until it reaches the value required to lift the load. This pressure level is given by $p_l = F/S$, where $S$ is the projected area of the recess in the direction perpendicular to the applied load.

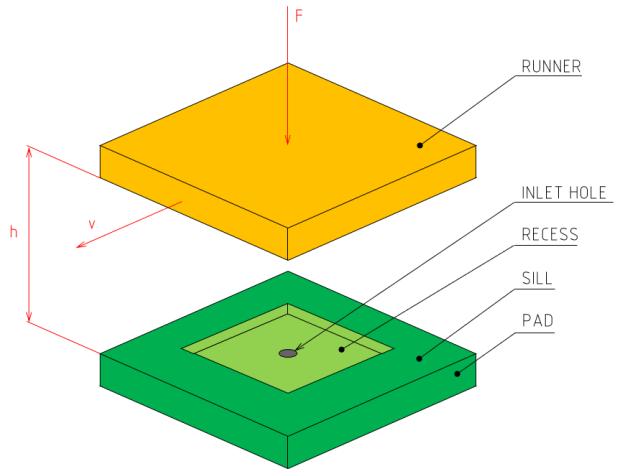


Figure 2 Scheme of hydrostatic bearing contact.

At this moment, separation of the sliding surfaces occurs, and a lubricating film is formed. Pressurized lubricant then begins to flow through the bearing. As the lubricant passes through the throttling region (land), a pressure drop occurs, followed by outflow and return of the lubricant to the reservoir. Different load levels result in different recess pressures $p_r$ and corresponding lubricating film thicknesses $h$ [3].

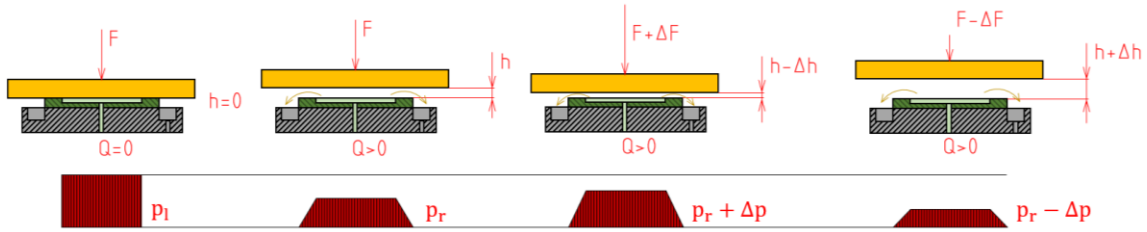


Figure 3 Principle of a hydrostatic bearing: pressure distribution in an axial bearing.

Hydrostatic bearings offer several benefits. Continuous separation of frictional surfaces ensures minimal wear and low friction even at low rotational speeds, same as no stick-slip effect [15]. They exhibit high positional accuracy and substantial stiffness, making them ideal for precision engineering applications. They can carry heavy loads and provide excellent damping, which helps suppress vibrations [16–18]. When properly designed and maintained, hydrostatic bearings have a long service life. However, these advantages are offset by certain drawbacks. Their operation requires a complex fluid supply and filtration system, increasing both initial investment and operational costs [19]. Continuous fluid pumping raises energy consumption, and sensitivity to contamination necessitates high-quality filtration. In some cases, thermal management issues may affect lubricant viscosity and system stability.

### 2.1.1 Hydraulic system

Hydrostatic bearings operate on the principle of externally supplied pressurized lubricant that forms a load-carrying film. However, it is strongly dependent on the design and reliability of the hydraulic supply system. The primary task of the supply system is to sustain a stable lubricant film thickness over a wide range of loads and operating conditions. Accurate regulation of lubricant pressure and flow rate is therefore fundamental. The hydraulic system must continuously deliver an adequate quantity of pressurized fluid to the bearing recesses so that load support is maintained without surface contact. According to the method by which lubricant is supplied to the pads, hydrostatic bearing systems are generally classified as constant-pressure or constant-flow systems.

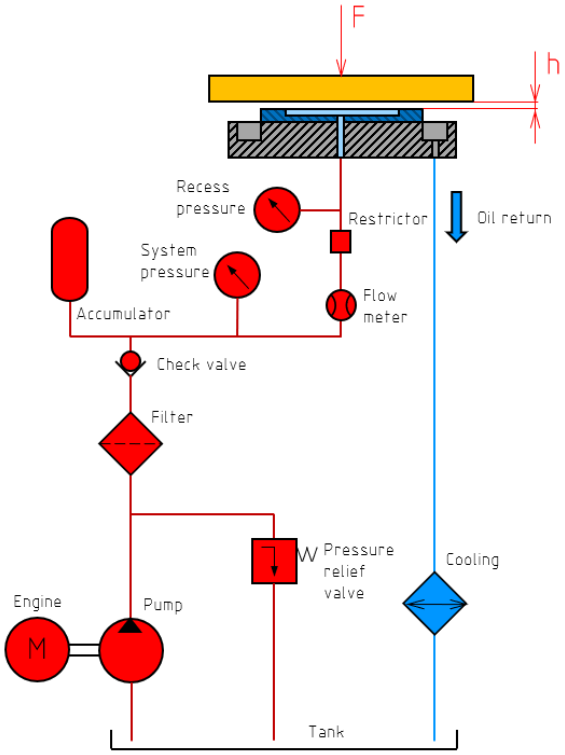


Figure 4 Scheme of hydrostatic bearing hydraulic system parts.

To ensure stable and safe operation, hydrostatic bearing systems incorporate a range of auxiliary hydraulic components (Figure 4), largely independent of the chosen supply principle. These typically include pressure relief valves, check valves, and throttling elements. Temperature control of the lubricant is achieved by means of cooling units, maintaining viscosity within a defined operating window. As the lubricant is often discharged to atmosphere and subsequently returned to the reservoir, effective filtration is essential to prevent particulate contamination that could damage the bearing surfaces. For increased operational safety, hydraulic accumulators and redundant supply lines may also be integrated.

Within a hydrostatic lubrication circuit, the accumulator [20] serves as a critical safety component during abnormal or transient conditions. It consists of a pressure vessel containing a deformable separation element—most commonly an elastomeric membrane—that isolates the incompressible lubricant from a compressible gas volume.

During normal operation, the accumulator is charged to system pressure and stores a reserve quantity of pressurized fluid. Proper functionality requires installation in conjunction with a check valve, which prevents backflow toward the pump and ensures that any discharge from the accumulator is directed solely at the bearing pads. In the event of a sudden pump failure, the pressure within the bearing recesses would otherwise collapse rapidly, potentially causing contact between sliding surfaces while relative motion is still present. Such a scenario can lead to severe surface damage. The accumulator mitigates this risk by temporarily sustaining pressure and supplying lubricant, thereby providing sufficient time to decelerate and stop the bearing motion under lubricated conditions. Additionally, due to the elastic behavior of the membrane, the accumulator attenuates pressure pulsations originating from pump operation, contributing to improved stability of the lubrication film. The use of multiple accumulators can further reduce hydraulic pulsation levels.

For applications demanding uninterrupted operation, critical elements of the hydraulic supply—such as filters, auxiliary pumps, heat exchangers, and accumulators—may be installed in parallel redundant branches. Under conventional arrangements, maintenance or failure of any of these components would necessitate system shutdown and loss of lubrication. With a parallel configuration, the affected line can be isolated while lubrication is maintained through the backup circuit, preserving pressure and flow to the bearing. Although this approach increases system complexity and initial cost, it substantially improves long-term operational reliability and fault tolerance of both the hydraulic system and the hydrostatic bearing.

**Constant flow system**

The defining requirement of a constant-flow hydrostatic system is that each bearing pad receives the same volumetric flow rate (Figure 5). Under this condition, uniform lubricant film thickness across all pads can be achieved. Implementing this principle in practice presents challenges, particularly as the number of pads increases. Each pad requires an independent flow source, which traditionally implies the use of multiple pumps. Because individual pumps exhibit variations in internal leakage and efficiency, mechanical synchronization is often required to ensure equal delivery. In gear pump arrangements, for example, the pump shafts may be mechanically coupled to enforce identical displacement per revolution. Modern constant-flow systems increasingly rely on actively controlled [21,22] hydraulic components to achieve uniform flow distribution.

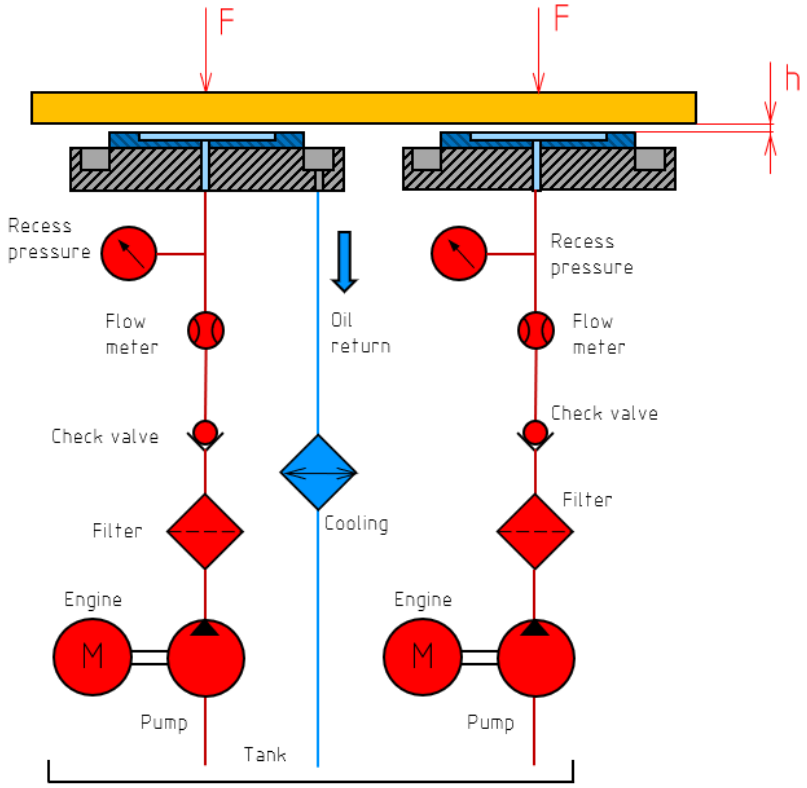


Figure 5 Constant flow hydraulic system.

Proportional or servo-controlled flow valves can adjust the supplied flow based on feedback signals from flow sensors installed in each branch. While this approach offers flexibility and precision, it necessitates advanced control hardware and sensor infrastructure. The overall effectiveness of such regulation depends on the dynamic response of the control system and the accuracy and stability of the measured feedback signals.

**Constant pressure system**

Constant-pressure systems are designed to provide approximately equalized supply pressure to all bearing pads [23]. A single central pump (Figure 6) delivers pressurized lubricant to the bearing through throttling elements (restrictors) that create a controlled pressure drop between the supply manifold and the recesses [24]. When the bearing is subjected to disturbances such as load asymmetry, the pressure loss across the restrictor allows each recess pressure to adjust autonomously [25]. Without restrictors, lubricant would preferentially flow toward the least-loaded pad, starving heavily loaded regions and causing a reduction in local film thickness.

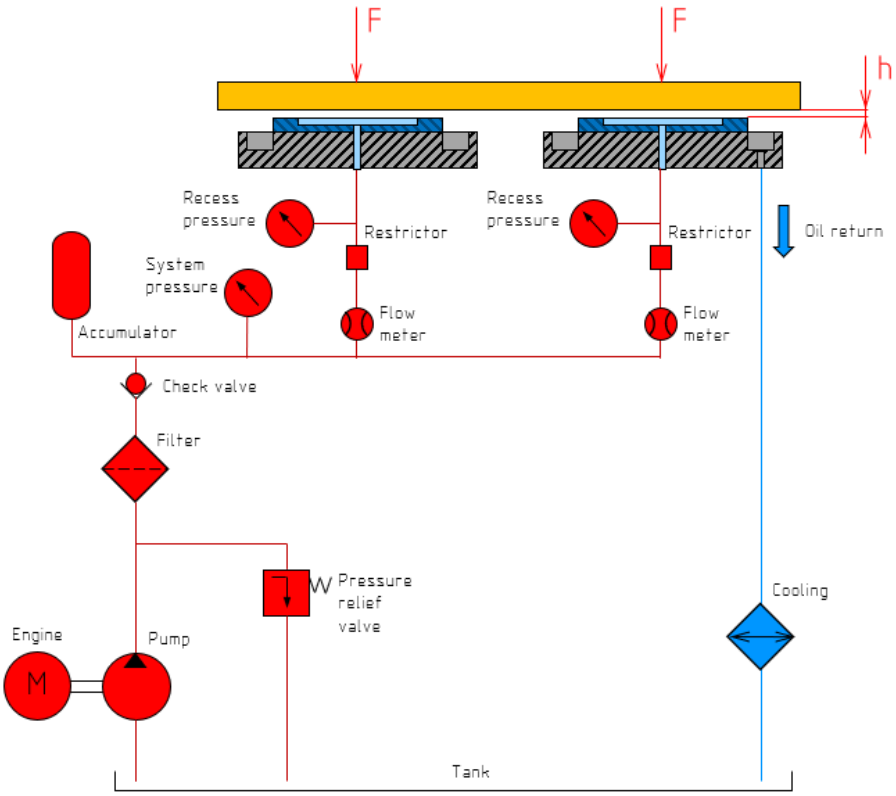


Figure 6 Constant pressure hydraulic system.

The restrictor counteracts this tendency by limiting the flow into unloaded pads in proportion to the pressure difference, thereby redirecting lubricant toward more heavily loaded pads. This mechanism promotes a more balanced pressure distribution and stabilizes the lubricant film across the bearing. Compared with constant-flow systems, constant-pressure configurations require fewer pumps and simpler hydraulic layouts, but their performance is highly sensitive to the proper selection and design of the restrictor elements.

**Restrictors**

Restrictors, also referred to as compensation elements, are essential components in constant-pressure hydrostatic systems. Their function is to generate a pressure drop that enables recess pressure to increase as the bearing clearance decreases. Restrictors can be classified as fixed, adjustable, passive self-regulating, or actively controlled.

Fixed restrictors possess invariant geometry and include orifice plates and capillary tubes. Orifices [9,26,27] are short flow passages typically operating under turbulent or transitional conditions, whereas capillaries [28–30] are long, narrow tubes designed for laminar flow. Due to the absence of moving parts, fixed restrictors are simple, robust, and highly reliable. They are dimensioned such that a substantial pressure drop occurs at nominal operating flow, enabling effective compensation for clearance variations.

Adjustable restrictors, such as needle valves or throttle valves, allow manual adjustment of flow resistance during system commissioning or maintenance. Once set, they operate as fixed restrictors during normal operation but can be readjusted to accommodate changes in load or manufacturing tolerances. This flexibility is particularly valuable in large-scale bearings where precise machining of identical restrictors is impractical.

Passive self-adjusting restrictors respond automatically to pressure variations. Membrane-based restrictors [31–34] employ an elastic diaphragm that deflects under pressure changes. An increase in recess pressure causes partial closure of the flow path, increasing flow resistance and further elevating pressure, while a pressure decrease results in opening of the passage and increased flow. This self-regulating behavior provides strong compensation without external control.

Active restrictors [35] represent the most advanced class of compensation elements. Their flow characteristics are continuously adjusted using external actuators, such as piezoelectric or electromagnetic devices. By enabling real-time modulation of flow to individual pads, active restrictors allow hydrostatic bearings to adapt dynamically[36–39] to variations in load, speed, or misalignment, thereby maintaining optimal lubricant film conditions.

Hydrostatic bearings are always part of a larger hydraulic circuit, including a pump, accumulator, valves, filters, and piping. The pump provides fluid at the required pressure, the accumulator smooths pressure fluctuations and supplies fluid during temporary load peaks, filters remove contaminants that could damage the bearing or restrictors, and valves control flow direction and magnitude. Piping must minimize pressure losses and maintain system stability. Modern systems often integrate pressure, flow, and temperature sensors to enable real-time active control and diagnostics.

### 2.1.2 Large hydrostatic bearings

Large-diameter hydrostatic bearings necessitate a fundamentally different design philosophy compared with bearings of smaller scale. To classify a bearing as belonging to the large-diameter category, explicit geometric limits must be established; in practice, several engineering constraints naturally delineate this threshold. The sliding surfaces impose stringent requirements on flatness and low roughness, yet conventional machining and subsequent grinding inherently restrict the feasible size of clamped workpieces. Increasing diameter amplifies these manufacturing challenges, as maintaining micro-level precision across meter-scale surfaces becomes progressively more difficult. Transportability provides an additional boundary condition: components such as bearing races would form massive rings whose handling, transport, assembly, and servicing would be logistically prohibitive. Considering these constraints jointly, bearings with diameters on the order of 5 m can be reasonably designated as large-scale units.

At such dimensions, the design paradigm must shift toward segmentation of critical elements. Dividing the bearing slider and the hydrostatic pads into segments improves manufacturability, simplifies transport, and allows targeted maintenance. In the event of surface damage, a single pocket or slider segment can be replaced without dismantling the entire structure. Segmentation, however, introduces a new engineering challenge: maintaining the flatness and geometric continuity of the divided sliding surface, which is essential for preserving stable film thickness and uniform load distribution.

Large-scale hydrostatic bearings also operate under conditions that may fluctuate more substantially than in smaller systems. Variations in ambient temperature induce changes in lubricant viscosity, influencing load capacity and stiffness, while shifts in loading direction or magnitude—arising, for example, from structural movements or repositioning of the supported equipment—modify the pressure distribution within the film. These factors collectively necessitate a design and control approach that explicitly accounts for geometric segmentation, manufacturing tolerances, and variable operating conditions to ensure long-term reliability of large hydrostatic bearing systems.

Applications of hydrostatic bearings are broad, typically where precision, reliability, and high load capacity are required. In machine tools, they are used in spindles and linear guides, allowing micrometer-level precision even under heavy cutting loads. In astronomy, they support large telescopes and antennas, providing extreme stability and vibration suppression. In energy systems they are used in turbine and generator bearings. In aerospace and space applications, hydrostatic bearings are employed in precision gyroscopes, simulators and radar antennas. Bearing surface materials are selected for wear resistance, lubricant compatibility, and thermal conductivity. Traditionally, bronze, copper, or brass alloys are used, often with tin or lead additives to improve adhesion resistance. In modern precision applications, composite materials and ceramic coatings are also employed, combining low friction with high hardness. Shafts are typically hardened and finely ground or polished to ensure a uniform pressure film and minimize micro-vibrations.

The applicability of hydrostatic bearings in machining centers is best illustrated by the progression from precision tables and gantry machines to today’s large-scale systems, where an axis or table travels distances on the order of meters while stable micrometer-level accuracy is required. As machine dimensions increased, conventional rolling guides became a limiting factor due to restricted stiffness, significant vibration transmission, and rising friction. In contrast, hydrostatic guides with a thin oil film made it possible to maintain smooth motion and high load capacity without stick–slip effects, even over long travel lengths. In specific designs, this benefit is evident, for example in linear guides with film thicknesses of only a few micrometers implemented in a high-precision machining center, where stiffness was increased by up to an order of magnitude while simultaneously reducing the overall drive energy demand, without degrading accuracy over long table travels [40].

In large rotary tables of horizontal boring machines, hydrostatic axial and radial bearing surfaces support workpieces weighing tens of tonnes; here, optimization of pocket layout is deliberately aimed at limiting table deflection under eccentric loading and maintaining flatness of the clamping surface over diameters of several meters [41,42]. Complementary numerical and thermo-mechanical analyses of complete machine frames with hydrostatic guides show that bearing behavior cannot be separated from the large-scale structure, as temperature distributions and deformations over meter-long axes strongly affect film thickness uniformity and thus the resulting tool-path accuracy [43].

In turbines and generators, hydrostatic bearings gained importance when increasing shaft lengths and rotor diameters began to impose extreme demands on rotor stability during start-up, low-speed operation, and transient conditions. For machines with shafts on the order of meters in length, it became evident that purely hydrodynamic bearings cannot reliably prevent surface contact at low speeds while maintaining a uniform film thickness over the entire bearing segment. Hydrostatic support makes it possible to generate a consistent pressure cushion independent of rotor speed, thereby stabilizing massive shafts at moments when their dynamic behavior is most sensitive. Analysis of large axial thrust bearings in steam turbines shows that an auxiliary hydrostatic mode significantly suppresses torsional and bending vibrations, which otherwise accumulate in long rotors and may lead to unwanted contact [44]. In hydraulic turbines with rotor diameters exceeding several meters, pressure uniformity within the pocket system plays a decisive role, as pressure inhomogeneity in the axial bearing can induce tilting of the entire shaft assembly; numerical simulations and experimental measurements demonstrate that optimized oil supply to individual pads reduces thermal imbalance and uneven wear on large sliding surfaces [45].

In antenna and radar systems, hydrostatic bearings began to be adopted when increasing diameters of rotating platforms and supporting structures—commonly reaching meter-scale dimensions—simultaneously required high load capacity, extremely fine motion control, and minimal vibration generation. Deep Space Network (DSN) 64 m [46,47] antennas (later upgraded to 70 m [48]) use an azimuth hydrostatic thrust bearing: 3 rectangular pads each with 6 recesses, mounted via a self-aligning spherical joint. The supply system is designed for high pressures (pump capability up to 27.58 MPa) and film thickness over 127 μm level. In practice, these constraints translate into a clear operational requirement for deep-space antennas: maintain oil temperature/viscosity control, preserve runner flatness (shim control), and manage incremental mass additions of new instruments with pressure measurement.

In the development of large optical telescopes, hydrostatic bearings appear once the diameter of the primary mirror and the size of the supporting structure reach tens of meters and conventional rolling supports become insufficient in terms of both stiffness and motion controllability. In the Giant Magellan Telescope (GMT), hydrostatic axil (Figure 7) and radial segments support the alt-azimuth mount with a total mass on the order of thousands of tons; during sky tracking, the structure moves on an oil film approximately 50 μm thick, enabling smooth motion and pointing accuracy at the arcsecond level even under significant eccentric loading and seismic excitation [49].

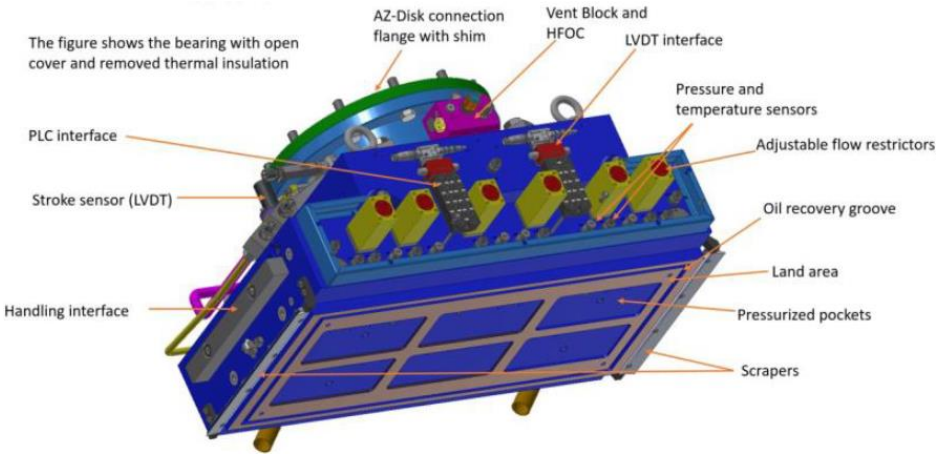


Figure 7 GMT hydrostatic pad [49].

A similar philosophy, realized in a concrete implementation, can be observed in the Very Large Telescope (VLT): its main axes are supported by hydrostatic bearings that allow rotation of the entire structure on an oil film ten of micrometers thick. The third stage of this evolution is represented by ESO's Extremely Large Telescope (ELT), whose azimuth axis is supported on a system of concentric circular tracks with diameters of approximately 51 m, 34 m, and 6 m, together with a radial guide; all of these tracks employ hydrostatic oil bearings (Figure 8) to allow the exceptionally large structure to deform in a controlled manner while retaining the required stiffness and smooth motion during tracking [50].

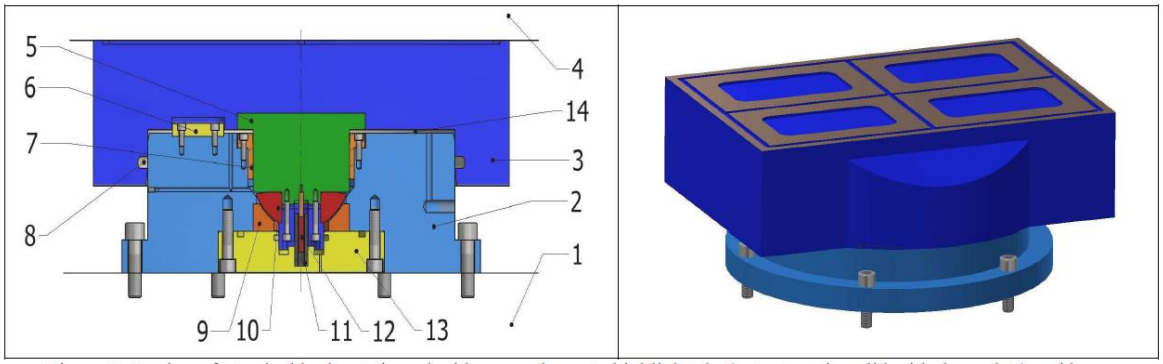


Figure 8. Section of a typical hydrostatic pad with some elements highlighted: 1) structure in solid with the pad, 2) pad base, 3) pad body with the oil pockets, 4) track, 5) central shaft, 7) bush, 8) seal, 9-10) spherical joint, 11-12) LVDT transducer, 13) cover, 14) oil rear chamber.

Figure 8 ELT hydrostatic pad scheme: [50].

Across all these domains, the adoption of hydrostatic bearings reflects a common set of functional requirements: high stiffness, excellent damping, minimal friction at wide range of speeds, and the absence of wear. Although the specific operating parameters vary widely between applications (Table 1), the underlying motivation remains the need for precise, stable, and durable support of critical machine elements.

Table 1 Examples of the largest hydrostatic bearings (azimuth bearings):

| **Application** | **Dimension (outer diameter)** | **Film thickness** | **Total flow** | **Recess pressure** |
|---|---|---|---|---|
| ELT | 52 m (3 tracks) [50] | - | 720 l/min [50] | - |
| VLT | ≈ 20 m | - | - | - |
| GMT | 21.2 m [49] | 65 - 70 um [51,52] | 276 l/min [52] | 3.5 MPa [52] |
| 64-meter antenna | 24.49 m [46] | 127 – 254 um [46] | 545.4 l/min [46] | 6.21 MPa [47] |
| 70-meter antenna | 24.49 m [48] | 127 – 250 um [48] | 594 l/min [48] | 10 MPa [48] |

## 2.2 Safety of lubrication film

The operational safety of hydrostatic bearings is governed by the integrity of the externally pressurized lubricating film. For large-scale bearings, the admissible operating range is defined not only by the nominal film thickness, but by its spatial distribution under realistic combinations of load, temperature, geometric errors and hydraulic disturbances. Each of these alters the local pressure field and thus the minimum film thickness, potentially driving parts of the contact towards critical contact conditions.

### 2.2.1 Lubrication-related failures

Failures associated with lubrication occur when the bearing is unable to sustain a continuous, sufficiently thick, and spatially uniform fluid film. Under such conditions, the fundamental separation between sliding surfaces is compromised, making the system sensitive to hydraulic, thermal, and contamination effects.

Material degradation may result from erosive action [53] caused by high-speed lubricant flow in narrow gaps, around recess boundaries, or within restrictors. Sustained high shear rates and localized turbulent jets progressively remove material, increase effective clearances, and distort the intended pressure field, thereby diminishing the bearing's load-carrying capability. When the lubricant contains solid contaminants, abrasive particles intensify erosion and may damage restrictor geometries, further destabilizing flow control and film formation. Hydrostatic bearings depend on accurately calibrated flow-control components to preserve pressure balance; even partial obstruction can induce asymmetric pressure distributions, localized film breakdown, and intermittent solid contact, rapidly degrading the bearing surfaces. Such blockages are commonly linked to particulate contamination, or lubricant ageing.

Thermal instability represents an additional failure pathway [54]. Excessive lubricant heating—caused by insufficient cooling, high shear in extremely small clearances, or externally imposed thermal loads—reduces viscosity and directly lowers film thickness (Figure 9). This may initiate thermal runaway, in which viscosity loss leads to further thinning of the film and increased heat generation, potentially culminating in complete film collapse if corrective measures are not implemented.

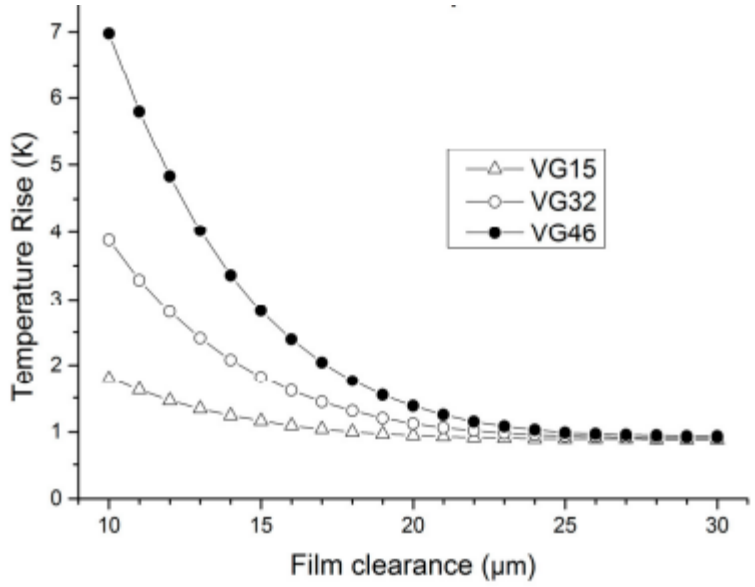


Figure 9 Change of oil film height with temperature for selected lubricants [54].

Among the most critical hazards is interruption of lubricant supply due to pump malfunction, cavitation, air entrainment, or pressure losses from leakage. Because hydrostatic bearings rely entirely on externally pressurized fluid to maintain separation, even brief supply disruptions can cause immediate surface contact, resulting in severe scoring, plastic deformation, or catastrophic seizure. In multi-pad configurations supplied from a common source, a localized supply failure may propagate instability throughout the entire bearing system.

### 2.2.2 Design-related failures

Failures attributable to design [55] arise either from inappropriate assumptions made at the early stages of development or from deviations between the intended and the realized geometry, materials, or assembly conditions of the bearing, even when the design documentation itself is formally correct. Such discrepancies may result in uneven pressure fields, misalignment, increased losses [56], or direct interaction between opposing sliding surfaces. The design of a hydrostatic bearing inherently requires consideration of elevated energy losses arising from lubricant flow through very thin clearances, as well as the continuous need to supply pressurised lubricant to the bearing interface.

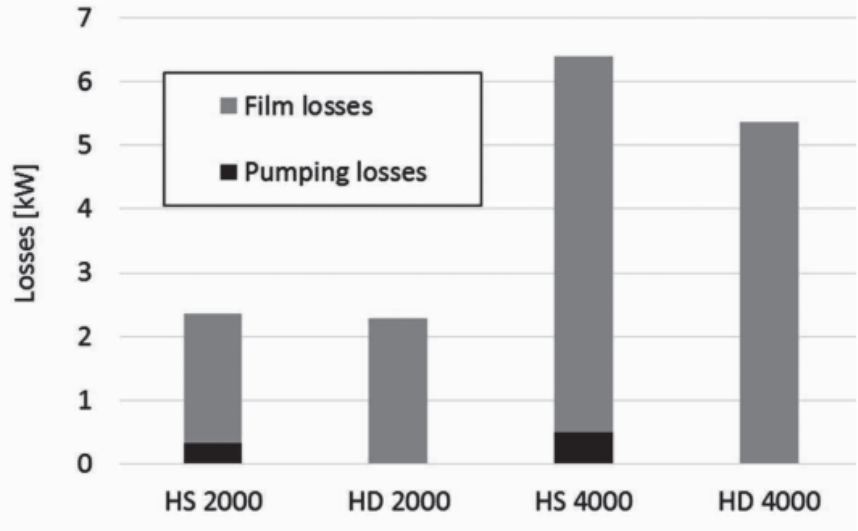


Figure 10 Comparison of losses in HS and HDf bearings at different rpms [56].

Errors in machining of recesses, pads, or the bearing slider can disturb lubricant flow paths and diminish bearing stiffness. Likewise, incorrect installation of pads or bearing surfaces may introduce local steps, alter recess geometry, or change the nominal clearance, leading to non-uniform load distribution and contact in locally overloaded zones. Differences in segment height, commonly referred to as offset, represent a significant geometric error in large-scale applications and must be explicitly considered in the design. To avoid direct surface contact, this deviation must be evaluated relative to the nominal thickness of the lubricating film, as the ratio [57] between the two governs the risk of film thinning (Figure 11).

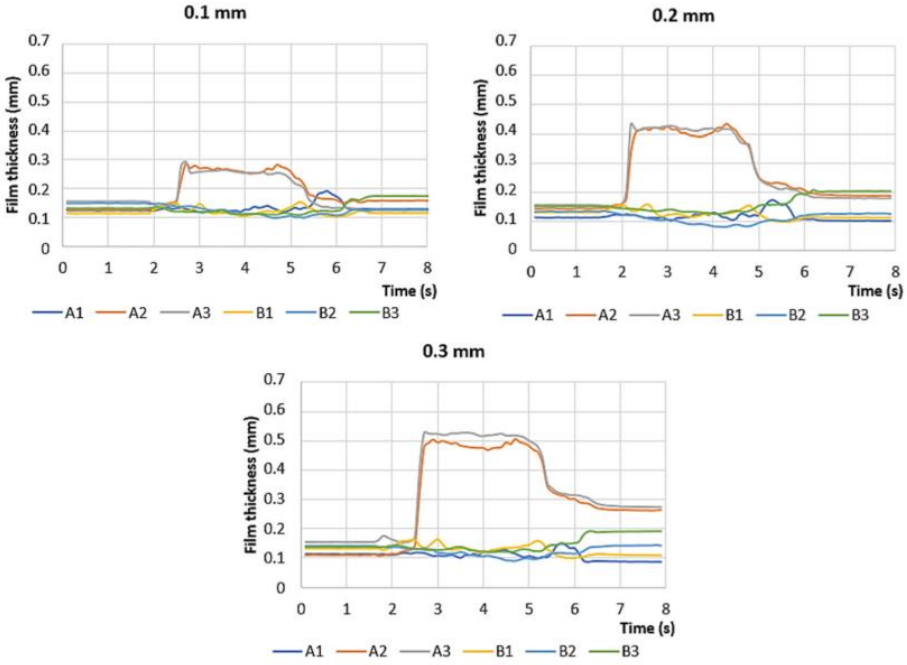


Figure 11 Film thickness distribution for step-up error [57].

Surface quality represents a particularly sensitive parameter. To achieve the designed film thickness and pressure distribution, hydrostatic bearings rely on surfaces [58–60] that are highly planar, smooth, and dimensionally stable. Deviations in the form of waviness, excessive roughness, or geometric inaccuracies [61] can generate localized pressure maxima (Figure 12), trigger collapse of the lubricating film, or induce instability under dynamic loading.

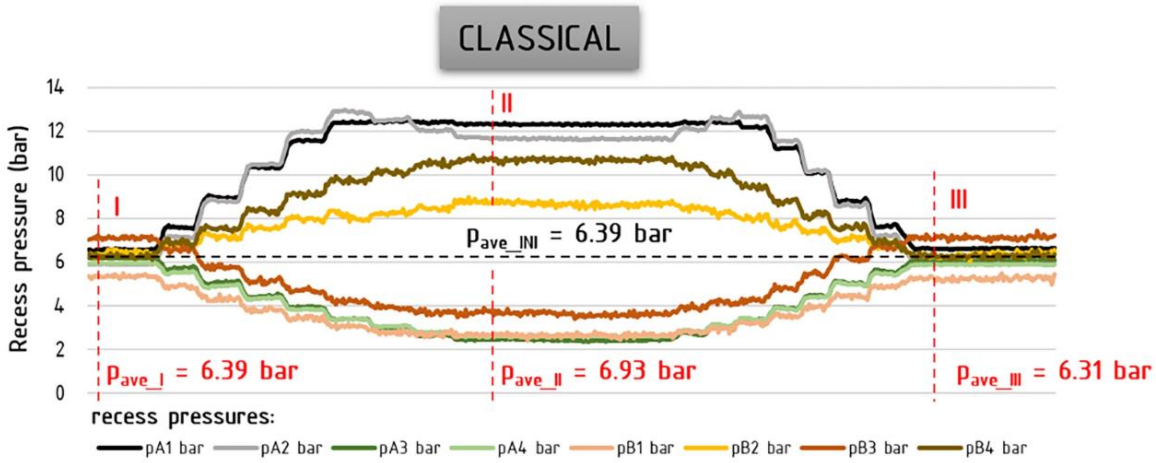


Figure 12 Recess pressure distribution during bearing overload (II.) [61].

Even small departures from straightness [62] or parallelism of the bearing lands shifts the pressure distribution (Figure 13) and therefore decreasing precision of carried object. The models of rough surfaces demonstrate that surface topography modifies both static capacity and dynamic stiffness; circumferential roughness can enhance stiffness, whereas radial roughness tends to reduce it [63,64]. Another work on topography confirms that neglecting realistic surface statistics can introduce errors exceeding 10 % in predicted load capacity [65]. From the perspective of safety, the manufacturing tolerance on flatness and waviness must therefore be chosen such that peak-to-valley deviations remain well below the minimum film thickness expected under the most adverse load and temperature conditions.

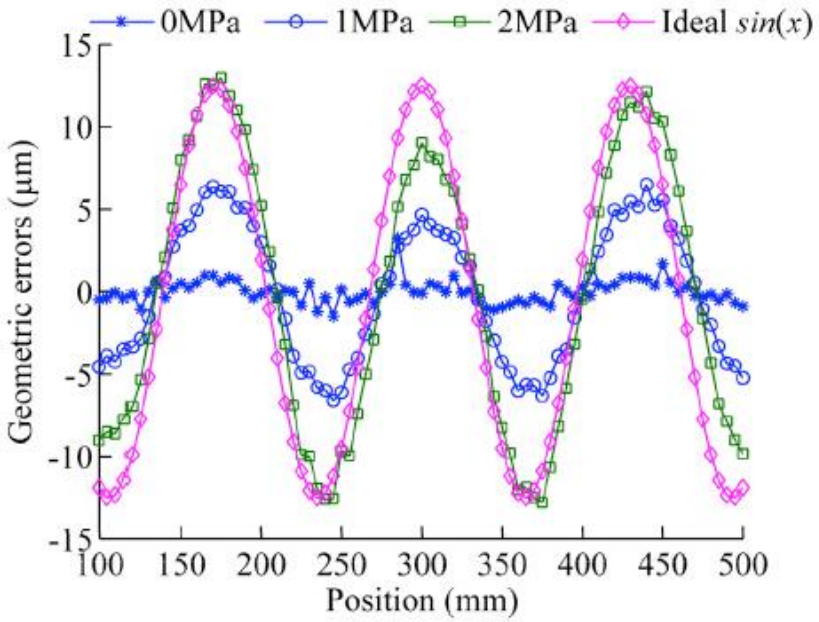


Figure 13 Results of the geometric errors of guide rail under different pressure [62].

Asymmetrical loading is inherent to many large hydrostatic bearings, for example in machine tool rotary tables, telescope mounts or repair turntables, where the resultant load does not remain at the geometric center. Under such conditions the lubricant tends to flow towards the least resistant path, i.e. towards unloaded pockets, which can lead to starvation in heavily loaded recesses. Load asymmetry, originating from inadequate structural support, unexpected shaft bending [66], or uneven mass distribution, can further amplify variations in flow and therefore in the film thickness. When such asymmetry coincides with unequal restrictor behaviour or geometric imperfections, it may cause pad tilting, partial loss of the lubricating film, or intermittent solid contact. In large bearings carrying massive rotating components, these effects can spread through the system and manifest as unstable vibrations or severe damage.

To further increase safety margins, actively controlled restrictors have been proposed. Servo-valve-based gap control and membrane-type active restrictors are capable of adjusting recess pressure (Figure 14) or flow in real time based on film thickness or pressure feedback [67], thereby compensating for asymmetrical loading and dynamic disturbances [68]. The design of control laws and feedback loops must therefore explicitly consider robustness against sensor noise and ensure that no excitation of self-oscillations in the film occurs, which could otherwise accelerate film collapse instead of preventing it.

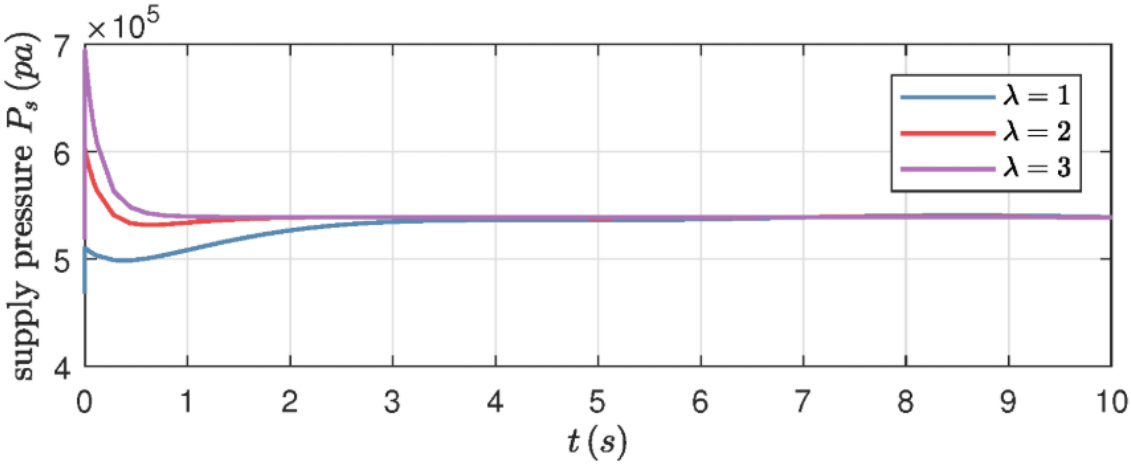


Figure 14 Influence of convergence rate on pressure feedback [67].

Another major contributor to design-related failure is deformation [69] of bearing components. Elastic compliance in the housing [70], pad supports, or the surrounding machine structure can cause the recess geometry to change under load [71], thereby altering the film thickness, and reducing stiffness (Figure 15). Thermal deformation produces analogous consequences [72,73], particularly in large-scale or high-speed applications where temperature gradients distort bearing lubricant, resulting in misalignment and degraded performance. With prolonged operation, accumulated mechanical and thermal deformations may displace the operating point sufficiently from its nominal condition to provoke instability, oscillatory behavior, or recurring contact events.

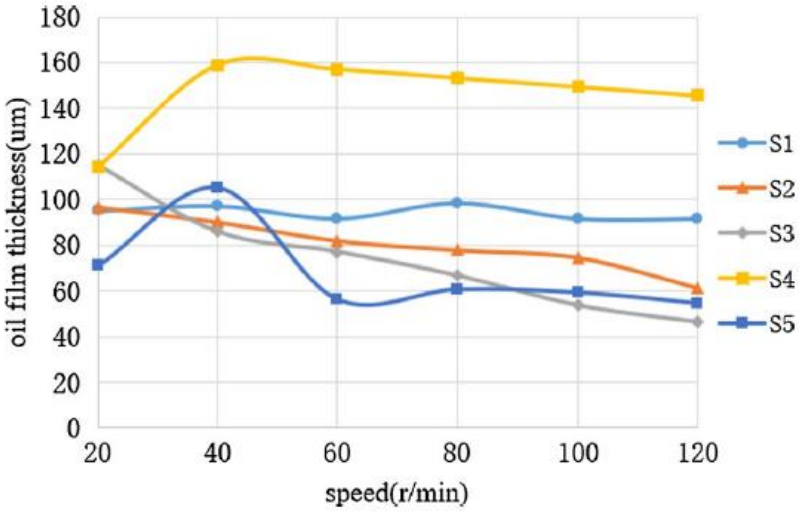


Figure 15 Film thickness distribution across pad for different rotational speeds [71].

Errors in material selection often stem from the implicit assumption of continuous full-film lubrication. This premise becomes critical during abnormal conditions such as loss of oil supply, when transient solid contact dominates the damage mechanism [74]. Benchmark tests under oil-starvation conditions have shown (Figure 16) that galvanized steel exhibits the most severe wear due to rapid removal of its protective coating, while structural steel and aluminium bronze are also unfavourable because of their combined wear, frictional, and thermal characteristics. From a safety-oriented design perspective, pairing structural steel with tin-based materials or PTFE offers superior robustness, as these combinations demonstrate low friction and limited heat generation, thereby mitigating the risk of scuffing during emergency operation.

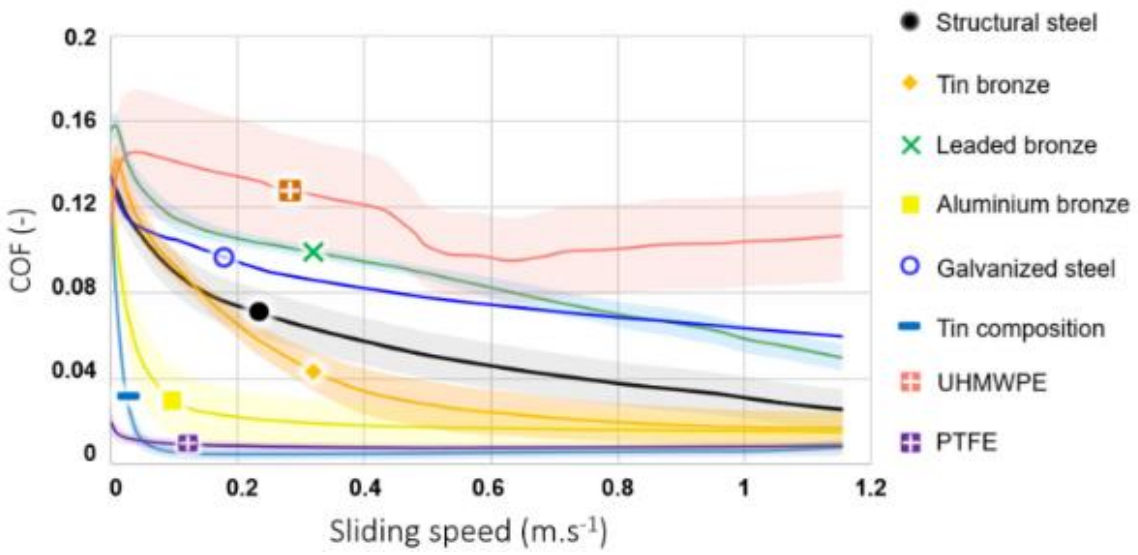


Figure 16 COF change with sliding speed of observed materials [74].

If extremely high stiffness and positioning accuracy are not required, compliant elements beneath the pads or within the pad structure can be introduced. Rubber or elastomeric blocks or engineered compliant supports allow the individual pads or pockets to tilt and adapt to local geometric imperfections, thereby redistributing pressure (Figure 17) and preventing local film collapse [75,76]. Experimental evidence indicates that compliant support can increase tolerable misalignment by several multiples compared with rigid supports, while maintaining sufficient load capacity for many large-scale applications [77]. The residual risk lies in the long-term stability and ageing of compliant materials and the potential for increased low-frequency deformations under varying loads, which must be addressed by appropriate material choice and periodic inspection.

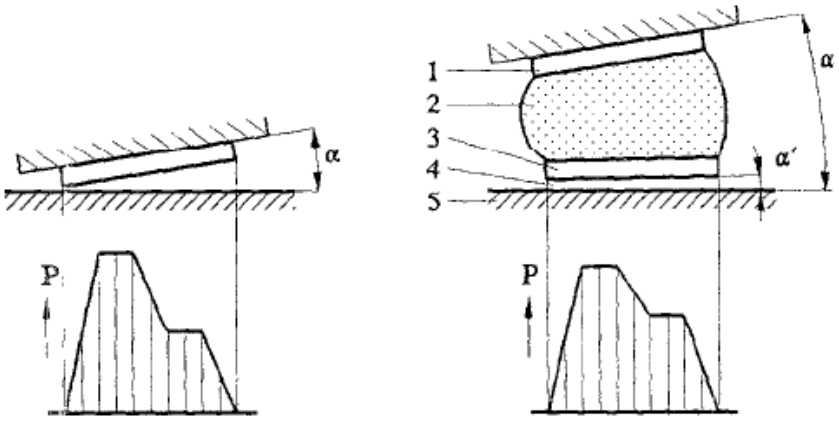


Figure 17 Rigid (left) versus comliant (right) bearing system: recess pressure influence comparison [75].

Finally, component replaceability should be addressed during the design phase. From the standpoint of material selection, assigning the softer material to the more easily replaceable part—typically the bearing pad—is advantageous. In the event of accidental contact, this approach minimizes repair costs and often simplifies maintenance by enabling replacement of the damaged pad rather than the more complex counter face.

# 3 ANALYSIS AND CONCLUSION OF LITERATURE REVIEW

Large-scale hydrostatic bearings constitute a distinct category of tribological systems whose principal advantage lies in their ability to support extremely high loads with negligible friction, including operation at zero or near-zero relative speed. This decoupling of load capacity from kinematic conditions enables applications that are unattainable with rolling or purely hydrodynamic bearings. At the same time, as bearing diameters increase to the order of tens of meters, the operating margin that guarantees safe separation of sliding surfaces becomes progressively smaller relative to geometric, hydraulic, and thermal disturbances. In such systems, safety can no longer be considered an automatic consequence of conventional design rules but must be treated as an explicit and primary design objective.

The realization of large hydrostatic bearings is inherently constrained by manufacturing precision, transportability, assembly, and serviceability. These constraints necessitate segmentation of bearing sliders, pads, and tracks, transforming otherwise continuous sliding surfaces into assemblies composed of multiple discrete elements [6]. While segmentation enables practical realization of large diameters, it introduces a fundamental safety challenge: the uniformity of the lubricating film can no longer be ensured solely by geometry. Each interface between segments represents a potential source of height offset, angular misalignment, or localized deformation. When compared with typical lubricating film thicknesses in large bearings—commonly on the order of several tens to a few hundreds of micrometres [46,47,50,52]—even small deviations may locally reduce the film to values approaching direct surface contact. Although such geometric imperfections are widely acknowledged in the literature [58–60,62], they are predominantly discussed in relation to stiffness reduction or positioning accuracy, rather than as direct safety risks governed by minimum film thickness.

To mitigate manufacturing and assembly inaccuracies, existing research has primarily focused on compensation strategies. Approaches relies on hydraulic compensation through restrictor design, pressure equalization, and, more recently, active control concepts [22,36,67,68]. These solutions aim to redistribute pressure and flow to reduce the influence of uneven loading and clearance variations. Under nominal conditions, such systems improve robustness against moderate disturbances. However, most studies implicitly assume ideal restrictor behaviour and uninterrupted lubricant supply. In practical large-scale applications, simple fixed restrictors—such as capillaries or orifices—are often preferred due to their simplicity and reliability, yet they are highly sensitive to contamination, lubricant degradation, and manufacturing tolerances. Partial or complete blockage can rapidly disturb pressure balance, leading to asymmetric film thinning and localized loss of separation.

While contamination and erosion effects are discussed in the context of lubrication-related failures [53], their impact on safety margins in segmented, large-diameter bearings is rarely examined in detail.

Another compensation strategy introduces mechanical compliance into the bearing system, most commonly through compliant pad supports [75–77]. Such solutions allow pads to adjust their orientation under load, increasing tolerance to misalignment and reducing local pressure concentrations. From a safety perspective, compliant supports expand the allowable range of geometric deviations. However, this benefit is achieved at the expense of reduced stiffness, long-term stability concerns related to material ageing, and increased susceptibility to low-frequency deformation. As a result, compliant solutions are unsuitable for applications where high stiffness and positional accuracy are required, such as precision machine tools, large telescopes, and antenna systems. For these rigid and safety-critical applications, compliance does not provide a generally acceptable solution.

Across the reviewed literature, lubricating film thickness is most often treated as a secondary parameter. It is commonly used to assess stiffness, damping, or load capacity [31,63]. While such approaches are sufficient for performance analysis, they do not fully reflect the role of film thickness in ensuring surface separation. From a safety standpoint, the minimum local film thickness determines the risk of direct contact. Design-related errors such as offset, waviness, and misalignment are frequently assessed using tolerance limits or pressure distributions, yet the direct relationship between these errors, the resulting distribution of film thickness, and proximity to contact conditions is seldom addressed. This limitation is particularly significant in large-scale bearings, where average values provide little information about local minima that control failure initiation.

Similarly, diagnostic strategies for hydrostatic bearings have historically emphasized hydraulic parameters such as pressure, flow rate, and temperature. While these quantities are essential for monitoring system operation, they provide only indirect information about the actual state of surface separation. Lubricating film thickness is typically estimated rather than measured. As a result, early-stage degradation processes—such as partial restrictor blockage, evolving geometric errors, or localized deformation—may remain undetected until the bearing approaches a critical condition. In large bearings supporting massive structures, even short contact events can cause severe and irreversible damage, highlighting the limitations of diagnostics that do not directly address film integrity.

**Knowledge gap:** Despite extensive research on the design, compensation, and optimization of large-scale hydrostatic bearings, the literature lacks a safety-oriented approach in which lubricating film thickness is treated as the primary governing parameter. There is a lack of experimentally supported methods that directly connect pad alignment, manufacturing and assembly errors, and fault scenarios—such as restrictor blockage—with the distribution and minimum value of the lubricating film. This gap is most evident in rigid, segmented bearings, where existing approaches rely on performance metrics rather than experimentally supported approaches that directly relate geometric and hydraulic disturbances to local minima and distribution of lubricating film thickness as indicators of safety-critical conditions.

# 4 AIMS OF THE THESIS

The main aim of this dissertation is to analyse and experimentally assess the influence of geometric imperfections, hydraulic disturbances, and operating conditions on the minimum lubricating film thickness in large-scale hydrostatic bearings, and to establish lubricating film thickness and its distribution as safety-relevant parameters for evaluating proximity to surface contact in rigid, segmented hydrostatic bearings.

To support this main aim, the following sub-objectives were defined:

- Assess the safety of the lubricating film in multi-recess hydrostatic bearings under non-ideal conditions, including hydraulic faults and geometric inaccuracies.
- Investigate the capability of large hydrostatic bearings to maintain a continuous lubricating film when local disturbances occur.
- Evaluate methods for achieving and verifying uniform lubricating film thickness distribution in real bearing installations.
- Examine the applicability of non-contact diagnostic and alignment techniques as tools for improving safety margins of hydrostatic bearings in practical operation.

## 4.1 Scientific questions and hypotheses

*Q1: How can optical methods increase the safety of large-scale hydrostatic bearings by enabling assessment and improvement of lubricating film thickness distribution under real operating conditions?*

*H1:* Optical non-contact measurement methods enable reliable determination of the distribution and minimum value of lubricating film thickness in large-scale hydrostatic bearings under real operating conditions where direct access or permanent installation of contact or embedded sensors is not feasible. The achievable accuracy, resolution, and repeatability of optical measurements are sufficient for safety-relevant diagnostics of the lubricating film, allowing identification of critical film thinning that governs the risk of surface contact and lubrication failure [22,23,55].

*H2:* Optical alignment method could have more accurate initial positioning of hydrostatic bearing pads in rigid, segmented bearings than conventional mechanical or pressure-based alignment techniques [46]. Higher alignment accuracy influences the resulting lubricating film thickness distribution, which could lead to increased uniformity and higher minimum film thickness values. By reducing the extent to which the bearing compensates geometric errors [58,62] through film thinning, optical alignment methods could increase the safety margin against local film collapse.

*Q2: How does restrictor failure affect the lubricating film thickness in multi-recess hydrostatic bearings?*

*H3:* If a capillary restrictor in a multi-recess hydrostatic bearing designed for nominal operating conditions becomes partially or fully blocked, the resulting change in flow distribution causes a measurable reduction in recess pressure and local lubricating film thickness in the affected recess [29,30,78]. This reduction can be experimentally detected through film thickness measurement and leads to a significant decrease in local load-carrying capacity, representing a safety-critical condition.

## 4.2 Thesis layout

The dissertation is structured as a sequence of three peer-reviewed journal papers that collectively address safety-relevant aspects of lubricating film behavior in large-scale hydrostatic bearings.

The first paper (**Paper 1**) is devoted to the development of a contactless method for measuring lubricating film thickness in hydrostatic bearings. The study introduces an optical point tracking approach that enables film thickness evaluation without mechanical interaction with bearing components and without the need for permanently installed sensors. The method is experimentally validated on a dedicated test rig and compared with analytical predictions and conventional proximity sensor measurements. Emphasis is placed on applicability in large-scale bearings, where access limitations and system complexity often restrict the use of traditional measurement techniques. This work establishes a practical basis for assessing lubricating film thickness as a safety-relevant parameter under real operating conditions. *[Q1; H1]*

The second paper (**Paper 2**) addresses the problem of pad alignment in large-scale, segmented hydrostatic bearings. Three alignment approaches—conventional mechanical leveling, pressure-based alignment, and optical coordinate measurement—are experimentally compared using a test rig with independently adjustable pads. The study examines how the choice of alignment method influences pad geometry, pressure distribution, and lubricating film thickness. Attention is given to alignment strategies that preserve bearing stiffness and geometric precision without relying on compliant support elements, which are commonly employed to absorb assembly inaccuracies. The results provide insight into the role of precise pad positioning in achieving a uniform lubricating film thickness distribution in rigid bearing systems. *[Q1; H2]*

The third paper (**Paper 3**) focuses on the behavior of a large hydrostatic bearing system under operating conditions representative of real installations. Using the hydrostatic bearing of the Very Large Telescope as a case study, the work examines the consequences of uneven or reduced lubricating film thickness and the associated risk of contact between sliding surfaces. The study compares conventional static measurement techniques with contactless sensing methods and investigates bearing response during simulated fault conditions, including disturbances in lubricant supply. This paper demonstrates the practical implications of lubricating film degradation in large-scale applications and highlights the importance of diagnostic and assembly-related considerations addressed in the preceding studies. *[Q2; H3]*

Taken together, the three articles form a coherent investigation of lubricating film safety in large-scale hydrostatic bearings. The dissertation structure reflects progression from development of suitable diagnostic tools, through evaluation of assembly-related influences, to analysis of bearing behavior under critical operating scenarios encountered in real systems.

**Paper 1**


MICHALEC, M., J. HURNÍK, J. FOLTÝN and P. SVOBODA. Contactless measurement of hydrostatic bearing lubricating film using optical point tracking method. *Proceedings of the Institution of Mechanical Engineers Part J-Journal of En*, 2023, vol. 237, no. 1, p. 76-84.

*[AIS Q3; Author's contribution 30 %]*

**Paper 2**


FOLTÝN, J., J. HURNÍK, M. MICHALEC, P. SVOBODA, I. KŘUPKA and M. HARTL. Pad Alignment Methods and Their Impact on Large Hydrostatic Bearing Precision. *Machines*, 2024, 12, 549

*[AIS Q2; Author's contribution 60 %]*

**Paper 3**

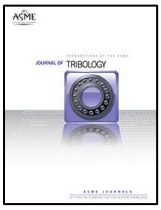


FOLTÝN, J., E. FLORES, M. TAPIA, N. ÁLVAREZ, M. MICHALEC and P. SVOBODA. Failure prevention procedure of the Very Large Telescope hydrostatic bearing pads based on lubricating film thickness measurement. *ASME. J. Tribol*, 2025, vol. 147.

*[AIS Q2; Author's contribution 60 %]*

# 5 MATERIALS AND METHODS

To address the scientific questions outlined in the previous chapter, it was necessary to establish a solid experimental framework and define the methods employed. These activities and their interrelations are illustrated in the schematic diagram (Figure 18).

| | | | |
|---|---|---|---|
| **Objective** | Film thickness measurement | Alignment | Safety procedure |
| **Device** | *2PAD* 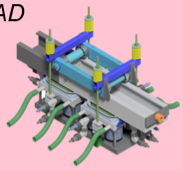 | *2PAD* 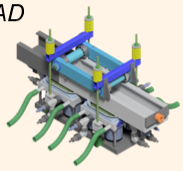 | *VLT* 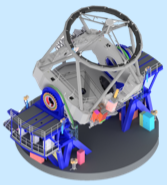 |
| **Methods** | Contact sensors<br>Optical method (OPT)<br>Prediction | Conventional gauges<br>Pressure method<br>Optical method (OCM) | Contact sensors<br>Non-contact sensors<br>Prediction |
| **Output** | Method of contactless film thickness measurement | Effect of alignment on film thickness distribution | Safety procedure for real bearing |
| | Paper 1<br>Q1 H1 | Paper 2<br>Q1 H2 | Paper 3<br>Q2 H3 |

Figure 18 Schematic representation of connection between methods and results.

The specific experimental objects, measurement systems, and analytical procedures are described in detail in the following chapter. This includes the design of the test rig, sensor selection and placement, data acquisition methods, and the processing of the collected data.

## 5.1 Experimental objects

Laboratory tests were carried out using a custom-designed test rig known as the Dual-Pad Experimental Hydrostatic Bearing (2PAD). This setup allowed for controlled testing of hydrostatic bearing behavior under various operating conditions, including different levels of pad misalignment, supply pressure, and restrictor settings. The test rig was equipped with a range of sensors to monitor film thickness, pressure distribution, flow rate, and temperature. The experimental setup enabled the simulation of bearing behavior in a simplified but representative environment, allowing for precise control and repeatability of test conditions.

Complementing the laboratory experiments, field measurements were performed under real operating conditions on the hydrostatic bearing system of the Very Large Telescope (VLT), located at the Paranal Observatory in Chile. The observatory is operated by the European Southern Observatory (ESO). These real-world measurements aimed to validate the laboratory findings and assess the performance of hydrostatic bearings in a full-scale astronomical application, considering environmental influences, operational loads, and long-term performance factors.

### 5.1.1 Experimental hydrostatic bearing

The so-called 2PAD device is a two-pad hydrostatic bearing developed in the laboratories of the Institute of Machine and Industrial Design. It is a linear bearing consisting of two independent pads arranged in series. The main components of the device are shown in Figure 19. The system includes a split runner, on which a loading frame rests. Using threaded rods, it is possible to apply a controlled load to the bearing pads. Each pad is freely adjustable in space, allowing simulation of typical assembly errors such as parallel offset (misalignment) and angular tilt. The adjustment is realized through four threaded support columns positioned at the corners of each pad. These supports can be replaced with compliant mounts (silent blocks) to evaluate the effect of flexible support structures. Due to the split design of the runner, artificial misalignments can also be introduced directly onto the runner itself. The experimental setup is equipped with an integrated sensor system that enables real-time measurement of load, lubricating film thickness, flow rate, pressure in the pads, and lubricant temperature at critical locations. The load is monitored using four strain gauge sensors, each with a maximum capacity of 10 kN and an accuracy of 2.5 N. The lubricating film thickness is measured by non-contact inductive displacement sensors with a resolution of 0.01 mm, calibrated at a nominal distance of 3 mm from the runner surface. Each pad is instrumented with three such sensors located near the corners, which is the minimum required to reconstruct the pad’s geometric plane. The lubricant temperature is measured using thermocouples placed at two key locations: at the outlet and inside the pad. The lubricant used in all laboratory experiments was mineral oil of ISO VG 46 grade. Additionally, both the ambient temperature and the temperature of the runner are recorded. The pressure in each pad is measured using pressure sensors with an accuracy of 0.5 bar. The flow rate of the lubricant is measured by a flow meter with an accuracy of 0.2 L/min.

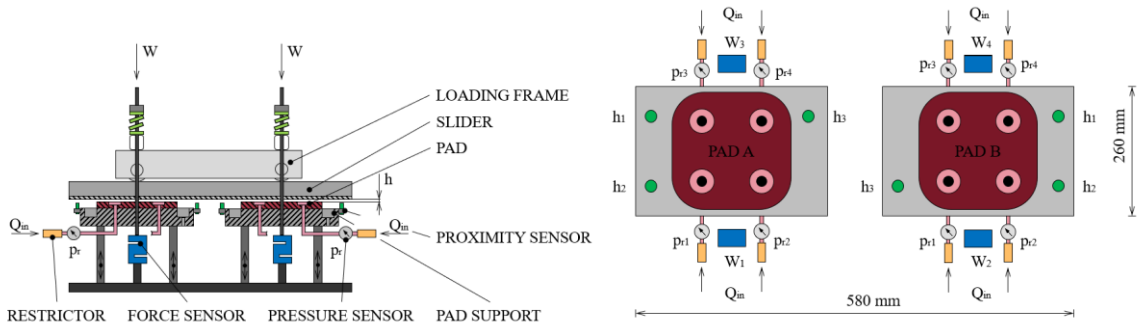


Figure 19 Scheme of laboratory device 2-PAD.

The hydrostatic bearing pad was designed with a four-recess configuration, where each recess has a circular geometry. The inlet to each recess is equipped with a throttle valve restrictor, ensuring mutual independence of the cells in terms of pressure distribution and flow behavior. The pressure loss generated by the throttle valve can be manually adjusted using a set screw, which alters the position of the internal slide element. This adjustment changes the flow area within the restrictor, thereby modifying the resulting pressure drop across the inlet. An integral part of the experimental setup is the hydraulic power unit, which ensures a continuous supply of pressurized lubricant to the bearing contact. Lubricant delivery is provided by a single gear pump, which necessitates the use of restrictors to distribute the flow evenly among the individual bearing recesses. To protect the sliding surfaces in the event of a lubricant supply failure, the system is equipped with a diaphragm accumulator. The hydraulic circuit includes a safety valve, which prevents overpressure by diverting excess fluid back to the reservoir if the system pressure exceeds a safe threshold. Since the lubricant exits the bearing cells to the atmosphere—where it may become contaminated—a filter is incorporated into the system to maintain fluid cleanliness. Lubricant cooling is handled passively through the reservoir walls, as the setup was designed for short-duration tests where significant lubricant heating was not expected. All outputs from the bearing sensors and the hydraulic system sensors were recorded using LabView software.

### 5.1.2 Very Large Telescope hydrostatic bearing system

The weight of the telescope was supported exclusively by hydrostatic bearings, which provide rotation, tilting, and centering of the telescope's main axes. Telescope azimuthal rotation was achieved using 16 axial hydrostatic pads. These pads operated against a track composed of two concentric rings (Figure 20), with 8 pads running on each ring. The total load transferred through the bearing system exceeded 500 tons.

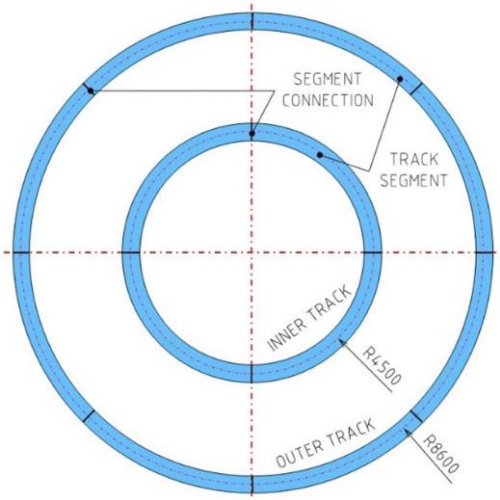


Figure 20 Scheme of azimuth hydrostatic bearing track rings with dimensions [79].

The testing focused on the axial hydrostatic pads of the outer, 20-meter-diameter ring. The pads used in the experiments are square-shaped, each containing four square recesses. A capillary-type restrictor was installed upstream of each recess to regulate the oil flow. Each pad was equipped with a pressure sensor placed in one of the recesses, and flow rate monitoring was possible via the flowmeter located in main line of the hydraulic system. Lubricating film thickness was measured twice per year using digital dial gauges.

## 5.2 Design of experiments and methodology

**Analytical Prediction of Bearing Parameters**

Prior to experimental measurements, analytical prediction of lubricating film thickness and recess pressure was performed to establish reference values and to determine the required measurement resolution. The analytical model was based on classical hydrostatic lubrication theory for multi-recess thrust pads [24]. The predicted flow $Q$ was calculated as a function of film thickness $h$, dynamic viscosity $\mu$, projected pad area $A_p$, applied load $W$, and geometry-dependent flow coefficient $q_f$.

$$Q = q_f \cdot \left(\frac{W}{A_p}\right) \cdot \frac{h^3}{\mu} \tag{1}$$

Carry capacity (W) was predicted from the recess pressure $p_r$ and pad geometry using pressure coefficient $p_f$ obtained from established design charts [19,24].

$$W = p_f \cdot A_p \cdot p_r \tag{2}$$

These calculations assumed rigid bearing surfaces, laminar flow, and constant lubricant temperature. The predicted values were used to assess whether the measured film thickness remained within a safe operating range.

**Film thickness measurement using optical point tracking method (OPT)**

In laboratory experiment, a fully contactless optical point tracking method was applied to measure lubricating film thickness (Figure 21). Circular targets with a diameter of 3 mm were attached to the bearing pad and slider surfaces using adhesive. A monocular monochromatic camera equipped with a fixed focal-length lens was positioned on a rigid tripod to observe the targets. Illumination was provided by a high-power LED light source to ensure sufficient image contrast. Camera calibration was performed using a planar checkerboard target to determine intrinsic camera parameters and lens distortion. The pixel-to-length conversion factor was obtained by imaging the calibration target in the measurement plane.

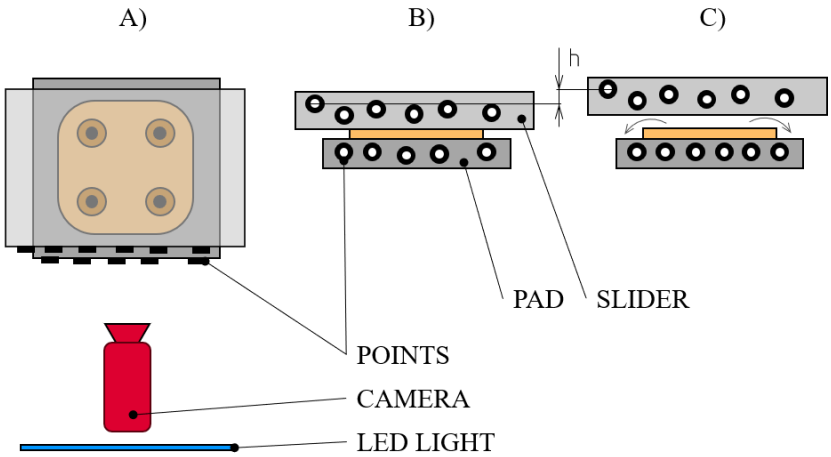


Figure 21 Scheme of OPT method: A) Measurement setup; B) Nominal position (no pressure); C) Film thickness measurement as difference from nominal state.

During the experiment, image sequences were recorded before and after pressurization of the bearing. The circular targets were detected with sub-pixel accuracy using ellipse fitting algorithms [80]. Rigid-body transformations describing translation and rotation of the pad and slider were calculated from the tracked target positions. The relative displacement between pad and slider in the direction normal to the bearing surface was interpreted as the lubricating film thickness. The method enabled measurement at multiple virtual probe locations corresponding to the positions of proximity sensors, allowing direct comparison between optical and contact-based measurements.

### Pad Alignment Based on Recess Pressure (Pressure Method)

The pressure-based alignment method relies on the assumption that uniform lubricating film thickness across a hydrostatic bearing pad corresponds to uniform pressure distribution in its recesses, provided that the lubricant flow rate to each recess is equal. In this approach, each recess inlet was equipped with a pressure sensor, and flow restrictors were adjusted to ensure identical flow conditions for all recesses prior to alignment. During alignment, the hydrostatic bearing was operated under pressurised conditions with the applied load acting on the pad. The pressure values in individual recesses were continuously monitored. If a recess exhibits a lower pressure compared to the others, it indicates locally increased film thickness or reduced load share, whereas elevated pressure indicates local overloading and reduced film thickness. Pad corner heights were then adjusted iteratively until the recess pressures converge to equal values within the accuracy limits of the pressure sensors.

### Pad Alignment Using Conventional Gauges

Alignment using conventional gauges is based on direct mechanical referencing of the bearing pad sliding surface. This method was implemented using a rigid straightedge and a precision spirit level. The straightedge was manufactured from an I-profile with a length of 1 m to ensure high bending stiffness in the direction perpendicular to the measured surface. Both contact faces of the straightedge were machined and ground to an accuracy of 0.01 mm to minimize geometric errors introduced by the measuring instrument itself. The spirit level used for tilt measurement had a sensitivity of 0.02 mm/m and featured a magnetic seating surface to ensure stable contact with the straightedge.

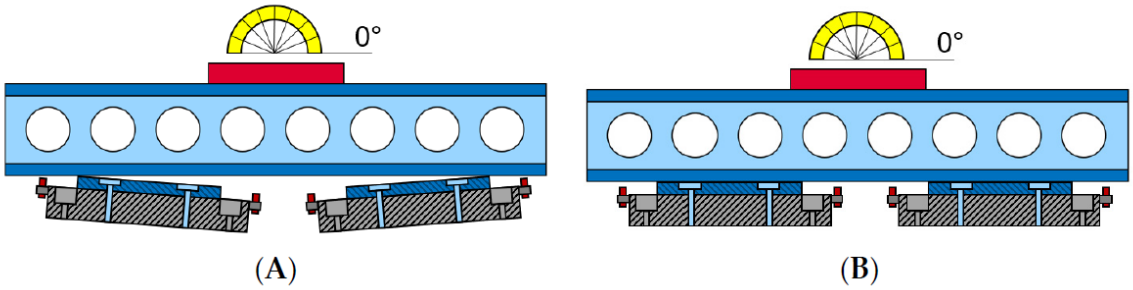


Figure 22 Scheme of: (A) Initial phase of planar aligning of the pad edges; (**B**) final state of the alignment by straightedge [81].

The alignment procedure was carried out by placing the straightedge successively across the outer and inner edges (Figure 22) of the bearing pad. First, the outer pad edges were levelled to establish a reference plane. Subsequently, the inner edges were adjusted by modifying the height of the pad supports until the spirit level indicated zero inclination in both orthogonal directions. Throughout the process, continuous visual inspection of straightedge contact was performed to detect local gaps indicative of surface tilt or height differences.

### Pad Alignment Using Optical Coordinate Measurement (OCMM)

The optical coordinate measurement method (OCMM) is a purely geometric alignment technique based on photogrammetric reconstruction of three-dimensional coordinates of selected points on the bearing pad surface. In the experiments, this method was implemented using a multi-point optical coordinate measurement system comprising a digital single-lens reflex camera, calibrated optics, coded circular targets, and dedicated photogrammetry software. Circular targets with a diameter of 3 mm were attached to the corners of the bearing pad. The measurement scene was captured from multiple camera positions, allowing triangulation of target coordinates in three-dimensional space. Scale bars with known length were placed in the scene to establish an absolute measurement scale.

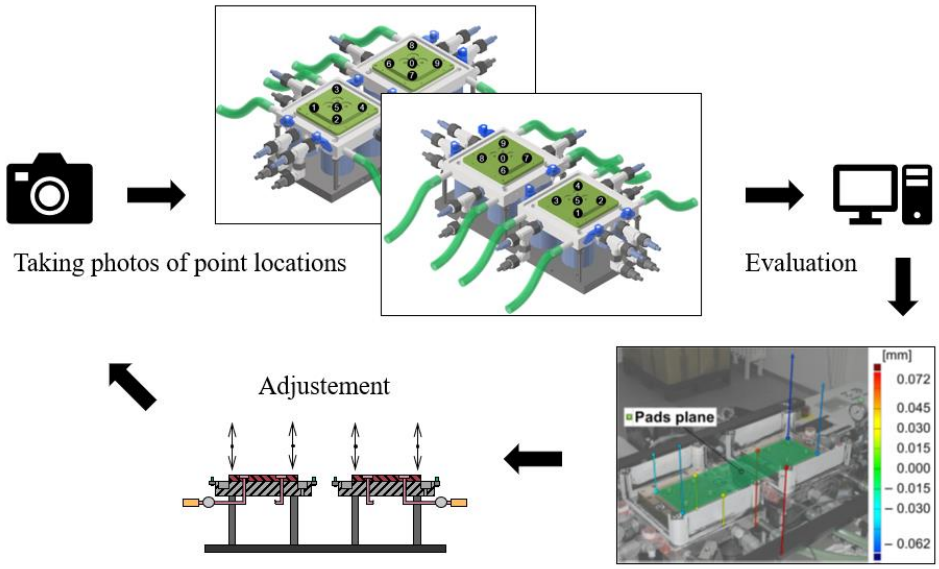


Figure 23 Scheme of iterative process of pad alignment [81].

The camera system was calibrated prior to measurement to determine intrinsic parameters and lens distortion. Based on the reconstructed target coordinates, a reference plane representing the ideal sliding surface was fitted using a best-fit algorithm. Deviations of individual pad corners from this plane were then computed. Alignment was achieved by iteratively adjusting the pad support screws to minimise the deviation of each target point from the fitted reference plane. After each adjustment step, the photogrammetric measurement was repeated until the deviations fell within a predefined tolerance band, typically on the order of ±0.01 mm.

### Film thickness measurement using dial indicators

In the field experiments on telescope bearings, lubricating film thickness was measured using digital dial indicators with a resolution of 1 µm. Measurements were conducted exclusively under static conditions to avoid damage to the precision track surface.

The hydraulic system of the bearing was first set to standby state, and the dial indicators were mounted at accessible corners of each pad using magnetic holders (Figure 24).


Figure 24 Setup for film thickness measurement by dial indicators [79].

The indicator tips were positioned perpendicular to the track surface and zeroed in unloaded condition. Subsequently, the hydraulic system was switched to operating mode, causing pressurization of the recesses and separation of the sliding surfaces. The resulting displacement of each indicator corresponded to the local lubricating film thickness and was recorded manually. After recording, the indicators were re-zeroed, and the hydraulic system was returned to standby to verify repeatability. On outer track pads, measurements were performed at all four corners, whereas on inner track pads only three corners were accessible due to spatial constraints. This method was primarily used as a reference technique for identification of severe faults such as significantly reduced film thickness caused by clogged capillaries.

**Film thickness measurement using inductive distance sensors**

To enable continuous and repeatable measurements, inductive contactless distance sensors with a resolution of 1 µm were employed. The sensors were mounted on rigid L-shaped brackets fixed to the bearing structure to ensure well-defined positioning relative to the track surface. Prior to measurements, each sensor was calibrated using precision shims to establish a known reference distance, typically 1.5 mm from the track surface, within the linear operating range of the sensor. Data acquisition was performed at a sampling frequency of 1 Hz, which was sufficient to capture changes during pressure build-up, steady-state operation, and controlled bearing motion. During measurements, film thickness, system pressure, recess pressure, telescope azimuth position, and rotational velocity were recorded synchronously. Measurements were carried out in several operating states, including hydraulic standby, pressure ramp-up, steady operating pressure, and controlled azimuth motion. This procedure allowed identification of film thickness variations caused by track segment transitions, surface waviness, and asymmetric loading.


Figure 25 Scheme of artificial clogging of capillary tube.

In addition, failure scenarios were investigated by deliberately blocking selected capillary restrictors using custom-manufactured caps (Figure 25), thereby simulating a clogged capillary. The resulting redistribution of film thickness across pad corners was used to evaluate the sensitivity of the method to early-stage bearing failures.

# 6 RESULTS AND DISCUSSION

To ensure a direct and verifiable connection between the defined research questions and obtained results, this chapter is structured into four parts: results organized according to research questions and hypotheses, discussion across all studies (Paper 1 – 3), limitations and uncertainties, and practical implications.

**Results related to Q1 / H1 (Optical diagnostics)**

The results of Paper 1 demonstrate that optical point tracking (OPT) enables reliable measurement of lubricating film thickness in hydrostatic bearings under real operating conditions. The average film thickness measured using the OPT method was 0.185 mm, compared to 0.192 mm obtained from proximity sensors, corresponding to a deviation of 3.6%. The confidence intervals of both methods overlapped, confirming consistency between measurement approaches. At the same time, the OPT method exhibited narrower confidence intervals, indicating higher measurement precision. From a safety perspective, this increased precision is critical, as safety margins in large-scale hydrostatic bearings are typically on the order of tens of micrometers, i.e., comparable to geometric deviations and elastic deformations. The achieved measurement resolution (up to 0.001 mm) allows detection of small changes in film thickness that are directly relevant to the risk of surface contact. These results confirm that optical methods provide sufficient accuracy, repeatability, and resolution for safety-oriented diagnostics of lubricating film thickness.

H1: VERIFIED

Optical methods increase safety by enabling direct measurement of minimum lubricating film thickness under real operating conditions. Experimental comparison showed average film thickness values of 0.185 mm (OPT) and 0.192 mm (proximity sensors), with overlapping confidence intervals.

Key results:

- Measurement deviation: 3.6%
- Measurement resolution: up to 0.001 mm

**Results related to Q1 / H2 (Alignment methods)**

The results of Paper 2 show that pad alignment has a direct and measurable influence on lubricating film thickness distribution and thus on bearing safety. The optical coordinate measurement method (OCMM) achieved the most uniform film thickness distribution, with a deviation of 7.4%, compared to 12.1% for the pressure-based method and 45.3% for conventional mechanical leveling. The positioning accuracy of the OCMM method reached ±0.01 mm. The pressure-based method provided acceptable results and offers potential for in-situ application; however, it showed higher variability.

In contrast, conventional mechanical leveling exhibited large deviations and strong dependence on operator skill, leading to non-uniform load distribution. Although average film thickness remained within nominal values for all methods, the high deviation in the mechanical approach resulted in significant local reduction of film thickness, thereby decreasing safety margins and increasing susceptibility to local film collapse. These results confirm that precise geometric alignment directly increases minimum film thickness and improves safety margins in rigid, segmented hydrostatic bearings.

H2: VERIFIED

Optical alignment method provides the highest positioning accuracy and results in the most uniform lubricating film thickness distribution. Deviation of film thickness distribution was 7.4% (OCMM), compared to 12.1% (pressure method) and 45.3% (mechanical leveling).

Key results:

- Alignment precision: ±0.01 mm
- Improvement vs mechanical method: approximately 6× reduction in deviation

**Results related to Q2 / H3 (Restrictor failure)**

The results of Paper 3 demonstrate that restrictor malfunction leads to significant local reduction of lubricating film thickness and represents a safety-critical condition. In experiments with artificially clogged capillaries, a local film thickness reduction exceeding 20 μm was measured in the affected recess. Additionally, dynamic measurements revealed film thickness fluctuations of up to 40 μm during operation, associated with track segmentation and load redistribution. The deviation between analytically predicted and experimentally measured film thickness reached up to 32%, indicating that simplified models do not fully capture real-system effects such as deformation, thermal influences, and assembly inaccuracies. Although direct surface contact was not observed, the minimum film thickness approached critical values comparable to surface roughness and geometric deviations. This condition represents a safety-critical state, even when global bearing operation is maintained. These findings confirm that a single restrictor failure can significantly reduce local load-carrying capacity and must be considered a critical failure mode.

H3: VERIFIED

Restrictor blockage leads to significant local reduction in film thickness and represents a safety-critical condition. Measured local film thickness reduction exceeded 20 μm under simulated capillary blockage.

Key results:

- Film thickness drop: >20 μm
- Dynamic fluctuation: up to 40 μm

- Safety criterion: A safety-critical state is defined as a condition where minimum film thickness approaches the scale of surface roughness and geometric deviations.

**Integrated discussion across studies**

The results collectively demonstrate that lubricating film thickness must be treated as a primary safety parameter rather than a secondary performance indicator. The first study establishes that film thickness can be measured with micrometer-level precision under realistic conditions. The second study shows that geometric alignment directly determines film thickness distribution and minimum values. The third study confirms that hydraulic faults lead to localized degradation of film thickness that cannot be reliably detected using pressure-based diagnostics alone. A key finding across all studies is that minimum film thickness, rather than average values, governs the risk of surface contact. This is particularly critical in large-scale segmented bearings, where local deviations dominate system behavior. The results also show that traditional design approaches based on ideal assumptions underestimate the influence of real disturbances, including misalignment, restrictor blockage, and structural deformation. Therefore, safety evaluation must be based on verified film thickness distribution rather than solely on analytical predictions.

**Limitations and uncertainties**

Several limitations must be considered. Analytical models used in this work assume rigid surfaces, laminar flow, and constant temperature. Optical measurement methods, while highly precise, are not suitable for continuous monitoring due to their setup complexity. Experimental validation was performed on a limited number of configurations and operating conditions. In real large-scale systems, additional factors such as thermal gradients, deformation, and wear may further influence film thickness distribution and should be considered in future studies.

**Practical implications**

The presented results provide directly applicable tools for improving safety in large-scale hydrostatic bearing systems. Optical diagnostics can be used during commissioning and maintenance to identify critical film thinning. Optical alignment enables precise geometric setup without reducing system stiffness. Continuous monitoring using inductive sensors allows early detection of hydraulic faults such as restrictor blockage. These methods are particularly relevant for high-value installations such as astronomical telescopes, large machine tools, and energy systems, where failure leads to significant downtime and economic losses. The measurable benefit lies in the ability to detect film thickness changes on the order of tens of micrometers and thus prevent transition to contact conditions.

Check for updates

Original Article

Institution of MECHANICAL ENGINEERS
Journal of ENGINEERING TRIBOLOGY

Proc IMechE Part J:
J Engineering Tribology
1–9
© IMechE 2022
Article reuse guidelines:
sagepub.com/journals-permissions
DOI: 10.1177/13506501221108138
journals.sagepub.com/home/pij
SAGE

# Contactless measurement of hydrostatic bearing lubricating film using optical point tracking method

**Michal Michalec[1], Jakub Hurník[1], Jan Foltýn[1] and Petr Svoboda[1]**

## Abstract

Hydrostatic bearings are vital part of numerous industrial applications of various sizes. Especially large-scale bearings are often encountered with complications caused by pad alignment and levelling. For such cases, a contactless measurement method was developed for film thickness diagnostics of hydrostatic bearings. The proposed method is based on a monocular tracking method, which is versatile and easily applicable for in-field measurements and diagnostics of hydrostatic lubricating films. The optical method is compared with analytical calculation and film thickness data obtained from proximity sensors of the experimental device. The results show good agreement of the data obtained from proximity sensors and the analytical calculation compared to the optical measurement. The proposed method could be used to improve the hydrostatic bearing pad levelling, alignment, or film thickness diagnostics of hydrostatic bearing pads to avoid costly maintenance that might arise due to collision of sliding surfaces in the case of lubricating film failure.

## Keywords

hydrostatic lubrication, large-scale bearings, film thickness measurement, optical methods, condition monitoring

Date received: 31 March 2022; accepted: 30 May 2022

## Introduction

Hydrostatic (HS) bearings are widely used in a variety of industrial applications, ranging from millimetres, up to tens of metres.[1] They find use in machining centres, turntables and guideways, giant telescopes, antennas, and similar applications.[2–6] HS bearings operate on the principle of requiring a continuous supply of pressurized fluid while working to separate the sliding surfaces with a thick lubricating film. This creates a significant reduction in driving force due to fluid friction and absence of stick-slip effect,[7] which occurs frequently in rolling and sliding elements. One of their key advantages is their operation at low speed or even at standstill. This is why HS bearings are frequently combined with hydrodynamic bearings (creating the so-called hybrid bearings), to improve machine safety and stability.[8] This type of bearing is frequently used in hydroenergetics.[9–11] Further advantages are: a large load carrying capacity, high stiffness, damping ability, very low friction, almost no wear, and very high movement precision.[12] In contrast, there are higher initial costs and the necessity of continuous pressure fluid supply while working.[13] A significant improvement in HS lubrication has been done since its introduction in the 19th century. Recent research on this topic shows an increasing trend of interest among the scientific community and industry.[14,15]

Compared to rolling bearings, HS bearings can be built in large areas in size over tens of metres.[1] Still, the alignment and levelling become a serious challenge.[16] Improper positioning of bearing sliding surfaces might cause decrease of the lubricating film performance or even lead to sliding surface damage and eventually bearing failure.[17] To ensure proper operation of HS bearings, a uniform and stable lubricating film must be maintained. Uneven loading or misalignment can be partially reduced by self-compensation,[18,19] compensatory devices implemented to the hydraulic circuit,[20,21] or using compliant members.[22–24] However, the most critical part is the levelling of bearing pads that is

[1]Institute of Machine and Industrial Design – Faculty of Mechanical Engineering, Brno University of Technology, Czech Republic

**Corresponding author:**
Michal Michalec, Institute of Machine and Industrial Design – Faculty of Mechanical Engineering, Brno University of Technology, Czech Republic.
Email: michal.michalec@vut.cz

directly influenced by the precision of the foundation and the manufacturing precision, especially in the case of large-scale HS bearings.

Optical measurement methods are often used for dimensional measurement in the industry. Many various measurement methods, based on camera images are present.[25] These methods are often advantageous due to their flexibility and versatility, e.g., in large measurement volumes. Here belong the photogrammetry methods, which could be used in industrial applications[25,26] to determine foundation precision even in large areas.[27] The biggest progress in this area was made throughout the era of digital cameras and computers expansion and continues to improve and open new possible applications.

The formation of HS thrust bearing lubricating films can be characterized as small, quasi-static two-dimensional movement. There are more optical methods that could be used for such applications. An example is the digital image correlation method (DIC), which is commonly used for similar applications.[28] This method is utilized by, e.g., optical extensometers. However, the measurement based on targets offers more flexibility at relatively high accuracy, since the contrast texture spray does not need to be applied on the body surface. Targets are widely used during the camera calibration,[29,30] accurate optical measurement[31] or object tracking[32] and their centre can be measured in image with an accuracy of 1/50–1/20 px.[33]

Bearing diagnostics throughout the service period are as important as proper setting. Usually used methods for film thickness evaluation require a large number of proximity sensors and data evaluation. As part of the modern industrial trends, such as Industry 4.0 and Internet of Things (IoT),[34,35] detailed information during service is provided and future maintenance can be predicted.[36] However, this means significantly higher initial costs, programming, and maintenance. In addition, sensors mainly provide information about the lubricating film while overall bearing behaviour is mostly overlooked after manufacturing, even though issues with levelling and unexpected body deformation often occur. Information about deformation or body movement can be tracked using coded targets.[30,32]

The progress in the fields of HS lubrication and modern technologies has opened new possibilities for HS bearing applications. Nevertheless, at the same time, new problems are emerging. Previous research on the use of optical diagnostic methods for large parts and areas has proposed new tools to improve the precision of large-scale HS bearings and on-site diagnostic. To date, an optical method for measuring the film thickness of large-scale HS bearings has not been proposed. Therefore, in this paper, we aim to investigate its measuring precision and possible applicability.

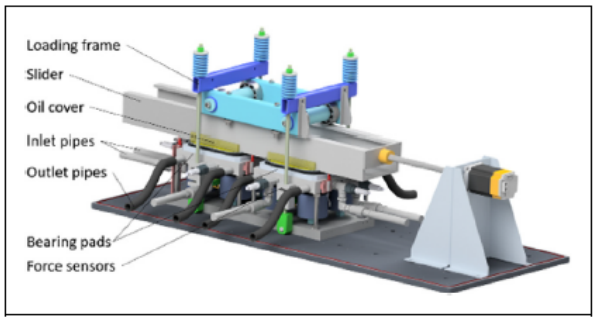


**Figure 1.** Overview of the experimental rig.

## Methods

Comparison of film thickness prediction, measurement using proximity sensors and optical method was performed on an experimental device described below.

### *Film thickness prediction*

The prediction of the lubricating film thickness was calculated based on the analytical calculation of the hydrostatic bearing with four circular recesses from reference[12]:

$$h = \sqrt[3]{\frac{12 \cdot Q \cdot \mu \cdot A}{F \cdot q_f}}$$

where $h$ is the film thickness, $Q$ is the supplied flow, $\mu$ is the dynamic viscosity, $A$ is the total pad area, $F$ is the applied force and $q_f$ is the flow factor (in this case 25.5).

### *Experimental hydrostatic bearing rig*

The experimental rig (2-PAD) consists of two HS bearing pads, slider, loading frame, and hydraulic aggregate for pressurized oil supply (Figure 1).

A detailed description of the rig can be found in Figure 2. Film thickness was directly measured using six proximity sensors mounted on pads with a resolution of 0.01 mm. The load was applied using four threaded rods with load cells of 1 N resolution. Four compression springs were placed between the nuts and the loading frame to ensure an even load distribution (Figure 1). The pads are supported on setting screws. Pressure and temperature sensors are used to monitor bearing performance. Pad levelling was done using calibration rods with a precision of $\pm$0.005 mm.

The pads were levelled using calibration rods and recess pressure information. After pad levelling and proximity sensor calibration, the 16 kN load was applied to the slider using the loading frame. Subsequently, the hydraulic pump started supplying a total of 9.8 L/min of lubricant with equally set restrictors to secure even supply to each of the recesses. The film thickness data from contact potentiometer proximity sensors of resolution 0.01 mm and 3 mm range were logged at 60 Hz frequency. The film thickness value was obtained from three proximity sensors of the examined bearing pad (Figure 2-2). Then the hydraulic pump was switched off and the measurement was repeated ten times to examine repeatability. Since the performed tests were relatively short, the temperature of oil was stable at 24 $\pm$ 1 °C

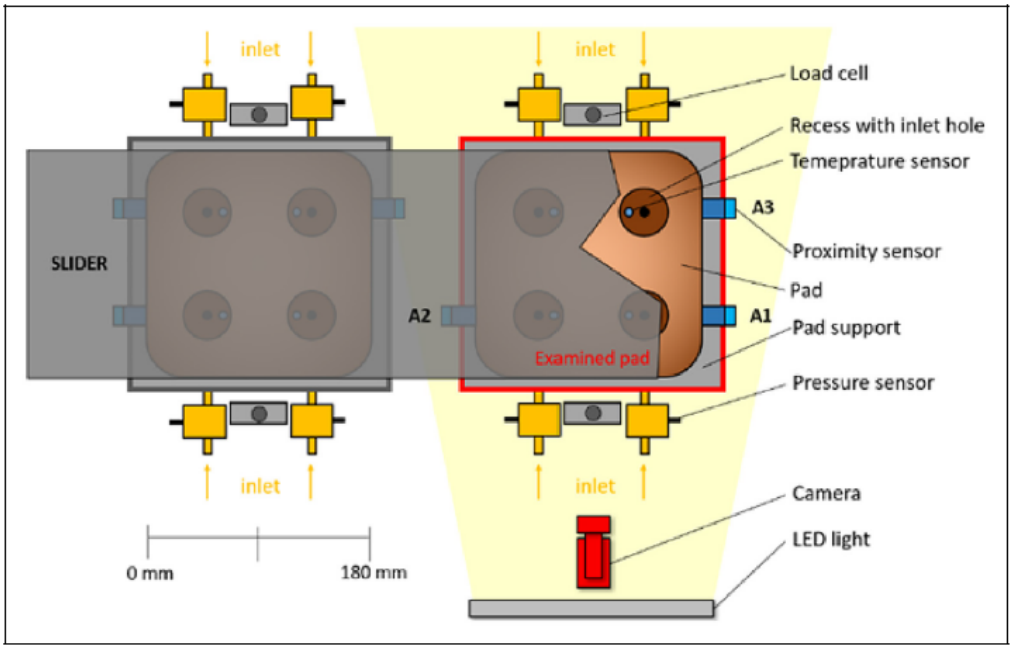


**Figure 2.** Schematical representation of the 2-PAD device.

during the whole measurement. The OPT measurement data were obtained throughout this process. The OPT film thickness measurement was calculated based on a sequence of 20 images. Twenty images were also used to determine the mean zero position of the slider.

## *Optical point tracking (OPT) method*

The optical lubrication film measurement was carried out by tracking the relative movement of the pad and the slider in a series of images using bundles of circular targets attached to the rigid bearing bodies (a pad and a slider). We assumed that in the case of linear bearing the 2D movement in direction of lubricating film formation was dominant. Thus, monocular camera measurement was used for optical measurements. The relative position of the pad and slider (both considered as rigid) was calculated based on the relative position and orientation of point clouds attached to these objects.

### *Experimental setup*

Because the front plane of the pad and the slider are not coplanar, lightweight 3-D printed plastic blocks were adhered to the slider, to allow measurement in one plane as much as possible (**Figure 3**). Three-millimetre calibration targets were attached both to the slider and the pad (over 50 pieces in both cases). The scene was captured using ZWO ASI 1600 MM monochromatic camera (16 Mpx CMOS sensor, rolling shutter). The camera was equipped with 35 mm Zeiss Interlock Compact lens. A strong LED light source (100 W) was used to illuminate the scene.

### *Camera calibration*

Firstly, the camera distortion parameters were calibrated using the Single Camera Calibrator App, available in MATLAB. This app uses Zhang's camera calibration method.[37] A $9 \times 12$, 15 mm checkerboard from calib.io was used. Three radial distortion, coefficients, tangent distortion, and skew were estimated. Thirteen images of a checkerboard calibration field were used. The achieved mean reprojection error was 0.47 px.

Subsequently, the px to mm ratio was calculated on-site, again based on the imaging of the calibration checkerboard. The checkerboard was placed horizontally on the plane with calibration targets, and the calibration image was taken. The image distortion is then removed. Checkerboard points are detected with sub-pixel accuracy in the image. The ratio $r_h$ and $r_v$ in both horizontal and vertical direction respectively is calculated based on the known mutual distance between two points of the checkerboard (provided in **Figure 4**). The ratio is calculated as $r = d_{mm} / d_{px}$. The thickness of the calibration checkerboard (6 mm) was compensated. The ratio $r_h$ and $r_v$ was calculated as 0.05894 and 0.05924 mm. These values show good agreement; therefore, the mean value $r$ is used as a unidirectional px to mm ratio.

### *Image processing*

In this section, the method for accurately obtain calibration target centres in an image is explained. Firstly, the image distortion is removed, and a light Gaussian image filtering is applied ($3 \times 3$ kernel, $\sigma = 0.5$) to remove noise. Canny edge operator[38] is applied to find the edges and according to certain criteria (ellipse size, the ratio between the minor and major axis of the ellipse, the ratio between the filled area of the closed edge and its convex envelope, and a result after an ellipse fitting to the contour). Star ellipse operator[33] is used to accurately compute the centers of the ellipse (Figure 5). In this work, 180 radial scanning rays were used.

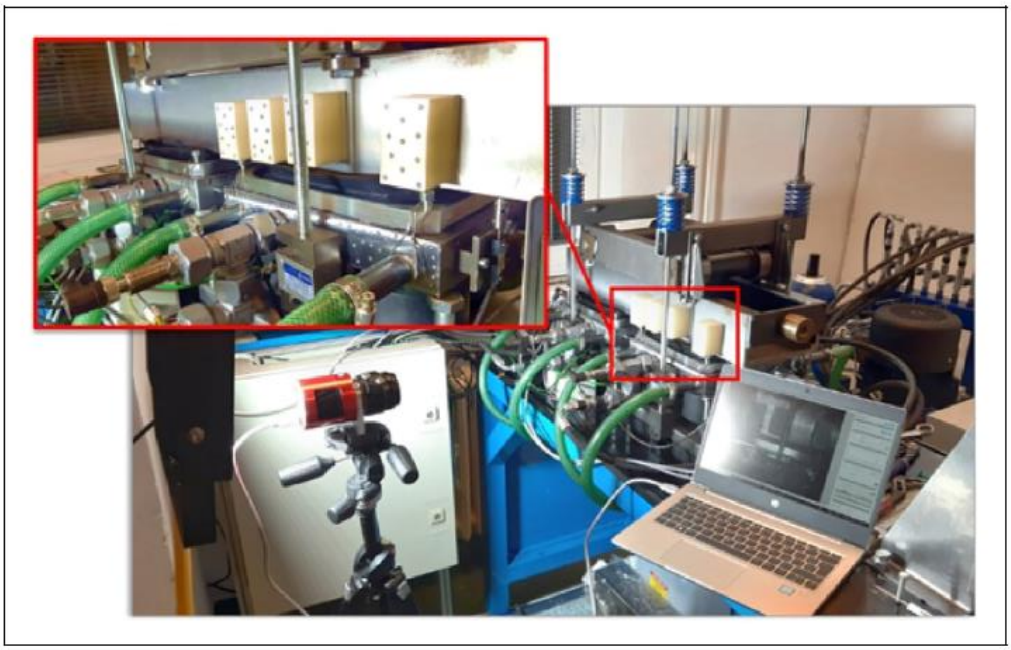

**Figure 3.** Experimental setup, detail of points on the bearing pad and slider, right – sample of measurement image.

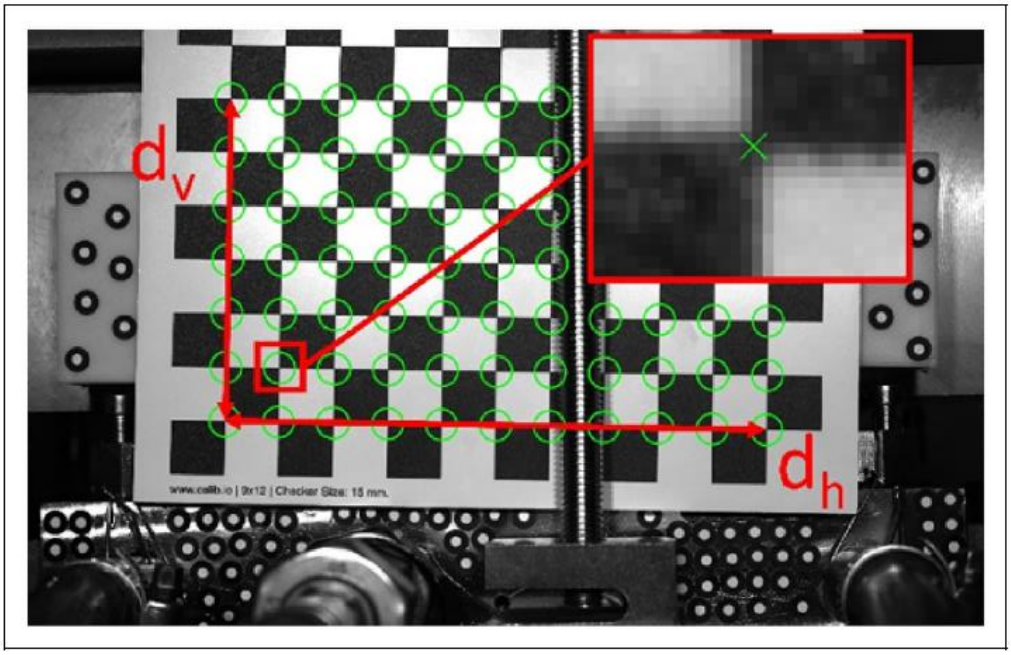


**Figure 4.** Pixel to millimeter ratio calibration. Green – subpixel checkerboard corners.

Moment-preservation sub-pixel method is used to compute the edges on the individual rays. The ellipse is then fitted to these subpixel edge points, and its centers is considered as the center of the target. The details of this method are introduced in.[30]

The target centers are tracked through the set of measurement images. Tracking assumes that the relative movement of the targets between the images is small. Therefore, instead of coding the targets or using target patterns, a simple condition of proximity is used. The result of target tracking is the sequence of coordinates of every target in the measurement series. In addition, the targets are sorted into pad targets (A) and slider targets (B), according to Figure 6.

*Movement calculation and results computation*

The travel of point cloud in a series of images is calculated as the transformation between the point cloud locations in subsequent images. Because the objects are rigid, we consider only translation in $x$ and $y$ axis and rotation. Considering that every point of the point cloud in the image is measured with a random error and the point cloud contains more than 3 points, an optimalization

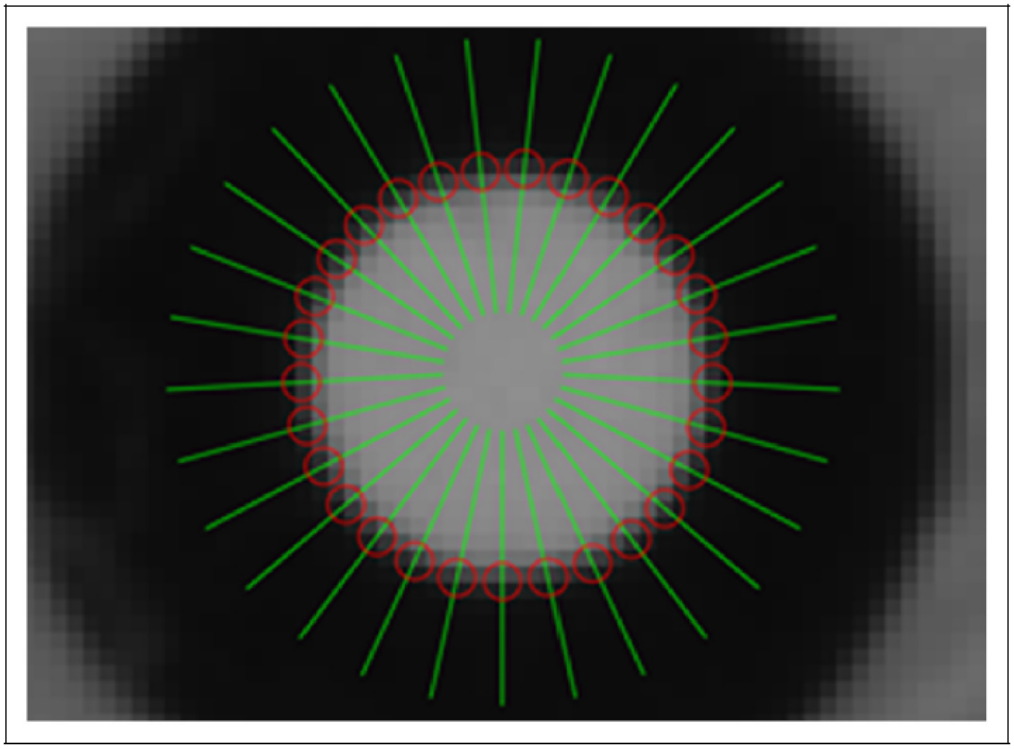

**Figure 5.** Illustration of star ellipse operator function. Green – radial scanning rays, red – edges detected with subpixel precision.

problem can be written:

$$\underset{\Delta x,\ \Delta y,\ \varphi}{argmin} \sum_{i=1}^{i=n} |\boldsymbol{X}_{m,i} - \boldsymbol{X'}_{m-1,i}|;$$

$$\boldsymbol{X'}_{m-1,i} = \boldsymbol{X}_{m-1,i} \cdot \boldsymbol{R}_{\varphi} + \boldsymbol{T}_{\Delta x,\,\Delta y}$$

where $\Delta x$ and $\Delta y$ are the translations in $x$ and $y$ directions, $\boldsymbol{T}_{\Delta x,\Delta y}$ is the translation vector, $\varphi$ is the rotation angle, $\boldsymbol{R}_{\varphi}$ is the rotation matrix, $m$ is the frame number in a series of measurement images, n is the number of targets in the point cloud, $\boldsymbol{x}$ and $\boldsymbol{x}'$ are the original and transformed image points, respectively.

The $||$ operator means the Euclidean distance. The optimization problem can be solved using the least-squares method.

In this application, it is important to compute only the relative movement of the pad and slider, which is considered as the thickness of the lubricating film or, more general, its difference over time. The workflow of this process is provided in Figure 2. We cannot consider both camera (which is mounted on a tripod) and pad (which is dynamically loaded) static. Therefore, both the camera and the pad movement are compensated in one step. This is carried out by calculating the camera/pad movement compensation transformation $T_C$ and $R_C$ This transformation is defined as the transformation from the pad targets $B_C$ in the current image to the targets $B_R$ in the reference image. This transformation is applied both to $B_C$ and $A_C$ targets, resulting in $B_{CC}$ and $A_{CC}$, which are the current targets with compensated camera or pad movement. Finally, the travel transformation $T_t$ and $R_t$ between the reference targets $A_R$ and $A_{CC}$ targets in the current image, with compensated camera/pad movement, is calculated.

However, the travel transformation $T_t$ and $R_t$ can't be directly used as a result. For comparison purposes with the contact film thickness measurement method, the auxiliary points ("probes") are placed at the same positions in the image, where the contact sensors are placed (two on the side of the camera system, as seen in Figure 7). The travel transformation $T_t$ and $R_t$ is applied to these points. The transformed auxiliary points are subtracted from the non-transformed, resulting in the travel in the locations of the sensors. The pixel-to-millimeter ratio $r$ obtained during camera calibration, is used to transform the travel into millimeters.

### *Consideration of measurement precision*

The key parameters for the estimation of the precision of the measurement system are the pixel resolution, the accuracy of the measurement of the target location in the image, and number of targets in the image. If we consider pixel equivalent of 0.06 mm, and an achievable accuracy of the ellipse location 1/50 px, the expected accuracy of the ellipse centre coordinates is within 0.0012 mm. However, the measurement accuracy depends on the movement parameters (translation and rotation), which has 3 parameters total. These parameters are calculated on more than 50 points, which means more than 100 conditions. Considering a sufficiently homogeneous distribution of targets in the image, the expected accuracy can be roughly expressed, based on the central limit theorem, as:

$$ac = \frac{ac_S}{\sqrt{\frac{n}{p}}} \cdot 2 \cdot 2$$

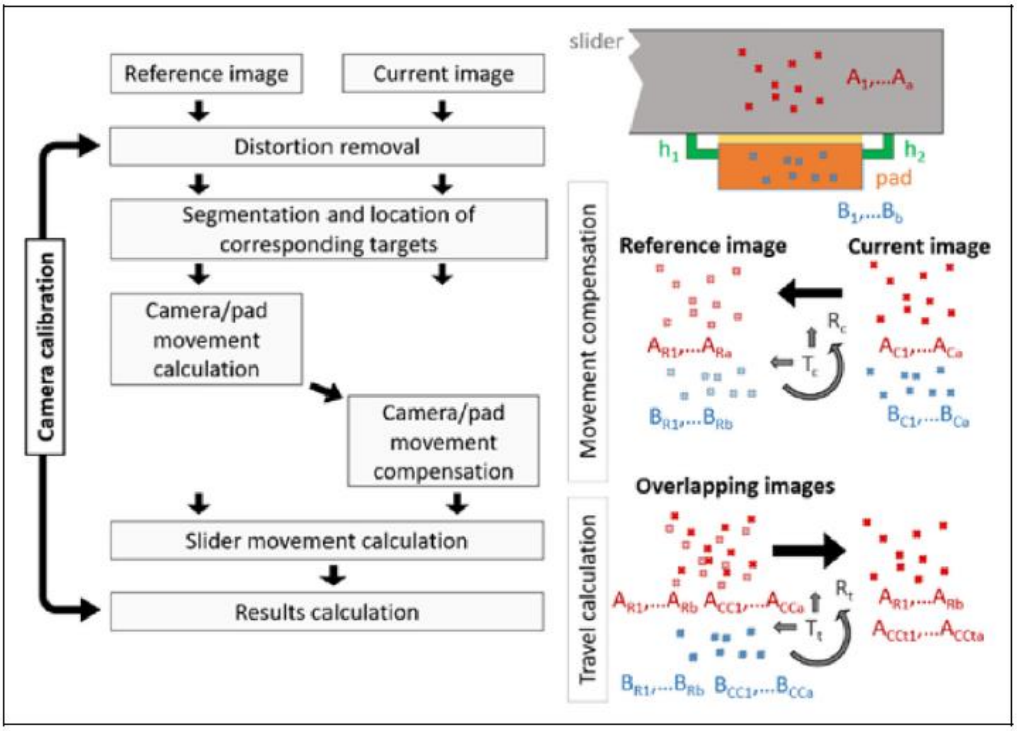


**Figure 6.** Workflow of the optical point tracking method.

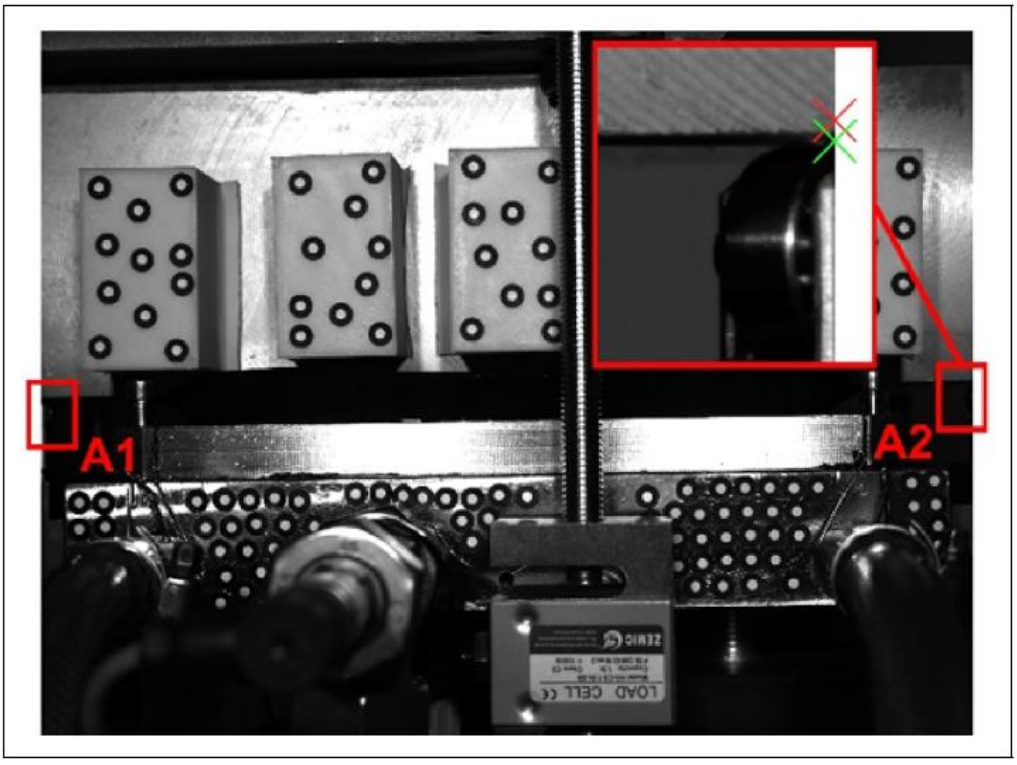


**Figure 7.** Reference measurement image. The magnified, lighten detail depicts the green, auxiliary measurement point (probe) and red, auxiliary point after the travel transformation, both points are in the contact of the distance sensor with slider. Placement of probes A1 and A2 are shown.

Where $ac$ is the considered measurement accuracy, $ac_S$ stands for the expected accuracy of a single point (0.0012 mm), $n$ for the number of applicable conditions (at least 100), $p$ for the number of movement transformation parameters (3) and the whole estimation is multiplied by 2, which is considered as the worst-case scenario, because the transformation parameters are calculated based on corresponding targets difference in reference and current image. The second multiplication by 2 is,

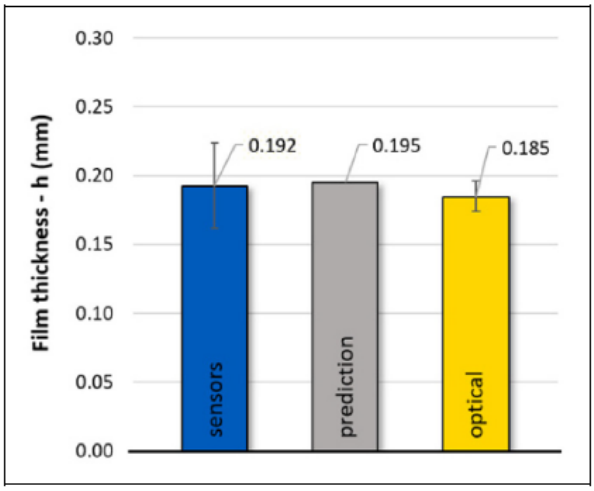


**Figure 8.** Lubricating film thickness prediction comparison with data from proximity sensors and OPT method results with their maximum and minimum recorded values.

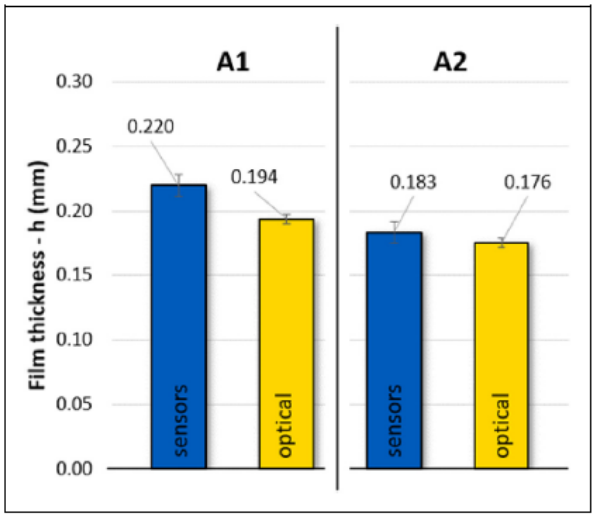


**Figure 9.** Comparison of film thickness measured in the location of point A1 and A2 using the compared methods, with their 95% confidence intervals.

again, the worst-case scenario, which considers the error of the camera/pad movement compensation. The rough estimation of the achievable accuracy is, therefore, 0.0008 mm.

## Results and discussion

The average film thickness obtained from proximity sensors was 0.192 mm, the interval of recorded values (average value on proximity sensors A1, A2, and A3 across all the measurements) was from 0.2239 to 0.1618 mm. On the other hand, the average film thickness obtained from OPT was 0.185 mm and the interval of recorded values (average value on probes A1 and A2) was from 0.1962 to 0.1738 mm. The results clearly indicate that the average value measured using the proximity sensors was in good agreement with the prediction, while the OPT method measured a lower thickness of the lubrication film (Figure 8). Although, the value measured by the proximity sensors showed a larger deviation compared to the OPT method, making OPT method more credible. In addition, the prediction may be larger than the actual thickness due to manufacturing and leveling errors, real geometry deviation compared to the prediction, or solid body deformations. However, the difference of the average film thickness measured by the compared methods or predicted is not significant – the intervals of recorded values overlap. For both measurement methods (proximity sensors or OPT), the recorded interval was significantly larger than assumed. This can be explained as the effect of the non-uniform film thickness over the area of the pad, which is also confirmed further.

To compare the precision of the measurement methods in detail, the mean measured values were compared at the locations of A1 and A2, as well as their deviations (Figure 9). The film thickness using the proximity sensors was $0.220 \pm 0.0086$ mm and $0.1835 \pm 0.0084$ mm at the locations of point A1 and A2, respectively. The average film thickness measured using OPT was $0.1940 \pm 0.0036$ mm and $0.1760 \pm 0.0033$ mm. All the intervals are considered for 95% confidence. Proximity sensors of higher precision would most certainly provide smaller deviations; however, the price of such sensors is increasing with their precision and the overall price of HS bearing mounted with numerous precise but expensive sensors would rise significantly. Moreover, the proximity sensors need to be mounted and isolated from the lubricant, calibrated and the logged data must be evaluated to obtain information about the film thickness only at specific points, while OPT method allows us to investigate the film thickness almost everywhere by sticking the targets where it is desired, and the calibration process is far simpler than of the proximity sensors. As the results clearly indicate, the OPT method works at higher precision. Basically, any camera with sufficient light can be used for the OPT method, however, this will affect the resulting precision. Generally, the higher the camera quality, the higher the measurement precision.

In case of both OPT probes, the standard deviation was larger than considered – the indicated precision was on the order of thousandths of millimetre. However, this might have been caused by the fluctuations of the film thickness caused by the pump and manufacturing or levelling error. The minor influence could also have the rolling shutter effect, which was caused by small movements or vibrations in the laboratory environment during the measurement.

## Conclusions

In the presented paper the OPT method was introduced for possible use in HS bearing condition investigation. The lubricating film is usually 0.01–0.2 mm thick, and its stability is crucial for proper operation. The proposed method offers a quick and versatile measurement of the thickness of the HS bearing film with a potential precision of 0.001 mm; thus, could be also used for bearings with lower film thickness. Compared to the prediction, a good agreement was achieved with the results obtained from proximity sensors and using

the OPT method. Any camera can be used for the OPT method measurement, although the better camera performance, the higher the result precision. Moreover, this setup (after method customization) might also be suitable for deformation, or unexpected movement investigation, since those effects are not easily measured using proximity sensors. In addition to that, optical methods provide new ways of positioning and levelling of large-scale multi-pad HS bearings to achieve best possible performance and minimize assembly errors. Although this method is not tailored to provide on-line diagnostics, it might serve as a valuable tool for on-field performance investigation and precision improvement, either throughout the assembly or during operation. The OPT method is ready for use for bearing diagnostics in a wide size range. Further research could be aimed at field measurements on an actual site to prove its applicability, precision, and effectiveness.

Presented at WTC 2022 Lyon.

## Acknowledgements

This research was carried out under the project FW03010357 with financial support from the state budget by the Technology Agency of the Czech Republic and the Ministry of Industry and Trade within the TREND Programme. The research was co-funded by Faculty of Mechanical Engineering, Brno University of Technology internal specific project FSI-S-20–6296.

## Declaration of conflicting interests

The author(s) declared no potential conflicts of interest with respect to the research, authorship, and/or publication of this article.

## Funding

The author(s) disclosed receipt of the following financial support for the research, authorship, and/or publication of this article: This work was supported by the Vysoké Učení Technické v Brně, Technology Agency of the Czech Republic, (grant number FSI-S-20–6296, FW03010357).

## ORCID iDs

Michal Michalec https://orcid.org/0000-0002-8803-9043
Jan Foltýn https://orcid.org/0000-0001-6715-642X
Petr Svoboda https://orcid.org/0000-0003-3091-4025

## References

1. Michalec M, Svoboda P, Křupka I, et al. A review of the design and optimization of large-scale hydrostatic bearing systems. *Eng Sci Technol an Int J*. 2021; 24(4): 936–958.
2. Johns M, Hull C, Muller G, et al. Design of the giant magellan telescope. *Ground-based Airborne Telesc V* 2014; 9145: 91451F.
3. Bernstein RA, McCarthy PJ, Raybould K, et al. Overview and status of the giant magellan telescope project. *Ground-based Airborne Telesc V* 2014; 9145: 91451C.
4. Zha J, Chen Y and Wang Z. A tolerance design method for hydrostatic guideways motion accuracy based on error averaging effect. *Procedia CIRP* 2018; 75: 196–201.
5. Jang S-H, Choi Y-H, Kim S-T, et al. Development of core technologies of multi-tasking machine tools for machining highly precision large parts. *J Korean Soc Precis Eng* 2012; 29: 129–138.
6. Wang Y, Liu Z, Zhao Y, et al. Design of an intelligent monitoring system for hydrostatic turntable service performance evaluation. *J Ambient Intell Humaniz Comput* 2018; 0: 0.
7. Awrejcewicz J and Olejnik P. The occurrence of stick-slip phenomenon. *J Theor an Appl Mech* 2007; 45: 33–40.
8. Bouyer J, Wodtke M and Fillon M. Experimental research on a hydrodynamic thrust bearing with hydrostatic lift pockets: influence of lubrication modes on bearing performance. *Tribol Int* 2022; 165: 107253.
9. Martinez Esparza LF, Cervantes De Gortari JG and Chicurel Uziel EJ. Design of hybrid hydrostatic/hydrodynamic journal bearings for optimum self-compensation under misaligning external loads. *J Tribol* 2017; 139: 1–12. Epub ahead of print 1 July 2017.
10. Childs DW and Esser P. Measurements versus predictions for a hybrid (hydrostatic plus hydrodynamic) thrust bearing for a range of orifice diameters. *J Eng Gas Turbines Power-Transactions Asme* 2019; 141: 1–12. Epub ahead of print 2019.
11. Rowe WB. Advances in hydrostatic and hybrid bearing technology. *Proc Inst Mech Eng Part C J Mech Eng Sci* 1989; 203: 225–242.
12. Khonsari MM and Booser RE. *Applied tribology: bearing design and lubrication*. 3rd ed. Wiley, 1970, p.653.
13. Bassani R and Piccigallo B. Hydrostatic lubrication. *Tribol Ser* 1992; 22: 541.
14. Liu ZF, Wang YM, Cai LG, et al. A review of hydrostatic bearing system: researches and applications. *Adv Mech Eng* 2017; 9: 1–27. Epub ahead of print 2017.
15. Li XB, Wang X, Li M, et al. The research status and progress of heavy/large hydrostatic thrust bearing. *Adv Mech Eng*. 2014; 2014: 9.
16. Jang J and Khonsari M. On the characteristics of misaligned journal bearings. *Lubricants* 2015; 3: 27–53.
17. San Andres L. The effect of journal misalignment on the operation of a turbulent flow hydrostatic bearing. *J Tribol* 1993; 115: 355–363.
18. Zuo X, Li S, Yin Z, et al. Design and parameter study of a self-compensating hydrostatic rotary bearing. *Int J Rotating Mach* 2013; 2013: 1–10.
19. Xu C and Jiang S. Analysis of the static characteristics of a self-compensation hydrostatic spherical hinge. *J Tribol* 2015; 137: 1–5.
20. Singh N, Sharma SC, Jain SC, et al. Performance of membrane compensated multirecess hydrostatic/hybrid flexible journal bearing system considering various recess shapes. *Tribol Int* 2004; 37: 11–24.
21. Rajasekhar Nicodemus E and Sharma SC. Orifice compensated multirecess hydrostatic/hybrid journal bearing system of various geometric shapes of recess operating with micropolar lubricant. *Tribol Int* 2011; 44: 284–296.
22. Michalec M, Polnický V, Foltýn J, et al. The prediction of large-scale hydrostatic bearing pad misalignment error and its compensation using compliant support. *Precis Eng* 2022; 75: 67–79.
23. Santos IF. Controllable sliding bearings and controllable lubrication principles-an overview. *Lubricants* 2018; 6: 12. Epub ahead of print 2018.
24. Van Beek A and Segal A. Rubber supported hydrostatic thrust bearings with rigid bearing surfaces. *Tribol Int* 1997; 30: 47–52.

25. Luhmann T. Close range photogrammetry for industrial applications. *ISPRS J Photogramm Remote Sens* 2010; 65: 558–569.
26. Hurník J, Zatocilová A and Paloušek D. Camera calibration method of optical system for large field measurement of hot forgings in heavy industry. In: Lehmann P, Osten W and Albertazzi Gonçalves A (eds) *Optical measurement systems for industrial inspection XI*. Munich: SPIE, 2019, p. 12.
27. Sapirstein P. Accurate measurement with photogrammetry at large sites. *J Archaeol Sci* 2016; 66: 137–145.
28. Pan B, Qian K, Xie H, et al. Two-dimensional digital image correlation for in-plane displacement and strain measurement: a review. *Meas Sci Technol* 2009; 20: 17. Epub ahead of print 2009.
29. Schneider D, Schwalbe E and Maas HG. Validation of geometric models for fisheye lenses. *ISPRS J Photogramm Remote Sens* 2009; 64: 259–266.
30. Hurník J, Zatočilová A and Paloušek D. Circular coded target system for industrial applications. *Mach Vis Appl* 2021; 32: 39.
31. Zhang D. Exploitation of photogrammetry measurement system. *Opt Eng* 2010; 49: 37005.
32. Hu H, Liang J, Xiao ZZ, et al. A four-camera videogrammetric system for 3-D motion measurement of deformable object. *Opt Lasers Eng* 2012; 50: 800–811.
33. Luhmann T, Robson S, Kyle S, et al. *Close range photogrammetry - principles, techniques and applications*. Dunbeath, Caithness KW6 6EG, Scotland, UK: Whittles Publishing, 2011.
34. Alcácer V and Cruz-Machado V. Scanning the industry 4.0: a literature review on technologies for manufacturing systems. *Eng Sci Technol an Int J* 2019; 22: 899–919.
35. Tao F, Cheng J, Qi Q, et al. Digital twin-driven product design, manufacturing and service with big data. *Int J Adv Manuf Technol* 2018; 94: 3563–3576.
36. Moore WJ and Starr AG. An intelligent maintenance system for continuous cost-based prioritisation of maintenance activities. *Comput Ind* 2006; 57: 595–606.
37. Zhang Z. A flexible new technique for camera calibration. *IEEE Trans Pattern Anal Mach Intell* 2000; 22: 1330–1334.
38. Canny J. A computational approach to edge detection. *IEEE Trans Pattern Anal Mach Intell* 1986; PAMI-8: 679–698.

machines

MDPI

*Article*

# Pad Alignment Methods and Their Impact on Large Hydrostatic Bearing Precision

**Jan Foltýn, Jakub Hurník, Michal Michalec, Petr Svoboda *, Ivan Křupka and Martin Hartl**

Faculty of Mechanical Engineering, Brno University of Technology, 61669 Brno, Czech Republic
* Correspondence: petr.svoboda@vut.cz

**Abstract:** Hydrostatic bearings are frequently used for moving large structures smoothly and precisely. In such applications, difficulties with manufacturing, transportation, and assembly arise. The safety and precision of the entire supported structure depend on the accuracy of the hydrostatic bearing alignment. There are several suitable methods for its alignment, yet it is not clear which method can achieve the highest bearing precision. This study provides a comparative experimental assessment of the three methods. The measurements were performed on a hydrostatic bearing test rig with independent positioning of the pads. Conventional measuring devices, a pressure distribution alignment method, and an optical method, OCMM (optical coordinate measuring machine), were compared. The accuracy of the selected methods and the difficulty of the aligning process were included in the comparison. The OCMM method was able to achieve an accuracy 1.6 times higher relative to the pressure method and 6 times higher compared to conventional measuring devices. This method is versatile and can be applied for a wide range of bearing sizes.

**Keywords:** hydrostatic bearing; large-scale bearing; alignment method; pad surface leveling; bearing precision

check for updates

**Citation:** Foltýn, J.; Hurník, J.; Michalec, M.; Svoboda, P.; Křupka, I.; Hartl, M. Pad Alignment Methods and Their Impact on Large Hydrostatic Bearing Precision. *Machines* **2024**, *12*, 549. https://doi.org/10.3390/machines12080549

Academic Editor: Xiang Li

Received: 18 July 2024
Revised: 9 August 2024
Accepted: 9 August 2024
Published: 13 August 2024

**Copyright** © 2024 by the authors. Licensee MDPI, Basel, Switzerland. This article is an open access article distributed under the terms and conditions of the Creative Commons Attribution (CC BY) license (https://creativecommons.org/licenses/by/4.0/).

## 1. Introduction

Hydrostatic bearings were first introduced by the engineer L. D. Girard in 1851 [1]. The original bearing was driven by pressurized water and was used in railway transport. This pioneering innovation was publicly unveiled at the prestigious Industrial Exhibition in Paris in 1878 [2]. The hydrostatic bearing working principle is based on a complete separation of the sliding surfaces by a lubricating film [3–8]. The external pressurized lubricant supply allows for operation even at zero speed [9]. Hydrostatic bearings are often used in combination with hydrodynamic bearings to increase safety and stability during start and stop phases [2,10]. Compared to hydrodynamic bearings, hydrostatic bearings operate with a relatively thick lubricating film [11].

Hydrostatic bearings exhibit exceptional load-carrying capacity [12] and a high degree of stiffness, thereby ensuring the precision and stability requisite for accurate machinery [13]. Additionally, the movement is performed with minimal frictional losses and extremely low wear [14]. They are often used in applications with low rotational speeds, unlike in the case of hydrodynamic bearings.

On the contrary, hydrostatic bearings require higher initial cost. The design of the bearing involves consideration of the hydraulic system and its components [15]. While the bearings themselves experience minimal energy losses [8], the hydraulic pump demands a continuous energy supply to deliver pressurized lubricant to the bearing. At the same time, the hydraulic system is, in part, more prone to failure. Despite these limitations, hydrostatic bearings find extensive utility in various fields such as spindles [16], tables and guides [3], machine tools, antennas, and telescopes [17], where the advantages outweigh the disadvantages.

In the case of large-scale bearings reaching sizes up to tens of meters, it is not possible for some parts to be created in one piece or to secure desirable machining precision. Moreover, they are difficult to transport and assemble [18]. Still, the sliding surface of the bearing requires very high geometric accuracy [19].

One way to achieve higher precision is creating parts, such as a pad and slider, separately in substantial proportions. While this approach enhances the precision of the sliding surfaces and facilitates transportation, it introduces a new challenge of aligning the separate pads, what is in the literature [6,20] known as a multi-pad bearing (Figure 1). In the case of large bearings, it is necessary to ensure that the bearing pads are accurately aligned [21]. Incorrect positioning of the sliding surfaces can result in a failure of the lubricating film thickness or a direct collision of the sliding surfaces [22,23].

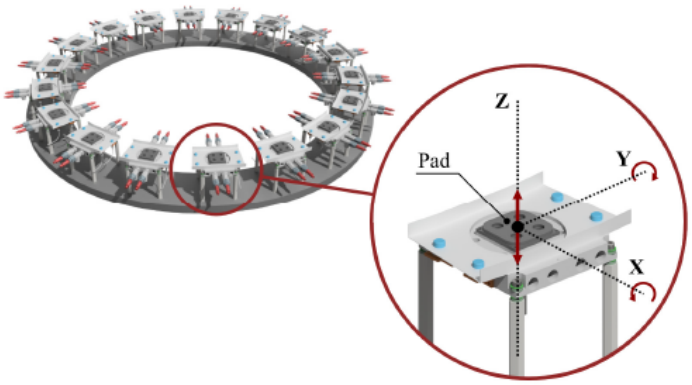


**Figure 1.** Scheme of multi-pad construction of hydrostatic bearing.

It is possible to use a compliant bearing pad support. This configuration allows the sliding surface to adapt its position, including height and tilt, to compensate misalignments within the deformations of the compliant member [24]. While this approach reduces the impact of manufacturing and assembly inaccuracies on the bearing structure, it significantly decreases the bearing's stiffness, rendering it unsuitable for high-precision applications [25].

In this case, where the stiffness of the bearing is crucial (machining centres, telescopes, etc.), compliant support cannot be used. In this case, the importance of accurate pad alignment is essential and directly affects the bearing precision and safety. Nonetheless, there is very limited knowledge of large-scale hydrostatic bearing pad alignment processes in the literature. The practical limits of the alignment methods are unknown; therefore, it is not clear which method should be chosen. There are three possible pad alignment methods, and each of them have advantages and disadvantages:

- Leveling using straightedge [26–28] and spirit level. This method is the simplest one and does not need any specialized equipment, which is an advantage. The disadvantage of this method is its complicated use on large scales.
- Leveling the pads using information about pressure from bearing recesses. The advantage of this method is that it can work online. The disadvantage is that the alignment is carried out based on indirect information and an estimation of the film thickness and could be compromised by the precision of machined sliding surfaces and pressure sensors.
- Leveling based on the coordinate measurement machine (CMM). Such systems are accurate (as the only method, its accuracy could be certified), but not portable, mainly in the case of large scales, and the leveling process can be time-consuming. Optical coordinate measurement machines can overcome the problem associated with portability and flexibility, ensuring sufficient accuracy [29]. Such methods offer the potential for greater alignment accuracy [30].

Although these advantages and disadvantages are straightforward, the evaluation of their real capabilities is not. The leveling of a large hydrostatic bearing several meters in diameter, with the desired accuracy in tenths of millimeters, or less, is a complicated task.

Moreover, the accuracy of the first two methods is not clear. In this study, the question of which alignment method provides the highest precision for large-scale hydrostatic bearings was investigated by comparing these possible methods head-to-head.

## 2. Materials and Methods

In this section, a comprehensive overview of the experimental setup used in the presented paper is provided, along with the alignment methods used. A detailed description of the experimental device is discussed, detailing the instruments and sensors used.

### *2.1. Prediction of Lubricating Film Thickness*

Analytical prediction of the lubricating film thickness was used to verify the proper design of the hydrostatic bearing pad geometry. This prediction was also used to evaluate the suitability of the selected alignment methods. The prediction follows the circular shape of a four-recessed pad,

$$h = \sqrt[3]{\frac{Q \cdot A \cdot \mu}{F \cdot q_f}}$$

where h is the thickness of the lubricating film, Q is the flow of the lubricant through the bearing, A is the projected area of the pad, μ is the dynamic viscosity of the used lubricant, F is the loading force, and $q_f$ is the flow factor. The recess pressure was again taken from the prediction relationship. The pressure prediction determines the carrying load capability of the hydrostatic bearing.

$$p_r = p_f \cdot \frac{F}{A}$$

The equation involves the recess pressure $p_r$, pressure coefficient $p_f$, force per pad F, and the projected area of the pad A. The coefficients $p_f$ and $q_f$ correspond to the geometry of the pad. These coefficients are read from the graph [31].

### *2.2. Experimental Hydrostatic Bearing Device*

The experimental hydrostatic bearing device (Figure 2) consisted of two pads, a load frame and a hydraulic unit. The pad geometry was designed with four circular recesses. Each of the recesses had a restrictor of the type throttling valve before the inlet. The lubricating film thickness measurement (h) was provided by contactless inductive proximity sensors with a precision of ±0.01 mm and a range of 3 mm. The pressure in the recess ($p_r$) was measured with a precision of ±0.56 bar. The load (F) was applied by tightening four threaded rods, at the end of which a force sensor with a precision of ±0.003 kN was mounted, and the load can be applied up to 60 kN. The hydraulic unit was designed to supply a flow rate (Q) of up to 10 L/min at a pressure of 100 bar. The flow rate was measured by a flow meter with a precision of ±0.2 L/min.

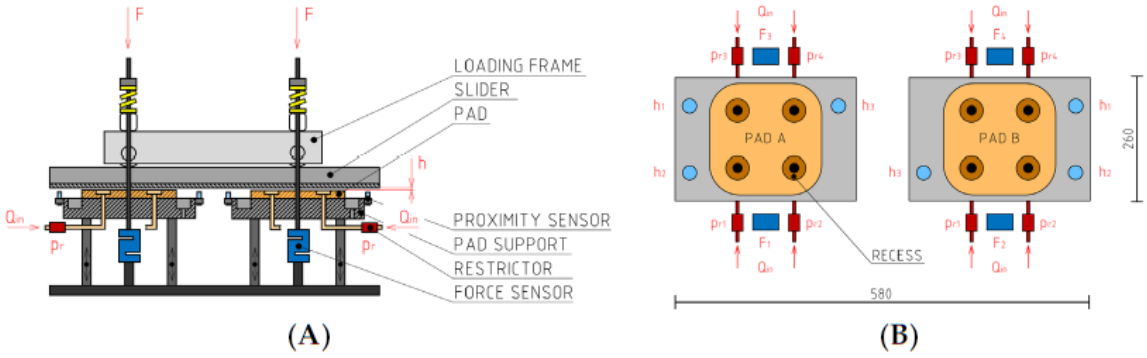


**Figure 2.** (A) Scheme of the experimental device 2PAD; (B) top view of experimental device 2PAD.

Prior to the actual measurement, elements generating errors in measured data were identified. The collective errors of the measuring elements are shown in the following table (Table 1) together with the measurement range.

**Table 1.** Errors of the sensors used on the experimental device 2PAD.

| | Max. Range | Precision |
|---|---|---|
| **Force gauge** | 14.7 kN | ±0.003 kN |
| **Flowmeter** | 15 L/min | ±0.2 L/min |
| **Proximity sensor** | 3 mm | ±0.01 mm |
| **Pressure gauge** | 160 bar | ±0.56 bar |
| **Thermometer** | 100 °C | ±1 °C |

There were also other errors in terms of calculation and manufacturing. Since the calculation consists of the reading coefficients from the graph, an 8% reading error was considered. At the same time, the pads were manufactured to a dimension with a certain tolerance. This tolerance affected the projected bearing area, which further affected the bearing load capacity. To determine the effect of the error on thickness and pressure, the maximum and minimum were entered into the corresponding prediction equation. Finally, the total measurement error was taken for the worst-case scenario. The sum of the calculated errors was determined using the raw data (the values displayed in the table were rounded after the calculation). Lubricating film thickness and recess pressure were selected as the most important hydrostatic bearing parameters to be assessed. The distribution of both thickness and pressure determined the safety of the bearing. Therefore, the influence of the defined errors on the thickness and pressure was considered (Table 2).

**Table 2.** Effect of error on thickness and pressure from highest influence to lowest.

| **Influence on Pressure** | |
|---|---|
| **Effect of $p_f$ coefficient reading error** | ±0.684 bar |
| **Effect of pressure measurement error** | ±0.56 bar |
| **Effect of manufacturing tolerance** | ±0.275 bar |
| **Effect of force gauge measurement error** | ±0.006 bar |
| **Total pressure measurement error** | **±1.525 bar** |
| **Influence on film thickness** | |
| **Effect of proximity sensor measurement error** | ±0.01 mm |
| **Effect of $q_f$ coefficient reading error** | ±0.0057 mm |
| **Effect of temperature error** | ±0.0027 mm |
| **Effect of flowmeter measurement error** | ±0.0018 mm |
| **Effect of manufacturing tolerance** | ±0.0015 mm |
| **Effect of force gauge measurement error** | ±0.00005 mm |
| **Total thickness measurement error** | **±0.02164 mm** |

### *2.3. Conventional Measurement Instruments*

Commonly available precise measuring devices were used for comparison. The instruments were needed to detect the relative tilt and relative height of the pads. To align the sliding surfaces, a straightedge made of an I-shaped profile with a length of 1 m was used. This shape guaranteed high stiffness in the direction perpendicular to the measured plane. The contacting surfaces were machined and grinded to an accuracy of 0.01 mm on both sides.

The tilt of the runner was measured in two axes with a precision spirit level. This spirit level had a magnetic seating surface, which ensured contact between the spirit level and the straightedge. The precision of the spirit level equated to 0.02 mm/m. The first part of the alignment consisted of leveling (Figure 3) the outer edges of the pads. This helped to simplify the whole measurement. Then, the remaining two inner edges of the pads had to

be adjusted in height. The angle in the two axes was constantly monitored, along with the contact of the straightedge with the pad surface.

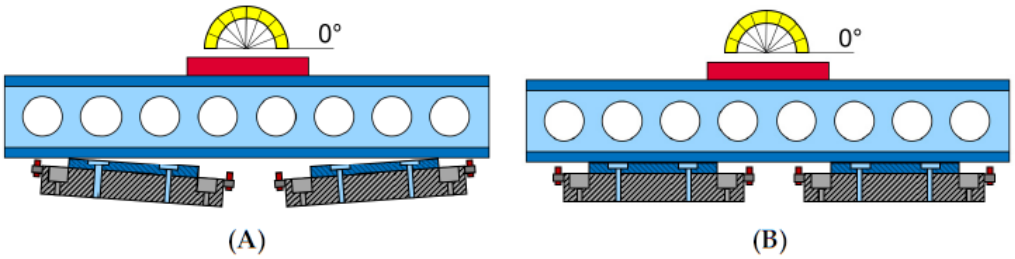


**Figure 3.** (**A**) Initial phase of planar aligning of the pad edges; (**B**) final state of the alignment by straightedge.

### *2.4. Pressure Method*

The second pad alignment method assumes that the lubricating film thickness was distributed evenly across the bearing pad; the pressure in the recess must also be equally distributed. If a pressure decrease occurs in a recess, the sliding surfaces are likely to contact. Flow control device restrictors were mounted at each pad inlet, securing the same flow; thus, even pressure is expected in each recess.

Alignment was then carried out by adjusting the corner height of the pad until the recess pressures (Figure 4) were equalized (within the accuracy of the sensors). If there was a pressure difference, the pad was recalibrated. For this reason, it was necessary to know the recess pressure information and the lubricating film thickness from at least 3 places on the pad. Therefore, the recess inlets needed to be equipped with pressure gauges and proximity sensors needed to be placed on the sides of the pad. Pressure gauges with a precision of ±0.56 bar were used.

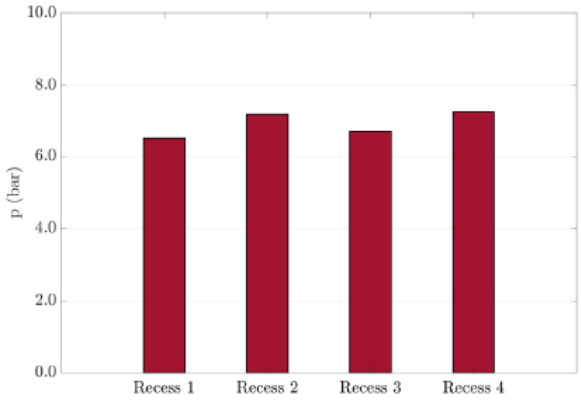


**Figure 4.** Resulting pressure distribution of pad B after setting.

### *2.5. Optical Measurement*

The alignment of the bearing pads can be assessed using a multi-point optical coordinate measurement machine (OCMM). The measurement result of such a system was 3D coordinates of special circular targets that adhered to the object's surface which were, in this case, the corners of the pad. A plane, representing an ideal planar surface of the slider, was fitted into these corner points using the best-fit method (Figure 5), and their deviations were calculated. These deviations were used to correct the position of pads.

The OCMM measurement includes imaging the scene with a digital camera from different angles, making it possible to accurately triangulate circular targets. Such photogrammetric measurement systems are accurate, portable, and can be used to measure a wide range of measurement volumes, up to the order of meters. This makes the method suitable for both small and large bearings. Moreover, no dedicated sensors on the bearing

are needed, which makes this option also economical. A disadvantage could be the lack of online pad alignment control.

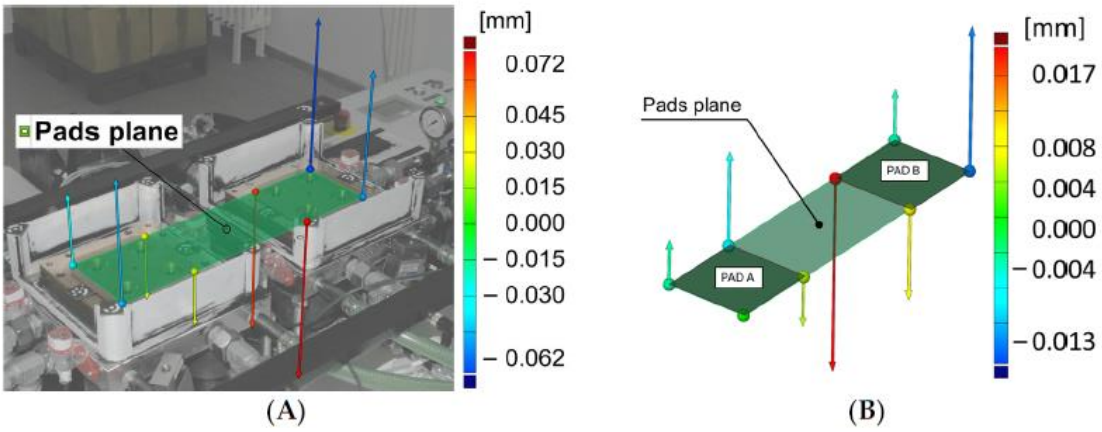


**Figure 5.** (A) Measurement setup of OCMM method; (B) final iteration–measured deviations.

In this work, the GOM TRITOP (Zeiss, Oberkochen, Germany) multi-point OCMM was used. It was based on a Nikon D300s camera (Nikon, Tokyo, Japan) equipped with a 24 mm Titanar objective (Schneider Kreuznach, Bad Kreuznach, Germany). The employed version of the TRITOP software was 7.5. Carbon fiber scale bars with approx. 1000 mm length and 3 mm targets were used. According to the quality indicators of the measurement project, the average distance of the image points to the respective reference points varied between 0.011 and 0.012 mm.

As the purpose of this work was to reveal the suitability of the alignment methods for hydrostatic bearings, there was a difference in the preparation phase of the experimental setup according to the respective method. The start-up phase of the bearing together with the data recording were already common. Thus, it will be possible to evaluate the change in the thickness with respect to the bearing initial condition and to determine the behavior of the bearing with manufacturing errors during operation. Also, the ambient conditions were unified to a total load of 20 kN and a total flow rate of 6 L/min. After setting up each method, the slider was moved to predefined positions. There were 4 positions defined in this way. The starting position for alignment included sliding 50 mm in the direction of pad A, sliding 50 mm in the direction of pad B, and returning to the starting position. Since the slider moves in a real situation, this movement reflects the actual conditions and ensures the repeatability of the measurements.

## 3. Results and Discussion

The average lubricating film thickness and average recess pressure were evaluated for each series of measurements using a particular method (Figure 6). The first series of results showed a comparison of pad A and pad B relative to the reference value (red line). In all cases, the error intervals are taken as the cumulative error of the measurement, sensing, and data logging. The OCMM method was able to achieve thicknesses of 0.136 mm and 0.141 mm. Such bearing film thicknesses agreed with the predicted thickness value of 0.155 mm. The deviation was due to manufacturing inaccuracies of the pocket and slider, which were not included in the analytical prediction of the ideal condition. Further, the pressure method set the bearing to a lubricating film thickness of 0.133 mm and 0.128 mm. From a safety point of view, the bearing is at a lower lubricating film thickness but still in agreement with the prediction. In contrast, the method using conventional measuring devices had the largest variation in lubricating film thickness. Despite the relatively high thickness value of 0.144 mm, the bearing had the worst thickness distribution between the pads. Pad B was more heavily loaded, resulting in a low average thickness value of 0.109 mm due to unsuitable load distribution.

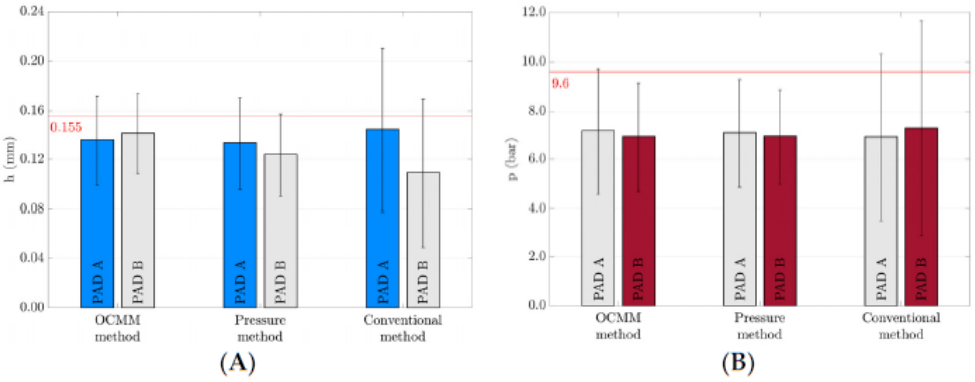


**Figure 6.** (**A**) Distribution of the average lubricating film thickness; (**B**) average pressure distribution.

The second set of data is focused on pressures that are generally dependent on the carried load by the hydrostatic bearing. From this point of view, the pressure values were at the same level since the load was the same in all cases. However, compared to the analytical prediction (9.6 bar line), there is a significant difference. The fact that the prediction does not consider inputs other than force, pressure coefficient, and bearing area may play a major role. Effects such as the type of restrictor used and manufacturing tolerances are not included at all. In addition, the biggest influence on the error rate in the pressure prediction calculation comes from reading the pressure coefficient from the graph.

The alignment of the pads is crucial for even lubricating film thickness distribution and thus for overall bearing precision; the methods were also compared from this point of view. The deviation of the measured values is plotted in the graph (Figure 7). The smallest error range was achieved using the OCMM method. Here, it can be concluded that the possible compensation of the irregularity by lubricating film will not have a fatal effect on the bearing operation. A similar result was achieved with the pressure method, although there was already a greater dispersion of thickness values over the surface. Hydrostatic bearing aligned with conventional measuring instruments shows the greatest differences in film thickness. The risk of lubricating film failure is greater in a hydrostatic bearing aligned using this method. Important aspects are selected in the table (Table 3). In the case of maximum deviations, the worst-case situation is taken, where such an unfortunate combination of errors can occur.

Based on the obtained results, we can conclude that using the OCMM method can allow for the most precise bearing alignment from the selected methods to be achieved. This method aligned the bearing to an accuracy of ±0.01 mm. This degree of accuracy is particularly important in applications requiring high precision and high stiffness. One of the key benefits of the OCMM method is that the lubrication film thickness achieves the highest average values. This ensures that the bearing operates in an optimal mode, which not only increases its lifetime but also secures a high precision. A uniform distribution of the lubricating film thickness is desirable in cases where there are some errors in the system (manufacturing, assembly), and this contributes to the overall reliability of the bearing. The OCMM method uses sensors as a verification element. This use of sensors is associated with ensuring the consistency of the measurement. However, it is important to note that the OCMM method itself does not require the acquisition of information from sensors to perform. Bearing leveling included five measurement leveling iterations. In each iteration, the bearing was measured and fixed according to the result (using the assembly personnel estimation). The reason why so many iterations were needed was the four-support pad mounting system, which was statically indeterminate. Therefore, it was not clear how the shift in support influenced the overall position of the pad. However, in the future, the pad mounting system can be created with only three supports to reduce the number of iterations.

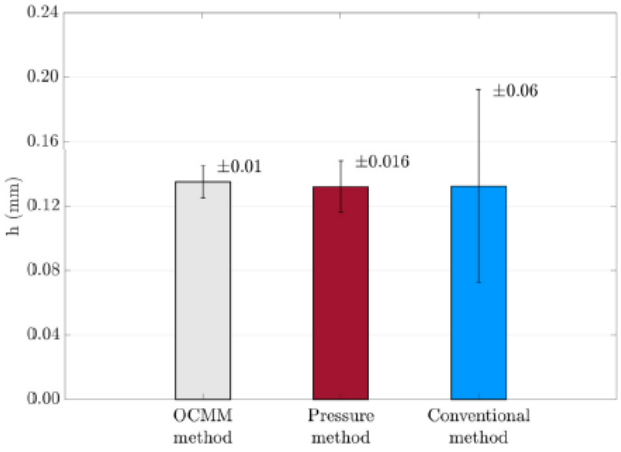


**Figure 7.** Comparison of film thickness distribution over pad area.

**Table 3.** Comparison of leveling methods.

| | OCMM Method | Pressure Method | Conventional Method |
|---|---|---|---|
| **Accuracy of alignment** | h ± 0.01 mm | h ± 0.016 mm | h ± 0.06 mm |
| **Deviation of film thickness** | 7.4% | 12.1% | 45.3% |
| **Repeatability** | High | High | Low |
| **Alignment difficulty** | Medium | Low | High |
| **Time consumption** | Medium | Low | High |

The pressure method is a different approach used to achieve relatively accurate bearing alignment. This method focuses on monitoring two key parameters: lubricating film thickness and pressure. To monitor these parameters, it is necessary to equip the bearing with sensors that allow for continuous data collection. The sensors allow for the actual lubrication film thickness and pressure to be monitored, allowing operators to react more accurately to changes and make necessary adjustments. This minimizes the risk of unwanted bearing wear or other lubrication-related problems. However, it must be considered that the pressure method is subject to sensor measurement errors. Inaccuracies in sensing lubricating film thickness or pressure can affect the accuracy of the entire process. This means that in addition to the advantages, this method can be sensitive to the quality and calibration of the sensors used.

The method of alignment using conventional measuring instruments enabled the bearing to be aligned to a sufficient condition. The lubricating film thickness reached positive values in all the measured points. However, there was a large variation in the lubricating film thickness values. Despite the theoretically good accuracy of the measuring instruments, the main limitation is the influence of the human factor. Significant thickness variations contribute to the instability of the whole bearing. Particularly in areas with lower film thicknesses, potential collisions and disruptions can occur. To minimize these uncertainties and achieve the highest degree of accuracy, the entire measurement procedure was repeated, with each repetition producing different results.

## 4. Conclusions

This study presents an experimental evaluation and assessment of alignment methods used for large hydrostatic bearings. The results indicate that it is possible to align the bearing using all the selected methods with a relatively high accuracy yet with different precision. This means that the averaged resulting film thickness values measured after the alignment are very similar, but the standard deviation from the average value differs significantly. The OCMM method showed the best results from the selected three approaches. It exhibited the best agreement with the predicted film thickness and recess pressure while maintaining minimal film thickness variation across the pad area. This method does not

require pressure or proximity sensors for alignment and is versatile for various hydrostatic bearing sizes. The pressure alignment method offers a way to achieve acceptable alignment precision; nonetheless, it requires information about pressure and film thickness. This relates to the necessity of equipping many sensors on the bearing and subsequent processing and evaluation of the obtained data. The alignment of pads using conventional methods is greatly influenced by the human factor during the performance of the aligning procedure. Its final precision was six times lower than that of the OCMM method. As the results show, the error magnitude was close to the range of the film thickness; thus, it is not satisfactory. Additionally, the size of the measuring instruments and the complexity of manipulation increase with the bearing size accordingly. Therefore, conventional measurement devices can be used for initial bearing alignment. For the further exploration of alignment methods, optical methods appear to be a promising approach. This approach effectively considers any manufacturing or assembly errors in bearing alignment. Hydrostatic bearing precision can be further improved by implementing feedback control, which can effectively handle any residual misalignment.

**Author Contributions:** Conceptualization, J.F. and P.S.; methodology, J.F.; software, J.H.; validation, J.F., J.H. and M.M.; formal analysis, M.M.; investigation, J.F., J.H. and M.M.; resources, J.F.; data curation, J.F.; writing—original draft preparation, J.F.; writing—review and editing, M.M.; visualization, J.H.; supervision, P.S., I.K. and M.H.; project administration, P.S.; funding acquisition, P.S. All authors have read and agreed to the published version of the manuscript.

**Funding:** This research was carried out under the project FW03010357 with financial support from the state budget by the Technology Agency of the Czech Republic and the Ministry of Industry and Trade within the TREND Programme. The research was co-funded by Faculty of Mechanical Engineering, Brno University of Technology internal specific project FSI-S-23–8340.

**Data Availability Statement:** The data presented in this study are available on request from the corresponding author.

**Conflicts of Interest:** The authors declare no conflict of interest.

## References

1. Girard, L.D. *Hydraulique Appliquée: Nouveau Système de Locomotion sur les Chemins de Fer*; Bachelier: Paris, France, 1852.
2. Rowe, W.B. Advances in Hydrostatic asnd Hybrid Bearing Technology. *Proc. Inst. Mech. Eng. Part C Mech. Eng. Sci.* **1989**, *203*, 225–242. [CrossRef]
3. Rowe, W.B. Application of Hydrostatic Bearings. In *Hydrostatic and Hybrid Bearing Design*; Elsevier: Amsterdam, The Netherlands, 1983. [CrossRef]
4. Bernstein, R.A.; McCarthy, P.J.; Raybould, K.; Bigelow, B.C.; Bouchez, A.H.; Filgueira, J.M.; Jacoby, G.; Johns, M.; Sawyer, D.; Shectman, S.; et al. Overview and status of the Giant Magellan Telescope project. In *Ground-Based and Airborne Telescopes V*; SPIE: Bellingham, WA, USA, 2014; ISBN 9780819496133. [CrossRef]
5. Wasilczuk, M. Friction and Lubrication of Large Tilting-Pad Thrust Bearings. *Lubricants* **2015**, *3*, 164–180. [CrossRef]
6. Rippel, H.C. *Cast Bronze Hydrostatic Bearing Design Manual*; Cast Bronze Bearing Institute: Cleveland, OH, USA, 1969.
7. Loeb, A.M. The Determination of the Characteristics of Hydrostatic Bearings through the use of the Electric Analog Field Plotter. *ASLE Trans.* **1958**, *1*, 217–224. [CrossRef]
8. Michalec, M.; Ondra, M.; Svoboda, M.; Chmelík, J.; Zeman, P.; Svoboda, P.; Jackson, R.L. A Novel Geometry Optimization Approach for Multi-Recess Hydrostatic Bearing Pad Operating in Static and low-Speed Conditions Using CFD Simulation. *Tribol. Lett.* **2023**, *71*, 52. [CrossRef]
9. Wang, Y.; Liu, Z.; Cheng, Q.; Zhao, Y.; Wang, Y.; Cai, L. Analysis and optimization of nonlinear carrying performance of hydrostatic ram based on finite difference method and Runge–Kutta method. *Adv. Mech. Eng.* **2019**, *11*, 1687814019856128. [CrossRef]
10. Bouyer, J.; Wodtke, M.; Fillon, M. Experimental research on a hydrodynamic thrust bearing with hydrostatic lift pockets: Influence of lubrication modes on bearing performance. *Tribol. Int.* **2022**, *165*, 107253. [CrossRef]
11. Wen, S.; Huang, P. *Principles of Tribology*; Wiley: Hoboken, NJ, USA, 2012; ISBN 9781119214892.
12. Bassani, R.; Piccigallo, B. *Hydrostatic Lubrication*; Elsevier: Amsterdam, The Netherlands, 1992; ISBN 044488498.
13. Neichel, B.; Mouillet, D.; Gendron, E.; Correia, C.; Sauvage, J.F.; Fusco, T. Overview of the Eu-ropean Extremely Large Telescope and its instrument suite. *arXiv* **2018**, arXiv:1812.06639.
14. Stachowiak, G.; Batchelor, A.W. *Engineering Tribology*, 3rd ed.; Butterworth-Heinemann: Oxford, UK, 2006.

15. Hamrock, B.J.; Schmid, S.R.; Jacobson, B.O. *Fundamentals of Fluid Film Lubrication*, 2nd ed.; CRC Press: Boca Raton, FL, USA, 2004; ISBN 0824753712.
16. Fang, C.; Huo, D.; Huang, X. A comprehensive analysis of factors affecting the accuracy of the precision hydrostatic spindle with mid-thrust bearing layout. *Int. J. Adv. Manuf. Technol.* **2021**, *114*, 949–967. [CrossRef]
17. Marchiori, G.; Rampini, F.; Ghedin, L.; Bressan, R. ELT design status: The most powerful ground telescope. In *Ground-Based and Airborne Telescopes VII*; SPIE: Bellingham, WA, USA, 2018; Volume 10700, ISSN 1996756X. [CrossRef]
18. Michalec, M.; Svoboda, P.; Křupka, I.; Hartl, M. A review of the design and optimization of large-scale hydrostatic bearing systems. *Eng. Sci. Technol. Int. J.* **2021**, *24*, 936–958. [CrossRef]
19. Zhang, P.; Chen, Y.; Zhang, C.; Zha, J.; Wang, T. Influence of geometric errors of guide rails and table on motion errors of hydrostatic guideways under quasi-static condition. *Int. J. Mach. Tools Manuf.* **2018**, *125*, 55–67. [CrossRef]
20. Khonsari, M.M.; Booser, E.R. *Applied Tribology*; Wiley: Hoboken, NJ, USA, 2017; ISBN 9781118637241. [CrossRef]
21. Jang, J.Y.; Khonsari, M.M. On the Characteristics of Misaligned Journal Bearings. *Lubricants* **2015**, *3*, 27–53. [CrossRef]
22. Andre's, L.S. Effects of Misalignment on Turbulent Flow Hybrid Thrust Bearings. *J. Tribol.* **2002**, *124*, 212–219. [CrossRef]
23. Dhanola, A.; Garg, H.C. Tribological challenges and advancements in wind turbine bearings: A review. *Eng. Fail. Anal.* **2020**, *118*, 104885. [CrossRef]
24. Van Beek, A.; Segal, A. Rubber supported hydrostatic thrust bearings with rigid bearing surfaces. *Tribol. Int.* **1997**, *30*, 47–52. [CrossRef]
25. Michalec, M.; Polnický, V.; Foltýn, J.; Svoboda, P.; Šperka, P.; Hurník, J. The prediction of large-scale hydrostatic bearing pad misalignment error and its compensation using compliant support. *Precis. Eng.* **2022**, *75*, 67–79. [CrossRef]
26. Yang, Y.; Wang, T.; Dai, L. Research on straightness calibration method of straight edge working face based on electronic level. In Proceedings of the MATEC Web Conferences: 5th International Conference on Advances in Materials, Machinery, Electronics (AMME 2022), Dali, China, 13–15 May 2022; Volume 363, p. 01013. [CrossRef]
27. Elmelegy, A.; Zahwi, S. Comparative study of error determination of machine tools. *Int. J. Adv. Manuf. Technol.* **2023**, *124*, 4575–4602. [CrossRef]
28. Gunnels, S. The Giant Magellan Telescope (GMT): Hydrostatic Constraints. In *Ground-Based and Airborne Telescopes III*; Stepp, L.M., Gilmozzi, R., Hall, H.J., Eds.; SPIE: Bellingham, WA, USA, 2010; Volume 7733. [CrossRef]
29. Michalec, M.; Hurník, J.; Foltýn, J.; Svoboda, P. Contactless measurement of hydrostatic bearing lubricating film using optical point tracking method. *Proc. Inst. Mech. Eng. Part J J. Eng. Tribol.* **2023**, *237*, 76–84. [CrossRef]
30. Zha, J.; Xue, F.; Chen, Y. Straightness error modeling and compensation for gantry type open hydrostatic guideways in grinding machine. *Int. J. Mach. Tools Manuf.* **2017**, *112*, 1–6. [CrossRef]
31. Loeb, A.M.; Rippel, H.C. Determination of Optimum Proportions for Hydrostatic Bearings. *ASLE Trans.* **1958**, *1*, 241–247. [CrossRef]


**Disclaimer/Publisher's Note:** The statements, opinions and data contained in all publications are solely those of the individual author(s) and contributor(s) and not of MDPI and/or the editor(s). MDPI and/or the editor(s) disclaim responsibility for any injury to people or property resulting from any ideas, methods, instructions or products referred to in the content.

ASME Journal of Tribology
Online journal at:
https://asmedigitalcollection.asme.org/tribology

**Jan Foltýn**[1]
Faculty of Mechanical Engineering,
Brno University of Technology,
Brno 61669, Czech Republic
e-mail: jan.foltyn@vut.cz

**Erito Flores**
European Southern Observatory,
Very Large Telescope,
Paranal 19001, Chile
e-mail: eflores@eso.org

**Mario Tapia**
European Southern Observatory,
Very Large Telescope,
Paranal 19001, Chile
e-mail: mtapia@eso.org

**Nicolás Álvarez**
European Southern Observatory,
Very Large Telescope,
Paranal 19001, Chile

**Michal Michalec**
Faculty of Mechanical Engineering,
Brno University of Technology,
Brno 61669, Czech Republic
e-mail: michal.michalec@vut.cz

**Petr Svoboda**
Faculty of Mechanical Engineering,
Brno University of Technology,
Brno 61669, Czech Republic
e-mail: petr.svoboda@vut.cz

# Failure Prevention Procedure of the Very Large Telescope Hydrostatic Bearing Pads Based on the Lubricating Film Thickness Measurement

*Maintaining a uniform film thickness is crucial for ensuring the safety of hydrostatic bearings in telescopes. If the lubricating film is disrupted, it can lead to the collision of sliding surfaces, resulting in costly and time-consuming repairs. Since hydrostatic bearings enable the telescope movement, repairs interrupt observations. By monitoring film thickness, potential errors in specific bearing pads can be detected and addressed at an early stage. The current film thickness measurement method, using dial indicators, is applicable only under static conditions and can be influenced by human error when setting or reading the values. In contrast, using contactless sensors provides a more reliable and efficient method, ensuring higher safety for hydrostatic bearing systems. However, factors such as working conditions and the number of required sensors need to be considered. In this study, field tests were conducted to evaluate the current dial indicator method and simulate the effects of clogged capillary errors. The proposed contactless sensor setup was also tested under real conditions on bearing pads. The results indicate a potential approach for interpreting telescope movement scenarios. Given the serious consequences of bearing failure, regular monitoring of film thickness should be prioritized to mitigate the risk of significant damage.* [DOI: 10.1115/1.4068788]

*Keywords: hydrostatic lubrication, oil film thickness, failure prevention, contactless measurement, bearings, diagnostics, fluid film lubrication*

## Introduction

Studying the Universe is one of the greatest challenges which lies before humanity. Studying objects and planets beyond our solar system may help to answer one of the oldest scientific questions "*Are we alone in the Universe?*". Such research would be impossible without the most advanced astronomical telescopes. The operation of a telescope requires a smooth service of many mechanical elements. A malfunction can disrupt valuable observation time and delay scientific breakthroughs. The component responsible for the altitude and azimuth axis movement of the telescope is the hydrostatic bearing (HBS). If a malfunction occurred in this system, the telescope would turn into an immovable mass of steel.

**Theoretical Background.** Hydrostatic bearings are sliding bearings where two surfaces are divided by a thin layer of fluid [1]. Separation is done by pressurizing the fluid in an external source (pump), thus hydraulic system must be incorporated. Hydrostatic bearings are often combined with hydrodynamic bearings to reduce wear [2] during the start and the stop phases [3]. The primary advantages of using hydrostatic bearings in large-scale applications such as reactors [4], machining centers [5], hydrogenators [6], and telescopes include their exceptional stiffness, effective damping characteristics, and high load-carrying capacity [7,8]. However, they also have certain limitations, such as the need for precisely machined sliding surfaces [9], a significant upfront investment, and high repair costs in the event of a failure.

The hydrostatic bearing (Fig. 1) consists of a pad in which one or more recesses are manufactured [10]. This recess is supplied by pressurized fluid through the inlet hole. When the recess pressure reaches a certain level, the sliding surfaces are separated, and fluid starts to flow through a narrow gap.

The movement of fluid through the sill area is related to the pressure drop. On the outer edge of the pad, the pressure of the fluid is

[1]Corresponding author.

Contributed by the Tribology Division of ASME for publication in the Journal of Tribology. Manuscript received April 1, 2025; final manuscript received May 27, 2025; published online June 19, 2025. Assoc. Editor: Ali Beheshti.

 Copyright © 2025 by ASME 

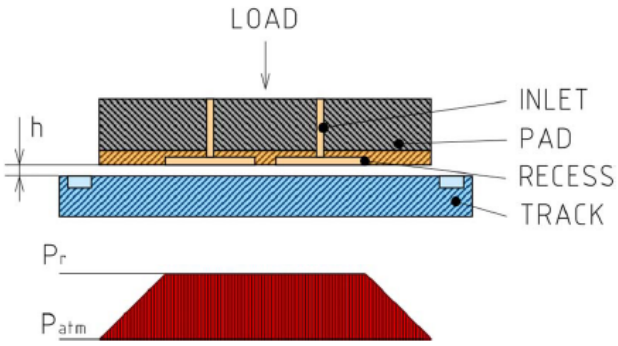


**Fig. 1 Scheme of hydrostatic bearing parts**

atmospheric. On the basis of load, geometry, and oil properties, the hydraulic parameters of the bearing can be calculated. The most important parameters are the recess pressure and the thickness of the film.

There are certain prediction approaches, such as numerical computational fluid dynamics [11,12], analytical, or experimental methods derived from the electrical field plotter [13]. These methods are based on the some ideal assumptions. Surfaces are perfectly smooth and flat, the load is evenly distributed, there are no deformations, the temperature doesn't change, and the pad and track are parallel. Real conditions, on the other hand, are not ideal. Manufacturing and assembly precision, uneven load [14,15], and temperature changes during the year, influence negatively resulting bearing performance. In the case of large-scale applications, manufacturing and assembly errors have a significant impact on the resulting positioning accuracy [16]. This is also due to the limitations in achievable manufacturing precision [17] caused by the large dimensions of the components. Bearing parts (pad, track) must be manufactured from multiple pieces to ensure transport and tight manufacturing tolerances [18]. The bearing composed of these segments incorporates misalignments [19] such as offset, incline, or tilt of connected pieces [20–23]. In a better case, these errors cause a decrease in the lubricating film thickness. The worst case, a fatal collision (metal-on-metal contact) of sliding surfaces can occur [24].

**Failure Investigation.** At the Paranal Observatory, the European Southern Observatory operates the Very Large Telescope (VLT), which comprises four unit telescopes (UTs). Each UT can function independently to conduct individual observations or work in unison as part of the VLT interferometer.

During the operation of UTs, the azimuth hydrostatic pads must be able to carry up to 500 $t$ with an oil film thickness of just 50 $\mu$m. The static part of the hydrostatic bearing, known as the track, consists of an outer ring and an inner ring (Fig. 2). The outer track ring reaches 20 m in diameter and consists of eight segments.

The track surface is not ideal from the perspective of hydrostatic bearing. There are errors that arise during the manufacturing process, such as surface roughness [25], surface waviness, and deviations from flatness, but also deformations caused by the oil pressure during the operation. There could be also some offset [26] between two track segments (Fig. 2). These conditions can lead to bearing failure or at least they influence the measurement of the film thickness.

As VLT telescopes reach 26 years of service, the probability of hydrostatic bearing-related failures may be increasing. There are two well-known failures of the hydrostatic bearing that have occurred in the last decade on UTs. The first is a clogged capillary. A capillary is a type of restrictor [27–29] that creates a pressure drop of the oil entering the recess of a hydrostatic bearing. The pressure drop is determined by the geometry of the capillary, specifically its length and internal diameter. In the case of UTs, the diameter is 1 mm. Although the hydraulic unit incorporates filters; particles

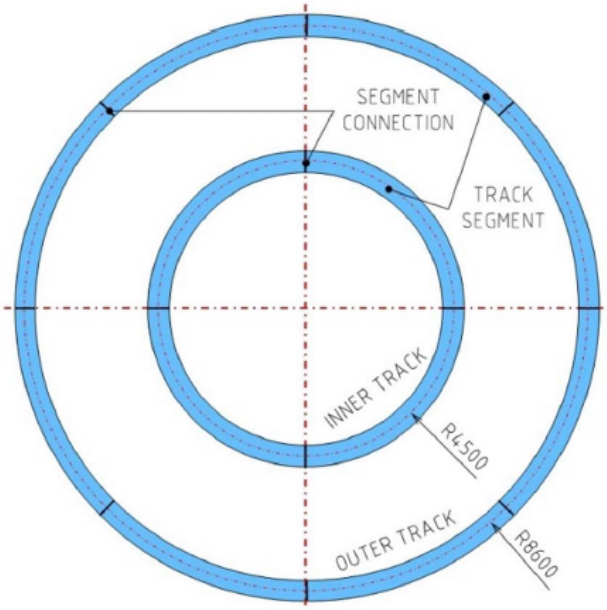


**Fig. 2 Scheme of track segments**

can reach the inlet of the capillary [30]. Clogging of one or more capillaries can cause failure of the pad. The pad should be able to operate with one clogged capillary, but the risk of failure increases dramatically. Another failure that can cause larger damage is the erosion of the glue between the bronze sliding surface and the steel foundation of the pad (Fig. 3).

Every pad has few spots where the glue can be exposed to pressured oil. Namely, those are the inlet hole to the recess, the hole of pressure sensor, and threated holes of fixing screws. These interfaces are sealed by O-rings, so theoretically, the oil should not reach the glue. Nonetheless, the investigation of an occurred failure showed that it is possible. The oil must have passed through one of these spots, as no other possibility was found.

A possible scenario is that there was some scratch or micro hole in the exposed surface of the glue layer. Under the pressure of the oil, the crack could propagate. Particles of glue could speed the whole process up due to abrasive behavior. The crack propagation continued, where the oil practically bypassed the bearing contact, and the pad lost its carrying capacity. Without oil flowing to the recess, there was no or very small recess pressure. The chamber over the pad is independent of the hydraulic system of the hydrostatic bearing, so it started to push the pad against the track even though there was no film thickness. Attempting to rotate the telescope resulted in scratches on both the pocket (Fig. 4) and the track.

Due to failure, other UT's bearing pads were checked. This problem was also found in another UT. In total, there were 33 hydrostatic pads that needed to be replaced. Such a failure required 2078 h of mechanical teamwork and nearly 7100€ for tools and items connected with repair. The hours of manufacturing new pads reached 70 h. However, the biggest impact was on observation time, which had to be postponed due to a malfunction. The key

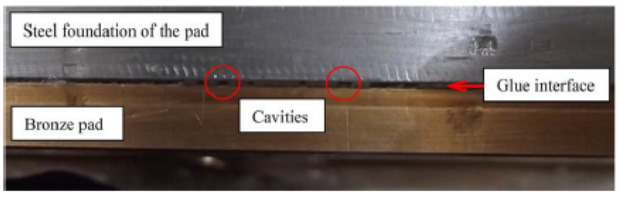


**Fig. 3 Detail of the interface between the steel and bronze part of the pad**

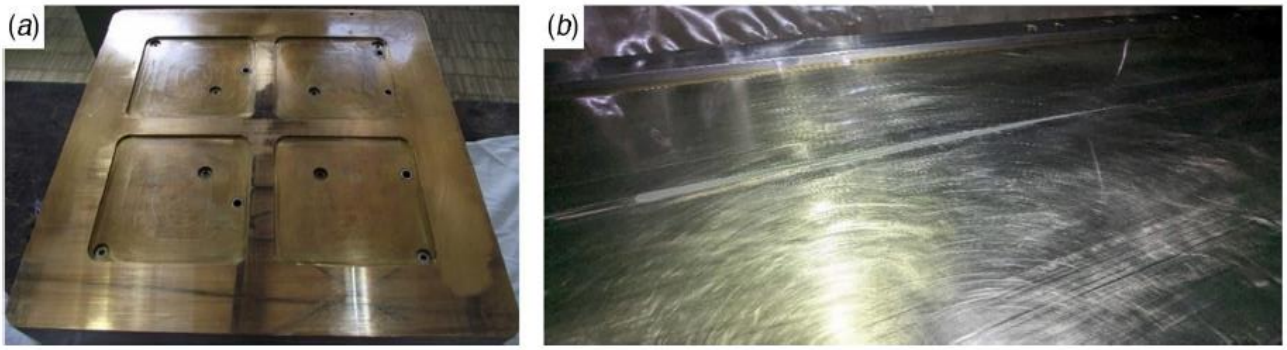


**Fig. 4** (*a*) Damaged sliding surface and (*b*) scratched track after pads glue failure—repaired by resin

highlights for incorporating film thickness measurement as warning criteria of the telescopes are as follows:

- For the safety measures, the oil film thickness measurement is a key procedure to understand the behavior of hydrostatic bearing.
- With incorporated film thickness measurement, the clogged capillary tube can be detected. Every pad has four capillary tubes. If one of them would be clogged by the particle in oil, the appropriate recess will lose carrying capacity and this behavior would be seen on the height of the corresponding pad corner. With only one recess pressure measurement, the clogged capillary can be detected with certainty only in 1 case out of 4.
- In the past, there was a failure of glue between the bronze sliding surface and the steel foundation of the pad. This state can be also captured by thickness measurement in the propagation stage (small cavity). The oil can erode the glue to the extent that oil will begin to flow through this cavity between bronze and steel. Since the layer of glue is around 2 mm, a fully propagated cavity will become the path for oil of the least resistance. Without oil in contact, the failure of oil film is inevitable. Here is the same situation as with the pressure measurement. Propagation would start from one recess, so it can be detected in 1 case out of 4.
- Based on the collected sensor data, preventive maintenance of the track can be done. In case where an offset between segments will be that large, the film thickness will be decreased on the critical value.
- If the mass of the telescope is out of the center of gravity it can overload part of the hydrostatic pads. Overload on one side of the telescope would be manifested in a decrease in the film thickness of the overloaded pads.
- One of the most severe failures during the operation of UTs is related to azimuth hydrostatic bearing pads.

## Material and Methods

From the mechanical point of view, the hydrostatic bearings of UTs are practically the same. Deviation that affects the film thickness measurement is different loads in each UT. The one with a higher load will have a smaller film thickness, or if the load changes (due new instrument, etc.), the film thickness will also change accordingly.

For each UT, the prediction of film thickness was calculated with respect to the UT's load. The resulting film thickness will give insights into what values should be expected and what resolution the sensors should have. Governing equations for load capacity and required flow are

$$W = p_r \cdot A_f \cdot \frac{(L-a)\cdot(l-b)}{L \cdot l} \tag{1}$$

$$Q = \frac{p_r \cdot h^3}{6 \cdot \mu} \cdot \left(\frac{l-b}{a} + \frac{L-a}{b}\right) \tag{2}$$

where $W$ (N) is the carried load by the hydrostatic pad, $p_r$ (Pa) is the recess pressure, $A_f$ ($m^2$) is the projected area of the pad, $Q$ ($m^3/s$) is the flowrate, $\mu$ (Pa · s) is the dynamic viscosity, $h$ (m) is the film thickness, and $L$, $l$, $a$, and $b$ (m) represent the lengths of the pad and recess sides.

The current film thickness measurement method uses digital dial indicators (Fig. 5). These indicators can be measured with a resolution of 1 $\mu$m. The measurements are done with a static telescope, because the movement of the dial indicator tip over a precise track could cause scratches during revolutions. The HBS pumping system is turned to standby and dial indicators are mounted on pads. In outer track is accessible even farther face of the pad so it is possible to mount all four corners with dial indicators. On the inner track, the situation is different. The far side of the pad is not accessible. That results in measurement only in three corners of the pad. Each axial pad is measured this way.

In the standby state, the dial indicators are zeroed. Then the pump is turned online and sliding surfaces are separated. Thickness is measured and written down. Then the dial indicators are zeroed again, and pumps are turned standby. The film thickness is checked again with regard to previous measurements to ensure repeatability.

The contactless measurement of the film thickness can overcome the disadvantages of the contact method. An inductive contactless distance sensor operates using electromagnetic induction to measure the distance to a conductive target. An excitation coil generates an alternating magnetic field, inducing eddy currents in nearby metal objects. This method ensures high precision, reliability, and immunity to dust or contaminants but works only with conductive materials. Measurement by dial indicators is done twice a year in each UT. With such a time frame, there is a very small chance of finding any failure in the propagation state. At the same time, the measurement with dial indicators is time-consuming and can be spoiled by human factors. The position of the dial indicator on the pad is not well restricted. The precision is dependent on the stiffness of the holding arm as well as on the precision of


**Fig. 5** Setup for film thickness measurement by dial indicators

positioning the tip on the track surface. These conditions incorporate uncertainties into the measured data. Contactless sensors on the other hand don't have these problems.

The pad has four degrees-of-freedom, one displacement and three rotations (Fig. 6). The displacement is caused by the chamber over the pad and allows movement in the *Z*-axis direction. The pad can also rotate around *X*, *Y*, and *Z* axes because of the pin tolerances located between the chamber and the pad.

From the film thickness measurement point of view, the rotation around the *Z*-axis has no impact on results. But rotations around *X*- and *Y*-axis can cause different heights on each corner of the pad. The sliding surface of the pad can be imagined as a 3D plane. With such degrees-of-freedom, the plane is unconstrained in space. To know exactly how the plane is oriented it is necessary to have at least three points of the plane, from the mathematical point of view. These points represent the necessary sensors to describe the sliding surface. If three points are known, the thickness under the last missing corner can be calculated. It must be stated that the calculated thickness will be approximated. Real thickness can be different due to deformations and surface imperfections.

Imperfections will influence the measurements of the film thickness. In the documentation of the design state, there was provided about expected deformations, tolerances, and other influencing errors. Deformation is present on the track under the surface of each pad and is caused by the applied pressure of oil. Generally, the sensors will be sensing undeformed areas of the track. The measured value of the lubricating film thickness could potentially be influenced by the deformation of surrounding bodies, resulting in a smaller thickness than predicted. Manufacturing conditions such as tolerances and surface roughness, on the other hand, would have a direct influence on measured values. Although the roughness value will be at the level of sensor sensitivity (1 $\mu$m), flatness (12 $\mu$m) can cause some fluctuation in height values. The same as that, the step or offset of 10 $\mu$m between each segment can negatively influence the data. These errors are not the only ones that can occur in UTs. They are numerically described. Influences such as uneven load of the telescope are not incorporated but can decrease the film thickness even more. On the other hand, the working temperature changes throughout the year. During hot days the film thickness would be smaller than on cold days because of changes in oil viscosity.

One pair of azimuth outer axial pads was mounted with eight distance sensors (four sensors on each pad). L-shape support was manufactured to hold the sensor at the exact location (Fig. 7). The used inductive sensors had a precision of 1 $\mu$m. The sensor was calibrated to a height of 1.5 mm between its tip and the track surface using precision shims. The dependence of the output voltage on the distance from the sensed object was linear within the 1.5 mm range. The data acquisition frequency was 1 Hz, at which a peak-to-peak noise level of 0 mV was reported.

## Results and Discussion

**Reference Measurement With Dial Indicators.** The procedure of measurement by dial indicators was executed. First, the dial indicators were mounted on the first half of the outer track pads (totally

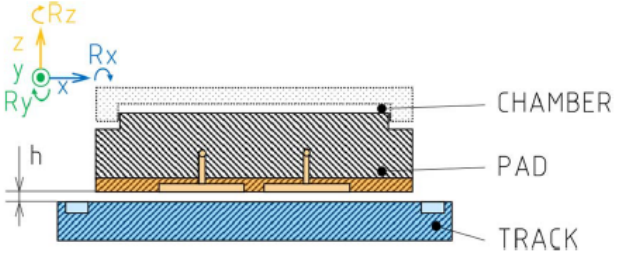


**Fig. 6 Scheme of the possible pad movement**

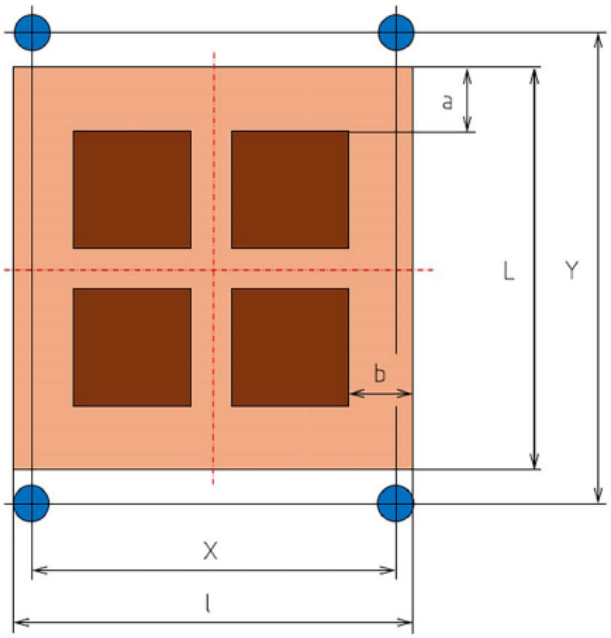


**Fig. 7 Essential geometry definition and position of sensors to reproduce a plane**

eight pads). When the HBS was turned standby, the dial indicators were zeroed. After the pumps were turned online, the oil layer was established, and film thickness was acquired. Following the recording of data at the established lubricating film thickness, the deflection indicators were re-zeroed. After the hydraulic circuit of the bearing was turned off, the film thickness was measured again to assess the repeatability of the measurements. The same procedure was performed for the second half of the pads. Measurement was dependent on the perpendicularity of the tip axis against the sensed surface. Because the tip of the dial indicator could scratch the track, the measurement can be done only during static conditions. The same procedure was done with inner track pads. The only difference was that each of the inner track pads could be mounted only by three dial indicators per pad. The reason is that there is not enough space to fit the dial indicator assembly. The measurement results of UT1 outer axial pads are shown in Table 1:

The film thickness is not evenly distributed through the surface of the pad. Also, there is uncertainty in the data because film thickness values indicate the pad was deforming. More likely the dial indicators were not exactly perpendicular to the track surface or there was possible movement of the magnetic support. Even with previous imperfections, it was possible to locate corners with clogged capillary using the current measurement method of the dial indicators. This situation happened on the outer axial support 7, pad 2 (OAX 7.2) pad. The corner A had a noticeably lower film thickness compared to the other corners, while the diagonally opposite corner D exhibited a higher film height. This indicates a clear tilting of the pad. After analyzing the measurement, the capillary on the A position was exchanged. Repeated film thickness measurement revealed that the corner A raised to 35 $\mu$m. There can be seen impact on measuring film thickness. Without measurement, it would be impossible to locate the clogged capillary or do some preventive maintenance. The oil thickness below 20 $\mu$m is below the safe limit and there is a high risk of collision. The sum of track flatness error and step between track segments can decrease the thickness down to microns.

**Initial Measurement With Contactless Sensors.** Film thickness, position of azimuth, velocity, and system pressure were logged. With these values, it was possible to determine the state of the telescope (Fig. 8). The sample rate of all measured values

Table 1 Measured data of oil thickness by dial indicators

| | Film thickness ($\mu$m) | | | | | |
|---|---|---|---|---|---|---|
| Pad | A | B | C | D | Avg. | Predicted |
| OAX 7.1 | 31 | 45 | 55 | 35 | 41.5 | 54.1 |
| OAX 7.2 | 17 | 30 | 38 | 58 | 35.8 | |

was 1 s. The test started with the telescope in the park position (139.55 deg) and HBS in the standby state. Next, the HBS was turned online. At a system pressure of 35 bar, the accumulator started charging, resulting in a noticeable pressure drop and a corresponding reduction in the lubricating film thickness. Subsequently, the pressure stabilized at an operating level of 85 bar. With a short delay, the azimuth axis was turned online as well. The telescope was moved with a constant speed of 2 deg/s to position –90 deg and then back to the parking position. After this procedure, the axis and HBS were turned to the standby state. In each stage, the delay was incorporated for capturing steady-state.

The sensors were able to capture the changes in the telescope movement. During the movement of the telescope, the data of film thickness were scattered. The scatter represents the effect of influential factors (roughness, flatness). This implies that continuous film thickness measurement would not be ideal during the operation of the telescope. More promising were the stable sections that occurred during the HBS online state. It was observed that the film thickness barely changed after the movement. This situation can be used for the preparation of preventive procedures for the measurement of film thickness. The measured data scatter was investigated during movement of the azimuth axis (Fig. 9). There was visible symmetry in film thickness values during movement in both directions. Trend changes are caused by the crossing of the track segment. There is a clear influence of assembly and manufacturing errors of the track segments. The most important conclusion is that during azimuth revolution of 230 deg the change in film thickness can reach up to 40 $\mu$m, which is nearly nominal value. Peaks are related to track segments and represent real situation of segment alignment. On the other hand, the variations in the lubricating film thickness were often observed as an increase over the nominal value, which did not negatively impact the bearing performance.

**Mathematical Calculation of the Pad Fourth Corner.** The equation of the plane was calculated for results from sensor testing. Even though the position was measured, the corner D was chosen as "unknown." Results can be seen in Fig. 10. The graph represents the measured film thickness of corner D (solid line) with regard to calculated values of the same corner (dashed line). There is a significant difference in results, with the calculated film thickness being larger than the experimental by up to 32%. The reason for this difference could be related to measuring conditions. Either uneven loading of the telescope or manufacturing and assembly tolerances of hydrostatic bearing can lead to cumulative error in sensed value. The base of the hydrostatic bearing pad can be deformed by the weight of the telescope itself and by the oil pressure. Even though it was stated that a minimum of three sensors per pad should be used (which is still true), four sensors would provide significantly more trustworthy results. With only three sensors, the uncertainty will be incorporated into the whole methodology.

**Simulation of Clogged Capillary—Measurement With Distance Sensors.** A clogged capillary was observed during measurement with dial indicators. It was shown that there is a deviation in the film thickness between the pad corners. The test was

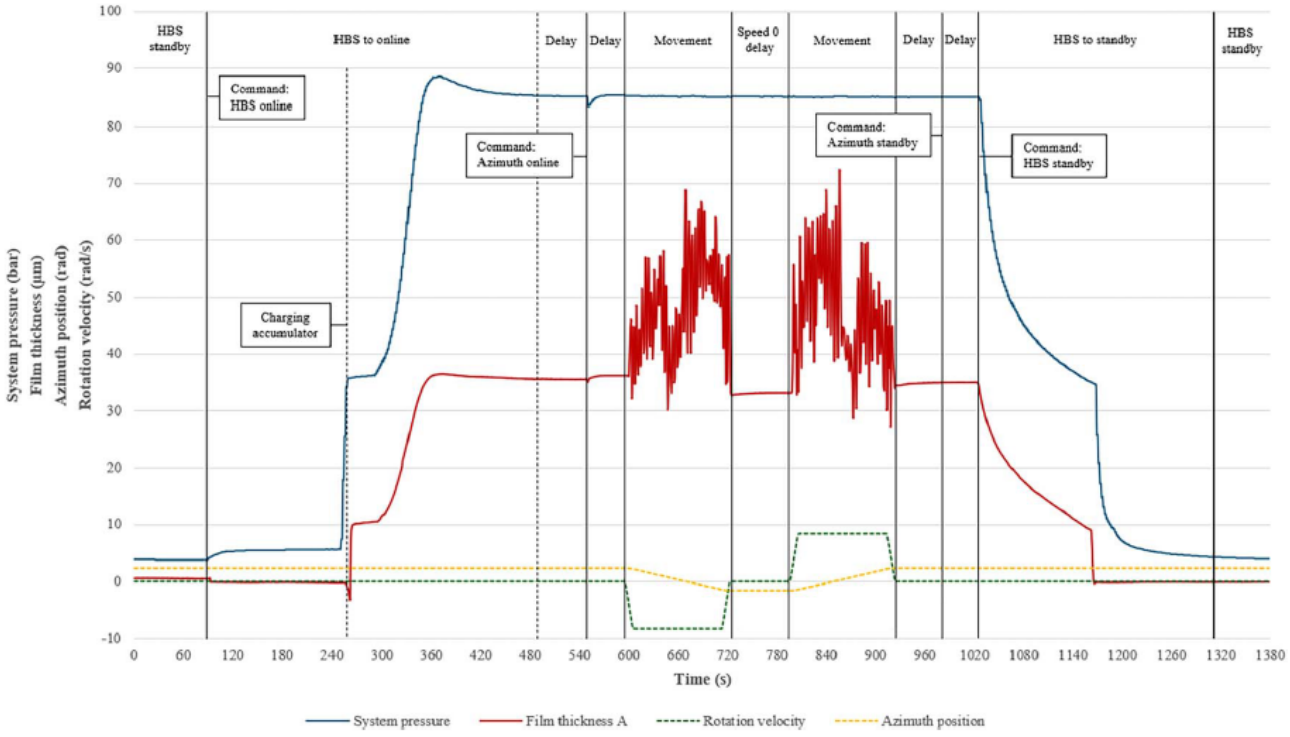


Fig. 8 Measurement procedure results of film thickness

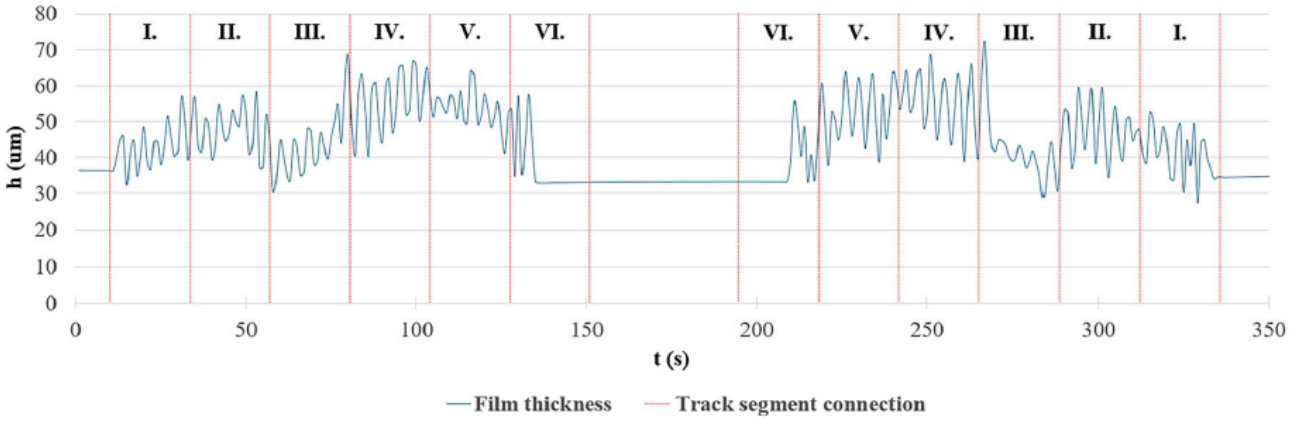


Fig. 9 Graph of lubrication film thickness data during telescope rotation

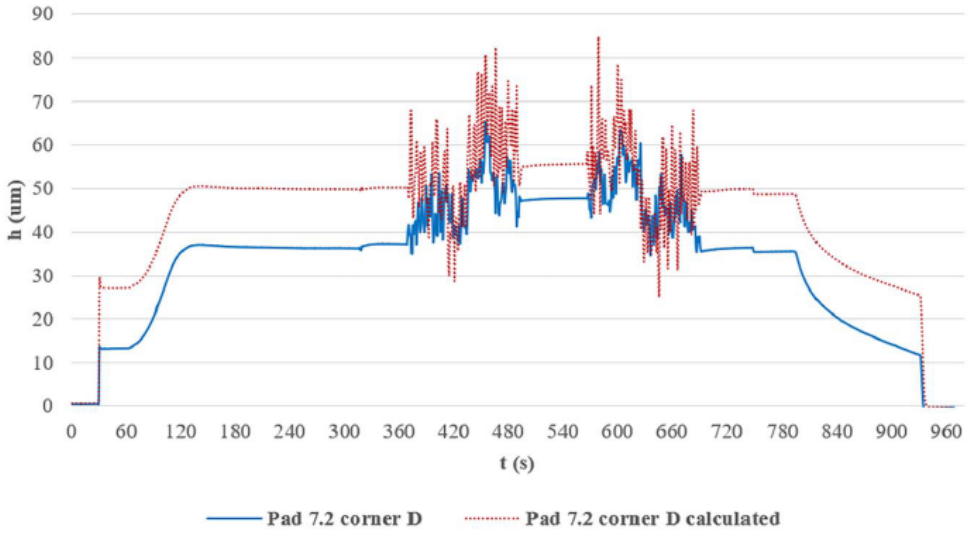


Fig. 10 Comparison of measured and calculated film thickness

reproduced with distance sensors. Special caps were manufactured to close the capillary inlet and outlet. The pad behavior was expected to be the same as that of clogged capillary. The clogged corner will be lower than the rest. The procedure of measuring film thickness with contactless sensors was followed by the measurement with dial indicators (Fig. 11). The test was carried out under static conditions. The film thickness logging started with telescope HBS on standby (I.). Then the HBS was changed to an online state (II.). After a delay (III.), the HBS was changed back to standby (IV.). This measurement was done before clogging capillary (A), during one capillary was clogged (B), and again with all four capillaries mounted (C).

The first graph (A) represents the initial state. All four capillaries were connected. The data logging started with HBS on standby. The pressure started to increase, the same as the film thickness. The change in the trend of curve was caused by filling the hydraulic accumulator. When the accumulator was fully charged with pressurized oil, film thickness continued to increase. Close to the system pressure 85 bar, observed a decrease in the film thickness. This process is caused by the control loop of the high-pressure pump, which tries to secure the pressure of 85 bar. The HBS entered the online state. To ensure stable results, the time delay was incorporated. During this stage, the average film thickness in four corners was calculated, as well as the standard deviation. The initial state was represented by similar film thickness on pads 7.1 and 7.2. The average film thickness on pad 7.1 was 42.2 $\mu$m and on pad 7.2 was 44.0 $\mu$m.

In the next stage (B), one of the capillary tubes was clogged, i.e., the capillary tube of pad 7.1 in corner B. Clogging was simulated by two caps: one closing capillary manifold and a second cap sealing inlet hole to recess. The data logging was similar to that in the first stage. On pad 7.2 can be seen an overall decreased film thickness of 1.4 $\mu$m with regards to the initial state. This was caused by the lower carrying capacity of pad 7.1. On pad 7.1 was situation more interesting. As predicted, the clogged corner had a very small film thickness (16 $\mu$m). The average film thickness decreased, and the corner thicknesses were dispersed.

Finally (C), the capillary tube was returned to its original position. The test was repeated. The pad behavior returned to its initial state. There can be seen small deviation in average film thickness. This difference would be caused by the redistribution of the load after turning the HBS online.

The precision of measurement with dial indicators can also be discussed. Each stage (A, B, C) was verified also by using dial indicators. Measurements were performed with the system powered on, then zeroed, and the change was recorded after the hydraulic system was switched off in order to assess repeatability. Contactless sensor measurement was better constrained (exact position, stiff connection with platform, and measured interface not in contact with sensor). The results are shown in Table 2.

The data obtained from contactless measurements demonstrate greater consistency. The discrepancy between the two measurement methods can reach up to 9 $\mu$m, which represents nearly 20%

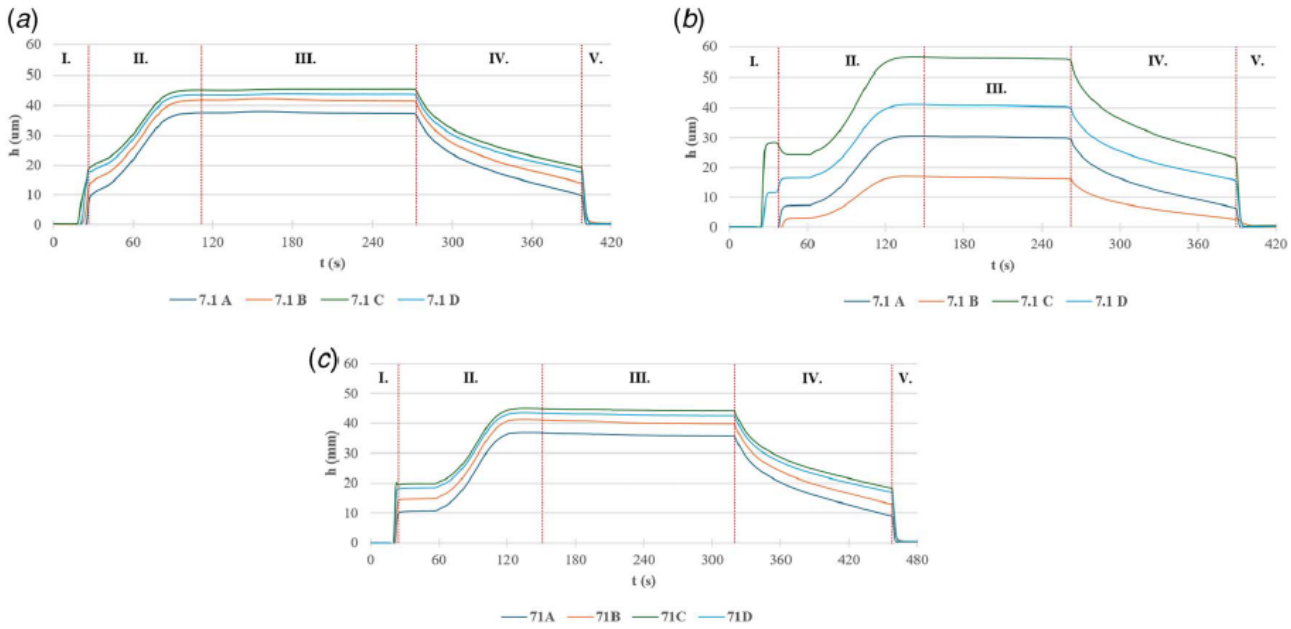


**Fig. 11 Results of capillary experiment with contactless sensors**

**Table 2 Comparison of contact and contactless measurement results**

| Initial state | 71A | 71B | 71C | 71D |
|---|---|---|---|---|
| Contactless sensor ($\mu$m) | 38 | 42 | 45 | 44 |
| Dial indicator ($\mu$m) | 38 | 44 | 51 | 47 |
| *Difference* ($\mu$m) | *0* | *2* | *6* | *3* |
| Clogged capillary | 71A | 71B | 71C | 71D |
| Contactless sensor ($\mu$m) | 30 | 16 | 56 | 41 |
| Dial indicator ($\mu$m) | 34 | 13 | 65 | 41 |
| *Difference* ($\mu$m) | *4* | *3* | *9* | *0* |
| Return to initial state | 71A | 71B | 71C | 71D |
| Contactless sensor ($\mu$m) | 36 | 40 | 44 | 42 |
| Dial indicator ($\mu$m) | 40 | 43 | 49 | 46 |
| *Difference* ($\mu$m) | *4* | *3* | *5* | *4* |

of the predicted film thickness. As previously mentioned, various uncertainties are introduced during the measurement process. The primary source of the observed difference appears to be the limited positioning accuracy of the contact sensors during installation. Although the tests with both contact and non-contact sensors were conducted in close succession, variations in temperature and humidity between measurements may contribute to the observed discrepancy. Temperature fluctuations directly influence the thickness of the lubricating film.

## Conclusions

The measurement of oil film thickness was assessed from the safety point of view. Unpredictable errors of the hydrostatic bearing can occur during operation. With the current measurement method, detecting failures such as a clogged capillary is challenging. Because the operation of UTs has been nearly 25 years, the possibility of a failure is relatively high. For this reason, the methodology of film thickness measurement was evaluated as a new failure prevention. The following conclusions based on the performed investigation were drawn:

- The described method and measurement approach apply to all types of pads in the telescope and can be used also in other large applications.
- Based on the online logging of film thickness, a new safety rule for the hydrostatic bearings system can be created.
- The measurement of oil film thickness can be used to detect the clogged capillary. It is also possible to execute maintenance procedures to mitigate any possible damage to track or pad surfaces.
- Although three sensors are sufficient to measure the thickness of the lubricating film—with the fourth corner position estimated computationally—the use of four sensors is preferable for improved safety and to reduce the risk of system failure, without introducing additional deviations or compromising robustness.
- The measured data can be different in each corner of the pad due to external conditions. Estimating deviations from the previous measured state is the proper way how to prevent failures of UT's bearings.

This methodology could be also used in the case of extremely large telescopes to prevent possible failures. Furthermore, the data from film thickness measurement can be used for the automatization of pad pressure adjustment in the future. This automated procedure could reduce the need for repetitive tasks.

## Acknowledgment

The research leading to these results has received funding from the project FW03010357 with financial support from the state budget by the Technology Agency of the Czech Republic and the Ministry of Industry and Trade within the TREND Program. I would like to express my sincere gratitude to ESO for the opportunity to conduct this research. I am especially thankful to my supervisors for generously sharing their invaluable knowledge and experience. I would also like to extend my heartfelt thanks to the members of the Paranal Mechanics and Electronics teams for their valuable support and collaboration throughout this work.

## Conflict of Interest

The authors declare no conflict of interest.

## Data Availability Statement

The data that support the findings of this study are available from the corresponding author upon reasonable request.

## References


[1] Bassani, R., and Piccigallo, B., 1992, *Hydrostatic Lubrication*, Elsevier, Amsterdam, The Netherlands.

[2] Litwin, W., Wasilczuk, M., Wodtke, M., and Olszewski, A., 2023, "The Influence of Polymer Bearing Material and Lubricating Grooves Layout on Wear of Journal Bearings Lubricated With Contaminated Water," Tribol. Int., **179**, p. 108159.

[3] Fillon, M., Wodtke, M., and Wasilczuk, M., 2015, "Effect of Presence of Lifting Pocket on the THD Performance of a Large Tilting-Pad Thrust Bearing," Friction, **3**(4), pp. 266–274.

[4] Rowe, W. B., 1989, "Advances in Hydrostatic and Hybrid Bearing Technology," Proc. Inst. Mech. Eng., Part C: J. Mech. Eng. Sci., **203**(4), pp. 225–242.

[5] Rowe, W. B., 1983, "Application of Hydrostatic Bearings," Hydrostatic and Hybrid Bearing Design, pp. 1–20.

[6] Bouyer, J., Wodtke, M., and Fillon, M., 2022, "Experimental Research on a Hydrodynamic Thrust Bearing With Hydrostatic Lift Pockets: Influence of Lubrication Modes on Bearing Performance," Tribol. Int., **165**, p. 107253.

[7] Khonsari, M., and Booser, R., 1970, "Applied Tribology," Tribol. Int., **3**(2), p. 116.

[8] Hamrock, B. J., and Schmid, S. R., 2004, *Fundamental of Fluid Film Lubrication*, 2nd ed., CRC Press, Boca Raton, FL.

[9] Jang, J., and Khonsari, M., 2015, "On the Characteristics of Misaligned Journal Bearings," Lubricants, **3**(1), pp. 27–53.

[10] Rippel, H. C., 1969, *Cast Bronze Hydrostatic Bearing Design Manual*, CBBI, Cleveland, OH.

[11] Michalec, M., Ondra, M., Svoboda, M., Chmelík, J., Zeman, P., Svoboda, P., and Jackson, R. L., 2023, "A Novel Geometry Optimization Approach for Multi-recess Hydrostatic Bearing Pad Operating in Static and Low-Speed Conditions Using CFD Simulation," Tribol. Lett., **71**(2), pp. 1–14.

[12] Wang, Z., Zhao, W., Chen, Y., and Lu, B., 2013, "Prediction of the Effect of Speed on Motion Errors in Hydrostatic Guideways," Int. J. Mach. Tools Manuf., **64**, pp. 78–84.

[13] Loeb, A. M., and Rippel, H. C., 1958, "Determination of Optimum Proportions for Hydrostatic Bearings," ASLE Trans., **1**(2), pp. 241–247.

[14] Li, X., Wang, X., Li, M., Ma, Y., and Huang, Y., 2014, "The Research Status and Progress of Heavy/Large Hydrostatic Thrust Bearing," Adv. Mech. Eng., **2014**(6), p. 982584.

[15] Zhang, Y. Q., Fan, L. G., Chen, Y., Li, R., Wu, T. Z., and Yu, X. D., 2014, "Deformation Analysis of Hydrostatic Thrust Bearing Under Different Load," Appl. Mech. Mater., **494–495**, pp. 583–586.

[16] Rajput, A. K., and Sharma, S. C., 2016, "Combined Influence of Geometric Imperfections and Misalignment of Journal on the Performance of Four Pocket Hybrid Journal Bearing," Tribol. Int., **97**, pp. 59–70.

[17] Zoupas, L., Wodtke, M., Papadopoulos, C. I., and Wasilczuk, M., 2019, "Effect of Manufacturing Errors of the Pad Sliding Surface on the Performance of the Hydrodynamic Thrust Bearing," Tribol. Int., **134**, pp. 211–220.

[18] Michalec, M., Svoboda, P., Křupka, I., and Hartl, M., 2021, "A Review of the Design and Optimization of Large-Scale Hydrostatic Bearing Systems," Eng. Sci. Technol. Int. J., **24**(4), pp. 936–958.

[19] San Andrés, L., 2002, "Effects of Misalignment on Turbulent Flow Hybrid Thrust Bearings," ASME J. Tribol., **124**(1), pp. 212–219.

[20] Michalec, M., Polnický, V., Foltýn, J., Svoboda, P., Šperka, P., and Hurník, J., 2022, "The Prediction of Large-Scale Hydrostatic Bearing Pad Misalignment Error and Its Compensation Using Compliant Support," Precis. Eng., **75**, pp. 67–79.

[21] Da Silva, H. A. P., and Nicoletti, R., 2019, "Design of Tilting-Pad Journal Bearings Considering Bearing Clearance Uncertainty and Reliability Analysis," ASME J. Tribol., **141**(1), pp. 1–11.

[22] Michalec, M., Foltýn, J., Dryml, T., Snopek, L., Javorský, D., Čupr, M., and Svoboda, P., 2023, "Assembly Error Tolerance Estimation for Large-Scale Hydrostatic Bearing Segmented Sliders Under Static and Low-Speed Conditions," Machines, **11**(11), p. 1025.

[23] Rajput, A. K., Yadav, S. K., and Sharma, S. C., 2017, "Effect of Geometrical Irregularities on the Performance of a Misaligned Hybrid Journal Bearing Compensated With Membrane Restrictor," Tribol. Int., **115**, pp. 619–627.

[24] Michalec, M., Daněk, L., Foltýn, J., Svoboda, P., Gachot, C., Hartl, M., and Křupka, I., 2024, "Comparative Wear and Friction Analysis of Sliding Surface Materials for Hydrostatic Bearing Under Oil Supply Failure Conditions," Adv. Eng. Mater., p. 2401733.

[25] Yacout, A. W., 2007, "The Surface Roughness Effect on the Hydrostatic Thrust Spherical Bearings Performance (Part 3 of 5, Recessed Clearance Type of Bearings)," ASME Int. Mech. Eng. Congr. Exposition Proc., **9**, pp. 431–447.

[26] Foltýn, J., Hurník, J., Michalec, M., Svoboda, P., Křupka, I., and Hartl, M., 2024, "Pad Alignment Methods and Their Impact on Large Hydrostatic Bearing Precision," Machines, **12**(8), p. 549.

[27] Sharma, S. C., Phalle, V. M., and Jain, S. C., 2011, "Performance Analysis of a Multirecess Capillary Compensated Conical Hydrostatic Journal Bearing," Tribol. Int., **44**(5), pp. 617–626.

[28] Ma, X., and Li, M., 2017, "Pad Attitude Adjusting Moment in Large Multi-pocket Pivoted Pad Used in Static Oil Journal Bearing," Ind. Lubr. Tribol., **69**(4), pp. 605–611.

[29] Sharma, S. C., Jain, S. C., and Bharuka, D. K., 2002, "Influence of Recess Shape on the Performance of a Capillary Compensated Circular Thrust Pad Hydrostatic Bearing," Tribol. Int., **35**(6), pp. 347–356.

[30] Wen, S., and Huang, P., 2016, *Principles of Tribology*, Wiley, New York.

# 7 CONCLUSIONS

This dissertation focused on improving the safety of large-scale hydrostatic bearings by addressing critical aspects of lubricating film integrity under realistic operating, assembly, and fault conditions. While hydrostatic bearings are widely recognized for their high load capacity, low friction, and suitability for precision applications, their safe operation at large scales is increasingly constrained by geometric imperfections, limited accessibility, and sensitivity to hydraulic disturbances. The central premise of this work was that the safety of such systems cannot be ensured solely through pressure-based design assumptions but must instead be evaluated and managed through direct consideration of lubricating film thickness and its distribution.

The first part of the dissertation addressed the challenge of diagnosing lubricating film thickness in large-scale hydrostatic bearings where conventional sensor installation is impractical. The developed optical point tracking method demonstrated that non-contact optical techniques are capable of providing film thickness measurements with accuracy and repeatability comparable to proximity sensors, while exhibiting reduced measurement dispersion. The ability to assess spatial and temporal variations of film thickness without mechanical interaction with the bearing components represents a significant advantage for safety-oriented diagnostics. These findings confirm that optical methods can reliably support assessment of minimum film thickness, which governs the risk of surface contact, particularly during commissioning, inspection, and fault investigation in large installations.

The second part of the work examined the influence of pad alignment on lubricating film thickness distribution and bearing safety. Experimental comparison of conventional mechanical leveling, pressure-based alignment, and optical coordinate measurement demonstrated that alignment accuracy has a direct and measurable impact on film uniformity. Optical alignment achieved the most uniform film thickness distribution and the highest geometric precision, without relying on compliant support elements that reduce bearing stiffness and positional accuracy. The results confirm that addressing assembly inaccuracies through precise geometric alignment, rather than compensating them through elastic deformation, is essential for maintaining both safety and precision in rigid, segmented hydrostatic bearings. Optical alignment methods thus represent an effective preventive measure against local film thinning and associated safety risks.

The third part of the dissertation investigated hydrostatic bearing behavior under fault conditions in a real large-scale application. Field experiments on the Very Large Telescope hydrostatic bearing system showed that local hydraulic faults, such as capillary blockage, produce pronounced and localized reductions in lubricating film thickness. Measured drops demonstrated that even a single restrictor malfunction can drive the bearing toward contact conditions, despite overall system redundancy. These results confirm that conventional restrictor-based design methodologies, which assume ideal and continuous function of all restrictors, do not adequately account for realistic fault scenarios. Continuous, contactless film thickness monitoring was shown to provide early identification of such critical states, enabling preventive intervention before catastrophic damage occurs.

The main contributions of the thesis can be summarized as follows:

- A safety-oriented approach to large-scale hydrostatic bearings was established, identifying lubricating film thickness and its distribution as the key parameters for safe operation.
- A contactless optical point tracking method was developed and validated for lubricating film thickness diagnostics in hydrostatic bearings under realistic conditions.
- Experimental data from one of the world's largest hydrostatic bearing installations were obtained and published, providing rare insight into film behavior under real operating and fault conditions.

Overall, this dissertation demonstrates that the safety of large-scale hydrostatic bearings can be significantly improved by adopting a focus that treats lubricating film thickness as a primary safety parameter. By combining optical diagnostics, precise alignment strategies, and continuous monitoring under real operating conditions, the presented work provides a coherent framework for identifying, preventing, and managing safety-critical states in hydrostatic bearing systems. The results extend existing knowledge beyond idealized design assumptions and contribute practical tools applicable to large, high-value installations where failure consequences are severe. Future work should focus on integrating optical diagnostics with automated decision-making tools, extending fault analysis to additional failure modes, and applying the proposed approach to large-scale hydrostatic bearing applications.

# 8 LIST OF PUBLICATIONS AND OUTCOMES

## 8.1 Publications related to the thesis topic

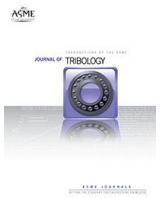


FOLTÝN, J., E. FLORES, M. TAPIA, N. ÁLVAREZ, M. MICHALEC, P. SVOBODA. Failure prevention procedure of the Very Large Telescope hydrostatic bearing pads based on lubricating film thickness measurement. *ASME. J. Tribol*, 2025, vol. 147. https://doi.org/10.1115/1.4068788 *[AIS Q2]*


FOLTÝN, J., L. MACCIONI, M. MICHALEC, F. CONCLI, P. SVOBODA. Uncertainty analysis of hydrostatic bearing working conditions with experimental, CFD, and analytical approach. *Forsch Ingenieurwes*, 2025, vol. 89. https://doi.org/10.1007/s10010-025-00836-9 *[AIS Q3]*


MICHALEC, M., J. FOLTÝN, P. SVOBODA, I. KŘUPKA, M. HARTL. Performance and stability comparison of hydrostatic bearing pad geometry optimization approaches. *Forsch Ingenieurwes*, 2025, vol. 89. https://doi.org/10.1007/s10010-025-00837-8 *[AIS Q3]*


MICHALEC, M., L. DANĚK, J. FOLTÝN, P. SVOBODA, C. GACHOT, M. HARTL, I. KŘUPKA. Comparative Wear and Friction Analysis of Sliding Surface Materials for Hydrostatic Bearing under Oil Supply Failure Conditions. Adv. Eng. Mater. 2025. https://doi.org/10.1002/adem.202401733 *[AIS Q2]*


FOLTÝN, J., MACCIONI, L., MICHALEC, M., CONCLI, F., SVOBODA, P. The Influence of Measurement Uncertainties and Input Parameters on Hydrostatic Bearing Performance: Analytical, Experimental, and Numerical Comparison. In: ISIEA 2024. Lecture Notes in Networks and Systems, vol 1124. Springer, Cham. https://doi.org/10.1007/978-3-031-70462-8_2


MICHALEC, M., FOLTÝN, J., SVOBODA, P., KŘUPKA, I., HARTL, M. Experimental Comparison of Hydrostatic Bearing Pad Geometry Optimization Approaches Under Static Conditions. In: ISIEA 2024. Lecture Notes in Networks and Systems, vol 1124. Springer, Cham. https://doi.org/10.1007/978-3-031-70462-8_1


FOLTÝN, J.; HURNÍK, J.; MICHALEC, M.; SVOBODA, P.; KŘUPKA, I.; AND HARTL, M. Pad Alignment Methods and Their Impact on Large Hydrostatic Bearing Precision. Machines 2024, 12, 549. https://doi.org/10.3390/machines12080549 *[AIS Q2]*


MICHALEC, M.; FOLTÝN, J.; DRYML, T.; SNOPEK, L.; JAVORSKÝ, D.; ČUPR, M.; SVOBODA, P. Assembly Error Tolerance Estimation for Large-Scale Hydrostatic Bearing Segmented Sliders under Static and Low-Speed Conditions. Machines, 2023, vol. 11, no. 11. https://doi.org/10.3390/machines11111025 *[AIS Q2]*


MICHALEC, M.; HURNÍK, J.; FOLTÝN, J.; SVOBODA, P. Contactless measurement of hydrostatic bearing lubricating film using optical point tracking method. PROCEEDINGS OF THE INSTITUTION OF MECHANICAL ENGINEERS PART J-JOURNAL OF EN, 2023, vol. 237, no. 1, p. 76-84. https://doi.org/10.1177/13506501221108138 *[AIS Q3]*


MICHALEC, M., POLNICKÝ, V., FOLTÝN, J., SVOBODA, P., ŠPERKA, P., HURNÍK, J.: The prediction of large-scale hydrostatic bearing pad misalignment error and its compensation using compliant support. Precis. Eng. 75, 67–79 (2022). https://doi.org/10.1016/j.precisioneng.2022.01.011 *[AIS Q1]*

## 8.2 Applied research outcomes

### 8.2.1 Utility models

SVOBODA, P.; POLNICKÝ, V.; MICHALEC, M.; FOLTÝN, J.; MARTINEK, J.; ROBENEK, V.; DRHA, V.; Brno University of Technology, Brno, Veveří, CZ Bosch Rexroth, spol. s r.o., Brno, Černovice, CZ: Device for testing the operational conditions of hydrostatic bearing. 37631, utility model (2024). URL: https://www.vut.cz/en/rad/results/detail/187147

### 8.2.2 Functional samples

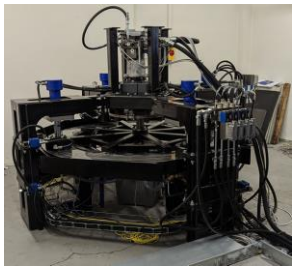

FOLTÝN, J.; MICHALEC, M.; POLNICKÝ, V.; SVOBODA, P.; MARTINEK, J.; ROBENEK, V.; DRHA, V.: Experimental device 4PAD; Hydrostatic turntable with mechatronic systems based on adaptive control loops. Laboratory B2/305 IMID, FME, BUT, Technická 2896/2 616 69 Brno, functional sample (2023) URL: https://intranet.ustavkonstruovani.cz/file-download/get-project-pdf/468.

FOLTÝN, J.; POLNICKÝ, V.; MICHALEC, M.; SVOBODA, P.; MARTINEK, J.; ROBENEK, V.: Experimental device 3PAD; Hydrostatic bearing with feedback film thickness control. Laboratory B2/305 IMID, FME, BUT, Technická 2896/2 616 69 Brno, functional sample (2022). URL: https://intranet.ustavkonstruovani.cz/file-download/get-project-pdf/467.

## 8.3 Other outcomes

ITC Fukuoka 2023

FOLTÝN, J., J. HURNÍK, M. MICHALEC, P. SVOBODA. Influence of Alignment Methods on Hydrostatic Bearing Performance. 9th International Tribology Conference 2023. 25.-30. 9. 2023, Fukuoka, Japan. [Poster presentation].

WTC2021
7th WORLD TRIBOLOGY CONGRESS
September 5-10 2021
LYON FRANCE

MICHALEC, M., J. HURNÍK, J. FOLTÝN, P. SVOBODA. Contactless measurement of hydrostatic bearing lubricating film using optical point tracking method. 7th World Tribology Congress 2022. 10.-15. 7. 2022, Lyon, France. [Poster presentation].

# 9 LITERATURE


1. Girard, L.-D. Hydraulique Appliquée. Nouveau Système de Locomotion Sur Les Chemins de Fer. 1852.
2. Rowe, W.B. Advances in Hydrostatic and Hybrid Bearing Technology. *Proceedings of the Institution of Mechanical Engineers, Part C: Mechanical Engineering Science* 1989, *203*, 225–242, doi:10.1243/PIME_PROC_1989_203_110_02.
3. Bassani, R.; Piccigallo, B. *Hydrostatic Lubrication*; Elsevier: Amsterdam, 1992; ISBN 044488498.
4. Li, X.; Wang, X.; Li, M.; Ma, Y.; Huang, Y. The Research Status and Progress of Heavy/Large Hydrostatic Thrust Bearing. *Advances in Mechanical Engineering* 2014, *6*, 982584, doi:10.1155/2014/982584.
5. Liu, Z.; Wang, Y.; Cai, L.; Zhao, Y.; Cheng, Q.; Dong, X. A Review of Hydrostatic Bearing System: Researches and Applications. *Advances in Mechanical Engineering* 2017, *9*, doi:10.1177/1687814017730536.
6. Michalec, M.; Svoboda, P.; Křupka, I.; Hartl, M. A Review of the Design and Optimization of Large-Scale Hydrostatic Bearing Systems. *Engineering Science and Technology, an International Journal* 2021, *24*, 936–958, doi:10.1016/j.jestch.2021.01.010.
7. ROWE, W.B. Application of Hydrostatic Bearings. *Hydrostatic and Hybrid Bearing Design* 1983, 1–20, doi:10.1016/b978-0-408-01324-6.50005-4.
8. Okahata, G.; Okuyama, S.; Yui, A. Numerical Study on Constant-Flow Hydrostatic Water Bearing for a Machine-Tool Table. *Adv Mat Res* 2011, *325*, 357–362, doi:10.4028/www.scientific.net/AMR.325.357.
9. Feng, H.H.; Xu, C.D.; Wang, F.F. Combined Influence of Misalignment and Orifice Diameter on the Static Performances of Hydrostatic, Water-Lubricated Journal Bearings. *Applied Mechanics and Materials* 2014, *607*, 608–611, doi:10.4028/www.scientific.net/AMM.607.608.
10. Du, J.; Liang, G. Performance Comparative Analysis of Hydrostatic Bearings Lubricated with Low-Viscosity Cryogenic Fluids. *Tribol Int* 2019, *137*, 139–151, doi:10.1016/j.triboint.2019.03.061.
11. Bouyer, J.; Wodtke, M.; Fillon, M. Experimental Research on a Hydrodynamic Thrust Bearing with Hydrostatic Lift Pockets: Influence of Lubrication Modes on Bearing Performance. *Tribol Int* 2022, *165*, 107253, doi:10.1016/j.triboint.2021.107253.

12. Concli, F. Pressure Distribution in Small Hydrodynamic Journal Bearings Considering Cavitation: A Numerical Approach Based on the Open-source CFD Code OpenFOAM®. *Lubrication Science* 2016, *28*, 329–347, doi:10.1002/ls.1334.

13. Dhande, D.Y.; Pande, · D W A Two-Way FSI Analysis of Multiphase Flow in Hydrodynamic Journal Bearing with Cavitation. 2017, *39*, doi:10.1007/s40430-017-0750-8/Published.

14. Guo, Z.; Hirano, T.; Kirk, R.G. Application of CFD Analysis for Rotating Machinery - Part I: Hydrodynamic, Hydrostatic Bearings and Squeeze Film Damper. *J Eng Gas Turbine Power* 2005, *127*, 445–451, doi:10.1115/1.1807415.

15. Mahdi, R.; Stephan, K.; Friedrich, B. Experimental Investigations on Stick-Slip Phenomenon and Friction Characteristics of Linear Guides. *Procedia Eng* 2015, *100*, 1023–1031, doi:10.1016/J.PROENG.2015.01.462.

16. Bonanno, A.; Pedrielli Imamoter -cnr, F. A STUDY ON THE STRUCTUREBORNE NOISE OF HYDRAULIC GEAR PUMPS. *Proceedings of the JFPS International Symposium on Fluid Power* 2008, *2008*, 641–646, doi:10.5739/ISFP.2008.641.

17. Ortwig, H. Experimental and Analytical Vibration Analysis in Fluid Power Systems. *Int J Solids Struct* 2005, *42*, 5821–5830, doi:10.1016/J.IJSOLSTR.2005.03.028.

18. Vibrations Induced by Internal Fluid Flow. *Flow-induced Vibrations* 2014, 157–195, doi:10.1016/B978-0-08-098347-9.00004-7.

19. Khonsari, M.M.; Booser, R.E. Applied Tribology. *Tribology* 1970, *3*, 116, doi:10.1016/0041-2678(70)90297-6.

20. Xian-ting, M. A Review of the Present Status of Hydraulic Accumulator. *Applied Mechanics and Materials* 2013, *246–247*, 629–634, doi:10.4028/WWW.SCIENTIFIC.NET/AMM.246-247.629.

21. Rehman, W.U.; Yuanxin, L.; Guiyun, J.; Yongqin, W.; Rehman, S.U.; Bibi, S.; Iqbal, N.; Zaheer, M.A.; Azhar, I.; Xiaogao, Y. Control of Oil Film Thickness for Hydrostatic Journal Bearing Using PID Disturbance Rejection Controller. In Proceedings of the 2017 IEEE 3rd Information Technology and Mechatronics Engineering Conference (ITOEC); IEEE, October 2017; pp. 543–547.

22. Khan, N.; Rehman, W.U.; Chen, W.J.; Ahmad, A.; Ayaz, M. Active Lubrication For Hydrostatic Journal Bearing Using Adaptive Control. 2019.

23. Zha, J.; Cheng, K.; Xue, F.; Wu, D.; Liu, X. Hydrostatic Guideways for Precision Machines: The State-of-the-Art and Future Perspectives. *Tribol Int* 2024, *200*, doi:10.1016/J.TRIBOINT.2024.110060.

24. Rippel, H.C. *Cast Bronze Hydrostatic Bearing Design Manual*; CBBI: Cleveland, 1969;

25. Halling, J.; Burton, R.A. Principles of Tribology. *Journal of Lubrication Technology* 1977, *99*, 305–306, doi:10.1115/1.3453090.

26. Sinhasan, R.; Jain, S.C.; Sharma, S.C. Orifice-Compensated Flexible Thrust Pad Bearings of Different Configurations. *Tribol Int* 1986, *19*, 244–252, doi:10.1016/0301-679X(86)90003-4.

27. Grinnell, S.K.; Richardson, H.H. Design Study of a Hydrostatic Gas Bearing With Inherent Orifice Compensation. *J Fluids Eng* 1957, *79*, 11–21, doi:10.1115/1.4012913.

28. Verma, S.; Jadon, V.K.; Gupta, K.D. Analysis of Capillary Compensated Hydrostaticjournal Bearing Operating with Micropolar Lubricant. *Industrial Lubrication and Tribology* 2011, *63*, 192–202, doi:10.1108/00368791111126617.

29. Sharma, S.C.; Phalle, V.M.; Jain, S.C. Performance Analysis of a Multirecess Capillary Compensated Conical Hydrostatic Journal Bearing. *Tribol Int* 2011, *44*, 617–626, doi:10.1016/J.TRIBOINT.2010.12.012.

30. Zhu, X.C.; Gao, W.G.; Liu, T.; Zhao, S.H.; Zhang, G.W.; Zhang, D.W. Analysis on Dynamic Characteristics of Closed Hydrostatic Guideway Throttled by Capillary. *Applied Mechanics and Materials* 2014, *607*, 594–599, doi:10.4028/WWW.SCIENTIFIC.NET/AMM.607.594.

31. Lai, T.H.; Chang, T.Y.; Yang, Y.L.; Lin, S.C. Parameters Design of a Membrane-Type Restrictor with Single-Pad Hydrostatic Bearing to Achieve High Static Stiffness. *Tribol Int* 2017, *107*, 206–212, doi:10.1016/J.TRIBOINT.2016.11.037.

32. Kang, Y.; Shen, P.; Chen, C.; Chang, Y.; Lee, H. Modified Determination of Fluid Resistance for Membrane-type Restrictors. *Industrial Lubrication and Tribology* 2007, *59*, 123–131, doi:10.1108/00368790710746084.

33. Chen, D.C.; Chen, M.F.; Pan, C.H.; Pan, J.Y. Study of Membrane Restrictors in Hydrostatic Bearing. *Advances in Mechanical Engineering* 2018, *10*, doi:10.1177/1687814018799604;ISSUE:ISSUE:DOI.

34. Lin, S.C.; Lo, Y.H.; Lin, Y.H.; Tung, W.T.; Lai, T.H. Design and Performance Analysis of Dual Membrane Restrictor for Hydrostatic Bearing. *Lubricants 2022, Vol. 10, Page 179* 2022, *10*, 179, doi:10.3390/LUBRICANTS10080179.

35. Lai, J.-Y.; Chen, Y.-R. *Adaptive Flow Rate Control of a Hydraulic Proportional Valve*; 1992;

36. Ur Rehman, W.; Wang, X.; Chen, Y.; Yang, X.; Ullah, Z.; Cheng, Y.; Kanwal, M. An Active Control for Hydrostatic Journal Bearing Using Optimization Algorithms. *Industrial Lubrication and Tribology* 2021, *73*, 316–324, doi:10.1108/ILT-07-2020-0272.

37. Rehman, W.U.; Khan, W.; Ullah, N.; Shahariar Chowdhury, M.D.; Techato, K.; Haneef, M. Nonlinear Control of Hydrostatic Thrust Bearing Using Multivariable Optimization. *Mathematics 2021, Vol. 9, Page 903* 2021, *9*, 903, doi:10.3390/MATH9080903.

38. Brungardt, M. V.; Shatokhin, S.N. Spindles with Multiply Adaptive Hydrostatic Bearings. *Russian Engineering Research* 2021, *41*, 10–15, doi:10.3103/S1068798X21010081.

39. Yu, X.; Sun, F.; Zhou, D.; Huang, D.; Zhan, S.; Han, F.; Jiao, J.; Jiang, H. Research on Influencing Factors of Oil Film Temperature Field Characteristics for Adaptive Hydrostatic Thrust Bearing. *Proc Inst Mech Eng B J Eng Manuf* 2024, *238*, 1727–1735, doi:10.1177/09544054231213678.

40. Fritz, M.; Groeb, M. Increasing Performance and Energy Efficency of a Machine Tool through Hydrostatic Linear Guideways with Single Digit Micrometre Fluid Film Thickness. *MM Science Journal* 2021, *2021-November*, 5241–5246, doi:10.17973/MMSJ.2021_11_2021175.

41. Dong, X.M.; Cai, L.G.; Zhao, Y.S.; Shi, X. Deformation Analysis for Hydrostatic Rotary Table of Heavy Duty CNC Machine Tool. *Applied Mechanics and Materials* 2013, *457–458*, 335–339.

42. Huang, H.C.; Yang, S.H. Thrust-Bearing Layout Design of a Large-Sized Hydrostatic Rotary Table to Withstand Eccentric Loads for Horizontal Boring Machine Applications. *Lubricants 2022, Vol. 10, Page 49* 2022, *10*, 49, doi:10.3390/LUBRICANTS10040049.

43. Stach, E.; Smolik, J.; Sulitka, M.; Lazak, T.; Divis, I.; Falta, J. THERMO-MECHANICAL ANALYSIS OF A MACHINE TOOL WITH HYDROSTATIC BEARINGS. *MM Science Journal* 2022, *2022*, 6180–6189, doi:10.17973/MMSJ.2022_12_2022153.

44. Brito, M.; Teixeira, L.; Canelas, R.B.; Ferreira, R.M.L.; Neves, M.G. Experimental and Numerical Studies of Dynamic Behaviors of a Hydraulic Power Take-Off Cylinder Using Spectral Representation Method. *J Tribol* 2018, *140*, doi:10.1115/1.4037464/378104.

45. Cui, W.; Raza, K.; Zhao, Z.; Yu, C.; Tao, L.; Zhao, W.; Chen, W.; Peng, S.; Xu, Q.; Ma, L.; et al. Role of Transfer Film Formation on the Tribological Properties of Polymeric Composite Materials and Spherical Plain Bearing at Low Temperatures. *Tribol Int* 2020, *152*, 106569, doi:10.1016/J.TRIBOINT.2020.106569.

46. Renzetti N A *The NASA/JPL 64-Meter-Diameter Antenna at Goldstone, California: Project Report*; Pasadena, 1974;

47. Bartos, I.P.; Bell, H.B.; Phillips, H.P.; Sweetser, B.M.; Rotach, O.A. *Implementation of the 64-Meter-Diameter Antennas at the Deep Space Stations in Australia and Spain*; 1975;

48. Bartos, R.D. *An Analysis of the 70-Meter Antenna Hydrostatic Bearing by Means of Computer Simulation*; 1993;

49. Weis, U.; Tomelleri, R.; Ippa, A.; Eisenträger, P.; Sust, E.; Todeschini, A. Hydrostatic Bearing System for the Giant Magellan Telescope.; SPIE-Intl Soc Optical Eng, August 28 2024; p. 57.

50. Marchiori, G.; Rampini, F.; Ghedin, L.; Bressan, R. ELT Design Status: The Most Powerful Ground Telescope. 2018, *1070021*, 68, doi:10.1117/12.2314947.

51. Sheehan, M.; Gunnels, S.; Hull, C.; Kern, J.; Smith, C.; Johns, M.; Shectman, S. Progress on the Structural and Mechanical Design of the Giant Magellan Telescope.; Stepp, L.M., Gilmozzi, R., Hall, H.J., Eds.; September 2012; p. 84440N.

52. *GMT SYSTEM LEVEL PRELIMINARY DESIGN REVIEW Section 6*; 2013;

53. Litwin, W.; Wasilczuk, M.; Wodtke, M.; Olszewski, A. The Influence of Polymer Bearing Material and Lubricating Grooves Layout on Wear of Journal Bearings Lubricated with Contaminated Water. *Tribol Int* 2023, *179*, doi:10.1016/j.triboint.2022.108159.

54. Huang, H.C.; Yang, W.H. Thermal Characteristics of a Vertical Hydrostatic Guideway System for Precision Milling Machine Applications. *Lubricants* 2022, *10*, doi:10.3390/LUBRICANTS10100247.

55. Zha, J.; Xue, F.; Chen, Y. Straightness Error Modeling and Compensation for Gantry Type Open Hydrostatic Guideways in Grinding Machine. *Int J Mach Tools Manuf* 2017, *112*, 1–6, doi:10.1016/j.ijmachtools.2016.10.002.

56. WASILCZUK, F.; WASILCZUK, M.; WODTKE, M. PROSPECTS OF DECREASING POWER LOSSES IN A HYDROSTATIC THRUST BEARING. *Tribologia* 2017, 91–96, doi:10.5604/01.3001.0010.6033.

57. Michalec, M.; Foltýn, J.; Dryml, T.; Snopek, L.; Javorský, D.; Čupr, M.; Svoboda, P. Assembly Error Tolerance Estimation for Large-Scale Hydrostatic Bearing Segmented Sliders under Static and Low-Speed Conditions. *Machines 2023, Vol. 11, Page 1025* 2023, *11*, 1025, doi:10.3390/MACHINES11111025.

58. Qi, E.; Fang, Z.; Sun, T.; Chen, J.; Liu, C.; Wang, J. A Method for Predicting Hydrostatic Guide Error Averaging Effects Based on Three-Dimensional Profile Error. *Tribol Int* 2016, *95*, 279–289, doi:10.1016/j.triboint.2015.11.032.

59. Cui, H.; Wang, Y.; Yue, X.; Huang, M.; Wang, W. Effects of Manufacturing Errors on the Static Characteristics of Aerostatic Journal Bearings with Porous Restrictor. *Tribol Int* 2017, *115*, 246–260, doi:10.1016/j.triboint.2017.05.008.

60. Zoupas, L.; Wodtke, M.; Papadopoulos, C.I.; Wasilczuk, M. Effect of Manufacturing Errors of the Pad Sliding Surface on the Performance of the Hydrodynamic Thrust Bearing. *Tribol Int* 2019, *134*, 211–220, doi:10.1016/j.triboint.2019.01.046.

61. Michalec, M.; Foltýn, J.; Svoboda, P.; Křupka, I.; Hartl, M. Performance and Stability Comparison of Hydrostatic Bearing Pad Geometry Optimization Approaches. *Forschung im Ingenieurwesen 2025 89:1* 2025, *89*, 65-, doi:10.1007/S10010-025-00837-8.

62. Zhang, P.; Chen, Y.; Zhang, C.; Zha, J.; Wang, T. Influence of Geometric Errors of Guide Rails and Table on Motion Errors of Hydrostatic Guideways under Quasi-Static Condition. *Int J Mach Tools Manuf* 2018, *125*, 55–67, doi:10.1016/j.ijmachtools.2017.10.006.

63. Lin, J.R. Surface Roughness Effect on the Dynamic Stiffness and Damping Characteristics of Compensated Hydrostatic Thrust Bearings. *Int J Mach Tools Manuf* 2000, *40*, 1671–1689, doi:10.1016/S0890-6955(00)00012-2.

64. Lin, J.R.; Hung, T.C.; Chou, T.L.; Liang, L.J. Effects of Surface Roughness and Non-Newtonian Micropolar Fluids on Dynamic Characteristics of Wide Plane Slider Bearings. *Tribol Int* 2013, *66*, 150–156, doi:10.1016/J.TRIBOINT.2013.05.004.

65. Lu, H.; Tian, Z.; Lu, H.; Tian, Z. Investigation of the Static Performance of Hydrostatic Thrust Bearings Considering Non-Gaussian Surface Topography. *Lubricants 2023, Vol. 11,* 2023, *11*, doi:10.3390/LUBRICANTS11060267.

66. Martinez Esparza, L.F.; Cervantes De Gortari, J.G.; Chicurel Uziel, E.J. Design of Hybrid Hydrostatic/Hydrodynamic Journal Bearings for Optimum Self-Compensation Under Misaligning External Loads. *J Tribol* 2017, *139*, 1–12, doi:10.1115/1.4035157.

67. Sha, Y.; Lu, C.; Pan, W.; Chen, S.; Ge, P. Nonlinear Control System Design for Active Lubrication of Hydrostatic Thrust Bearing. *Coatings 2020, Vol. 10, Page 426* 2020, *10*, 426, doi:10.3390/COATINGS10040426.

68. Renn, J.C.; Wu, G.Y. A Study on Active Closed-Loop Gap Control for Hydrostatic Bearing. *Applied Mechanics and Materials* 2019, *894*, 51–59, doi:10.4028/WWW.SCIENTIFIC.NET/AMM.894.51.

69. Zhang, Y.Q.; Fan, L.G.; Chen, Y.; Li, R.; Wu, T.Z.; Yu, X.D. Deformation Analysis of Hydrostatic Thrust Bearing under Different Load. *Applied Mechanics and Materials* 2014, *494–495*, 583–586, doi:10.4028/WWW.SCIENTIFIC.NET/AMM.494-495.583.

70. Manring, N.D.; Johnson, R.E.; Cherukuri, H.P. The Impact of Linear Deformations on Stationary Hydrostatic Thrust Bearings. *J Tribol* 2002, *124*, 874–877, doi:10.1115/1.1482118.

71. Yu, X.; Wang, F.; Zhou, D.; Huang, D.; Zhan, S.; Yu, M.; Jiao, J.; Wang, J. Deformation Characteristics of Adaptive Hydrostatic Thrust Bearing under Extreme Working Conditions. *Journal of the Brazilian Society of Mechanical Sciences and Engineering 2020 42:9* 2020, *42*, 489-, doi:10.1007/S40430-020-02571-4.

72. Yu, M.; Yu, X.; Zheng, X.; Jiang, H. Thermal-Fluid-Solid Coupling Deformation of Hydrostatic Thrust Bearing Friction Pairs. *Industrial Lubrication and Tribology* 2018, *71*, 467–473, doi:10.1108/ILT-07-2018-0262.

73. Yang, X.; Shao, J.; Xu, X.; Wang, Y.; Yin, C.; Jiang, H. Research on Velocity Influence on Thermal Deformation Field of Heavy Hydrostatic Thrust Bearing. *Adv Mat Res* 2010, *129–131*, 968–972, doi:10.4028/WWW.SCIENTIFIC.NET/AMR.129-131.968.

74. Michalec, M.; Daněk, L.; Foltýn, J.; Svoboda, P.; Gachot, C.; Hartl, M.; Křupka, I. Comparative Wear and Friction Analysis of Sliding Surface Materials for Hydrostatic Bearing under Oil Supply Failure Conditions. *Adv Eng Mater* 2024, *2401733*, doi:10.1002/adem.202401733.

75. Van Beek, A.; Segal, A. Rubber Supported Hydrostatic Thrust Bearings with Rigid Bearing Surfaces. *Tribol Int* 1997, *30*, 47–52, doi:10.1016/0301-679X(96)00021-7.

76. Van Beek, A.; Lepic, L. Rubber Supported Hydrostatic Thrust Bearings with Elastic Bearing Surfaces of Infinite Length. *Wear* 1996, *201*, 45–50, doi:10.1016/S0043-1648(96)06987-6.

77. Michalec, M.; Polnický, V.; Foltýn, J.; Svoboda, P.; Šperka, P.; Hurník, J. The Prediction of Large-Scale Hydrostatic Bearing Pad Misalignment Error and Its Compensation Using Compliant Support. *Precis Eng* 2022, *75*, 67–79, doi:10.1016/j.precisioneng.2022.01.011.

78. Rowe, W.B. Restrictors and Compensation of Hydrostatic Bearings. *Encyclopedia of Tribology* 2013, 2759–2766, doi:10.1007/978-0-387-92897-5_53.

79. Foltýn, J.; Flores, E.; Tapia, M.; Álvarez, N.; Michalec, M.; Svoboda, P. Failure Prevention Procedure of the Very Large Telescope Hydrostatic Bearing Pads Based on the Lubricating Film Thickness Measurement. *J Tribol* 2025, *147*, doi:10.1115/1.4068788.

80. Michalec, M.; Hurník, J.; Foltýn, J.; Svoboda, P. Contactless Measurement of Hydrostatic Bearing Lubricating Film Using Optical Point Tracking Method. *Proceedings of the Institution of Mechanical Engineers, Part J: Journal of Engineering Tribology* 2023, *237*, 76–84, doi:10.1177/13506501221108138.

81. Foltýn, J.; Hurník, J.; Michalec, M.; Svoboda, P.; Křupka, I.; Hartl, M. Pad Alignment Methods and Their Impact on Large Hydrostatic Bearing Precision. *Machines* 2024, *12*, doi:10.3390/machines12080549.

# LIST OF FIGURES